الجامعة الأردنيـــة
كلية الدراسات العليا

التاريـــخ: / /

نموذج رقم (١٨)
اقرار والتزام بقوانين الجامعة الأردنية وأنظمتها وتعليماتها لطلبة الماجستير

أنا الطالب: وائل محمد يونس محمود الرقم الجامعي: 8090092
التخصص: الكيمياء الكلية: العلوم

اعلن بأنني قد التزمت بقوانين الجامعة الأردنية وأنظمتها وتعليماتها وقراراتها السارية المفعول المتعلقة باعداد رسائل الماجستير والدكتوراة عندما قمت شخصيا" باعداد رسالتي / اطروحتي بعنوان:
preparation and characterization of Gold, copper and silver nanoparticles electrochemically deposited by application of a square wave potential regime

وذلك بما ينسجم مع الأمانة العلمية المتعارف عليها في كتابة الرسائل والأطاريح العلمية. كما أنني أعلن بأن رسالتي /اطروحتي هذه غير منقولة أو مستلة من رسائل أو أطاريح أو كتب أو أبحاث أو أي منشورات علمية تم نشرها أو تخزينها في أي وسيلة اعلامية، وتأسيسا" على ما تقدم فانني أتحمل المسؤولية بأنواعها كافة فيما لو تبين غير ذلك بما فيه حق مجلس العمداء في الجامعة الأردنية بالغاء قرار منحي الدرجة العلمية التي حصلت عليها وسحب شهادة التخرج مني بعد صدورها دون أن يكون لي أي حق في التظلم أو الاعتراض أو الطعن بأي صورة كانت في القرار الصادر عن مجلس العمداء بهذا الصدد.

توقيع الطالب: وائل التاريخ: ٢٨ / ٧ / ٢٠١١

تعتمد كلية الدراسات العليا
هذه النسخة من الرسالـــة
التوقيع........ التاريخ ٢٨.........

The University of Jordan
Authorization Form

I, wael mohammad mahamoud authorize the University of Jordan to supply copies of my Thesis/Dissertation to libraries or establishments or individuals on request.

Signature:
Date: 28/7/2011

PREPARATION AND CHARACTERIZATION OF GOLD, COPPER AND SILVER NANOPARTICLES ELECTROCHEMICALLY DEPOSITED BY APPLICATION OF A SQUARE WAVE POTENTIAL REGIME

By
Wael Mohammad Mahamoud

Supervisor
Dr. Mohammed Khair Hourani, prof.

This Thesis was Submitted in Partial Fulfillment of the Requirements for the Master's Degree in Chemistry

Faculty of Graduate Studies
The University of Jordan

July, 2011

COMMITTEE DECISION

This Thesis (Preparation and characterization of gold, copper, and silver nanoparticles electrochemically deposited by application of a square wave potential regime) was successfully Defended and Approved on 20/7/2011.

Examination Committee	Signature
Dr. Mohammed Khair Hourani, Chairman *Prof. of Analytical Chemistry*	Moh'd Hourani
Dr. Mahmoud Alawi, Member *Prof. of Analytical Chemistry and Environmental analysis*	
Dr. Ehab Al-Shamaileh, Member Associ. Prof. of physical Chemistry	Ehab Alshamaileh
Dr. Imad Hamadneh, Member Assist. Prof. of Materials Chemistry	
Dr. Ayman Issa, Member *Associ Prof. of Analytical Chemistry (Hashemite University)*	

DEDICATION

I dedicate this thesis to the candles that always lighten my life, my father and mother.

ACKNOWLEDGEMENT

Foremost, all thanks, obedience and appreciations to Allah for granting me this Success.

There are many people I would like to acknowledge whom contributed to the completion of my Master degree. First I would like to thank my parents for the love and enormous support they have provided throughout my entire life. You have been there for every decision I have made and help my dreams become reality. I hope I make you proud.
Second, I would like to thank my precious teacher Prof. Mohammed Hourani. Thank you for your inspiration, wisdom, supervision, and encouragement. Third, I would like to thank the members of the defense committee, Prof. Mahmoud Alawi, Dr. Ehab Al-Shamaileh, Dr. Imad Hamadneh and Dr. Ayman Issa, for their valuable suggestions, guidance, and comments. Finally, I would like to thank all Chemistry department staff.

LIST OF CONTENTS

LIST OF TABLES

LIST OF FIGURES

LIST OF ABBREVIATIONS

AE	Auxiliary Electrode
AR	Analytical reagent
CRT	Cathode ray tube
CV	Cyclic Voltammetry
EDX	Energy dispersive X-ray spectroscopy
EDS	Energy dispersive spectroscopy
GPIB	General Purpose Interface Bus
NT	Nanotechnology
PED	Pulse electrodeposition
PVA	Poly vinyl alcohol
RE	Reference Electrode
tr	Rest time
SEM	Scanning Electron Microscope
SMDE	Stationary mercury drop electrode
WR	Working Electrode
XRD	X-ray Diffraction

PREPARATION AND CHARACTERIZATION OF GOLD, COPPER AND SILVER NANOPARTICLES ELECTROCHEMICALLY DEPOSITED BY APPLICATION OF A SQUARE WAVE POTENTIAL REGIME

By
Wael Mohammad Mahmoud

Supervisor
Dr. Mohammed K. Hourani, Prof.

ABSTRACT

In the present study, we have prepared of nanostructure from the metals gold, copper and silver by applied square wave potential regime on tantalum wire electrodes. First we prepared 1.9×10^{-3} M gold stock solution by dissolving a calculated volume of chloroauric acid ($HAuCl_4$) in acidic media. Next we diluted to three different concentrations (10^{-2}, 10^{-3} and 10^{-4}) M. Then we adjusted the method parameters to the suitable values for gold nanometallic deposition. The main structural nanogold and microgold obtained was nanoparticles, epitaxial growth, needles, flower, co-flower, twinned, grain boundary, thorn and microcrystal.

For the silver, we prepared its three solutions from silver perchlorate hydrate ($AgCl_4.XH_2O$) of (10^{-2}, 10^{-3} and 10^{-4}) M in acidic media. Nanoparticles, spongy, microcrystal, dendrites, plates, nanoagglomeration and flower structures were formed.

Copper nanometallic structures were prepared in acidic and basic media on a copper and tantalum wire electrodes from copper (II) perchlorate hexahydrate Cu $(ClO_4)_2.6H_2O$ of (10^{-2}, 10^{-3} and 10^{-4}) M. The main nanostructured copper surface and microcopper obtained in basic media were needles, nanoparticles, nanorodes, nanofibers, spongy, plates, grain boundary, grain, plam leave-like and microcrystal CuO.

Nanoparticles, nanorodes, spongy, ear grain-like, nanofibers, coccolith, tree-like, flower and microcrystals were formed in acidic media.

The concentration, amplitude, the frequency, time and the low and high value affected the size, distribution and the shape of the nanometallic structures. The developed gold, silver and copper nanostructures were characterized by cyclic voltammetry, SEM and EDX.

1-INTRODUCTION

1.1. Nanotechnology:

Nanotechnology (NT) is the production and use of materials with purposely engineered features close to the atomic or molecular scale. NT deals with putting things together atom by- atom and with structures so small they are invisible to the naked eye. It provides the ability to create materials, devices and systems with fundamentally new functions and properties.

The promise of NT is enormous. It has implications for almost every type of manufacturing process and product. Potential NT applications in the next few decades could produce huge increases in computer speed and storage capacity, therapies for several different types of cancer, much more efficient lighting and battery storage, a major reduction in the cost of desalinating water, clothes that never stain and glass that never needs cleaning. While the benefits are almost limitless, they will be realized only if the potential adverse effects of NT are examined and managed (**J. Clarence (Terry) Davies).**

1.1. a. Nanomaterials:

Nanomaterials with wide applications in a variety of areas because of the unusual, and the size of Depends on the optical properties and magnetic, electronic and chemical.

Nanomaterials are from the surface of a very large proportion of the size and characteristics are determined mainly by the behavior of the surface. It is well known applications of nanotechnology in the areas of cosmetics and pharmaceutical products, paint, electronics, and polishing, semiconductors and catalysis, the design and development of novel nanomaterials with tunable physical and chemical properties region continues to grow.

1.1. b. Nanoparticles of gold:

Synthesis of metal nanoparticles Synthesis of metal nanoparticles by the transition of a different size and Forms attracted significant interest in the recent past due to its unique properties of electronic and visual stimulus. Gold nanoparticles received special attention because of this wonderful visual and catalytic.

It is generally recognized that the properties of metal nano-heavily dependent on the size and shape and morphology. For example , the anisotropic gold nanoparticles two distinct surface plasmon bands corresponding to the browser and linear absorption. Aspect ratio nanostructure controls the intensity and position of longitudinal bands.

1.1. c. Nanoparticles of silver:

Silver has used widely in a variety of applications such as catalysis, electronics, photonics and photography because of have unique properties. For example, silver has the highest electrical conductivity, thermal conductivity and reflectivity of all metals. Accordingly, it has been exploited widely in silver a variety of applications such as catalysis, through electronics and photonics and photography. Morphology influences not only the intrinsic chemical, optical, and catalytic properties of nanoscale metal crystals, but also their relevant applications in electronic, plasmonic and sensing fields. As one of the member of noble metallic nanomaterials family, nanoparticles can be used in antibacterial, cryogenic superconducting materials, bio-label materials, and optical materials. Because of its intrinsic shape-dependent properties and resulting application, the control of the morphology of silver nanoparticles has been a primary focus. Silver nanoparticles in particular, are in demand with the emergence of Ag-impregnated materials in consumer goods, textiles, and food processing, all attributed to their antimicrobial properties.

1.1. d. Nanoparticles of copper:

High conductivity and low cost make the copper material is a promising substitute compared with gold and silver. Moreover, copper nanowires may play a key role in linking the next generation of electronic nanodevices. Particularly copper nanoparticles, has received considerable attention because of their ability in the use of lubrication nanomaterials, thermal applications, nanofluids and catalysts. Reaction conditions are affected of the size, shape and structure of metallic copper nanoparticles.

Has developed several methods for the preparation of copper nano-technology, such as the reduction of sonochemical, reduction of chemical and techniques for microemulsion. Chemical reduction method is the most commonly used on large-scale. Synthesis copper nanoparticles stable, monodisperse, uniformly shaped the proven difficult. In addition, copper nanoparticles tend to assemble during the synthesis. Polymers, surfactants, ligands can be used to achieve stability in aqueous media, and to prevent combine to produce extremely stable, nano-
well dispersed metal.

1.2. Scanning electron microscopy:

The scanning electron microscope (SEM) is a microscope that uses electrons instead of light to obtain an image with higher magnification and better resolution than the optical microscopes. Since their development in the early 1950's, scanning electron microscopes have opened a new era of studies in the medical and physical science communities.

Theory:

In light microscopy, a specimen is viewed through a series of lenses that magnify the visible-light image. However, the scanning electron microscope (SEM) does not actually view a true image of the specimen, but rather produces an electronic map of the specimen that is displayed on a cathode ray tube (CRT).

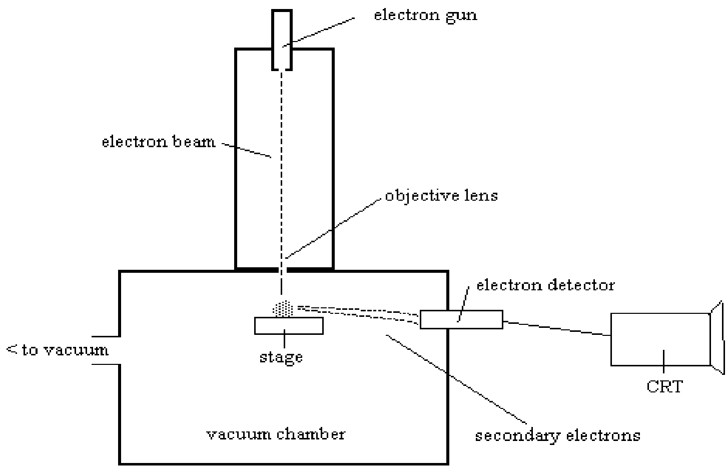


Figure 1: shows scanning electron microscopy.

The figure (1) above shows a schematic for a generic SEM. Electrons from a filament in an electron gun is beamed at the specimen in a vacuum chamber. The beam forms a line that continuously sweeps across the specimen at high speed. This beam irradiates the specimen which in turn produces a signal in the form of either x-ray fluorescence, secondary or backscattered electrons.

The SEM has a secondary electron detector. The signal produced by the secondary electrons is detected and sent to a CRT image. The scan rate for the electron beam can be increased so that a virtual 3-D image of the specimen can be viewed. The image can also be captured by standard photography.

By changing the width (w) of the electron beam, the magnification (M) can be changed where

$$M = \frac{W}{w}$$

And W is the width of the CRT. Since W is constant, the magnification can be increased by decreasing w.

1.3. Energy-dispersive X-ray spectroscopy (EDX):

Energy-dispersive X-ray spectroscopy (EDS or EDX) is an analytical technique used for the elemental analysis or chemical characterization of a sample. It is one of the variants of X-ray fluorescence spectroscopy which relies on the investigation of a sample through interactions between electromagnetic radiation and matter, analyzing X-rays emitted by the matter in response to being hit with charged particles. Its characterization capabilities are due in large part to the fundamental principle that each element has a unique atomic structure allowing X-rays that are characteristic of an element's atomic structure to be identified uniquely from one another.

To stimulate the emission of characteristic X-rays from a specimen, a high-energy beam of charged particles such as electrons or protons, or a beam of X-rays, is focused into the sample being studied. At rest, an atom within the sample contains ground state (or unexcited) electrons in discrete energy levels or electron shells bound to the nucleus. The incident beam may excite an electron in an inner shell, ejecting it from the shell while creating an electron hole where the electron was. An electron from an outer, higher-energy shell then fills the hole, and the difference in energy between the higher-energy shell and the lower energy shell may be released in the form of an X-ray. The number and energy of the X-rays emitted from a specimen can be measured by an energy-dispersive spectrometer. As the energy of the X-rays is characteristic of the difference in energy between the two shells, and of the atomic structure of the element from which they were emitted, this allows the elemental composition of the specimen to be measured.

1.4. Preparation of copper electrode:

The electrochemical behavior of copper in alkaline solution has been investigated by many workers. Two principle oxidation steps were suggested, (a) formation of Cu_2O, (b) formation of Cu $(OH)_2$ at room temperature or CuO at higher temperatures and a third step involving the formation Of Cu (III) oxide was postulated.

The nine peaks on the voltammogram shows figure (2) were analyzed and labeled as follows:

Anodic oxidation:

Ambrose et al studied the Cu-electrode in 1 M KOH and heir results can be summarized in the following chemical reaction:

Pre-peak (1): assigned to the formation of soluble species according

$$Cu + 2OH^- \longrightarrow Cu(OH)_2 + 2e^-$$

Peak (2): due to the formation of Cu_2O according to

$$2Cu + 2OH^- \longrightarrow Cu_2O + H_2O + 2e^-$$

Peak (3):

$$Cu_2O + 6OH^- + H_2O \longrightarrow 2Cu(OH)_4^{-2} + 2e^- \text{ initially}$$

$$Cu + 4OH^- \longrightarrow Cu(OH)_4^{-2} + 2e^- \text{ main reaction}$$

Peak (4):

$$Cu + 2OH^- \longrightarrow Cu(OH)_2 + 2e^-$$

and / or

$$Cu + 2OH^- \longrightarrow CuO + H_2 + 2e^-$$

Peak (5):

$$Cu(OH)_2 + 2OH^- \longrightarrow Cu(OH)_4^- + e^-$$

and / or

$$CuO + H_2O + 2OH^- \longrightarrow Cu(OH)_4^- + e^-$$

Cathodic reaction:

Peak (6): reverse of reactions occurring at peak 5.

Peak (7):

$$2Cu(OH)_4^{-2} + 2e^- \longrightarrow Cu_2O + 6OH^- + H_2O$$

Peak (8):

$$Cu_2O + H_2O + 2e^- \longrightarrow 2Cu + 2OH^-$$

For anodic excursions as far as peak 3.

Peak (9): no conclusion can be reached. The reactions are complex and the peak is probably due to more than one surface reaction.

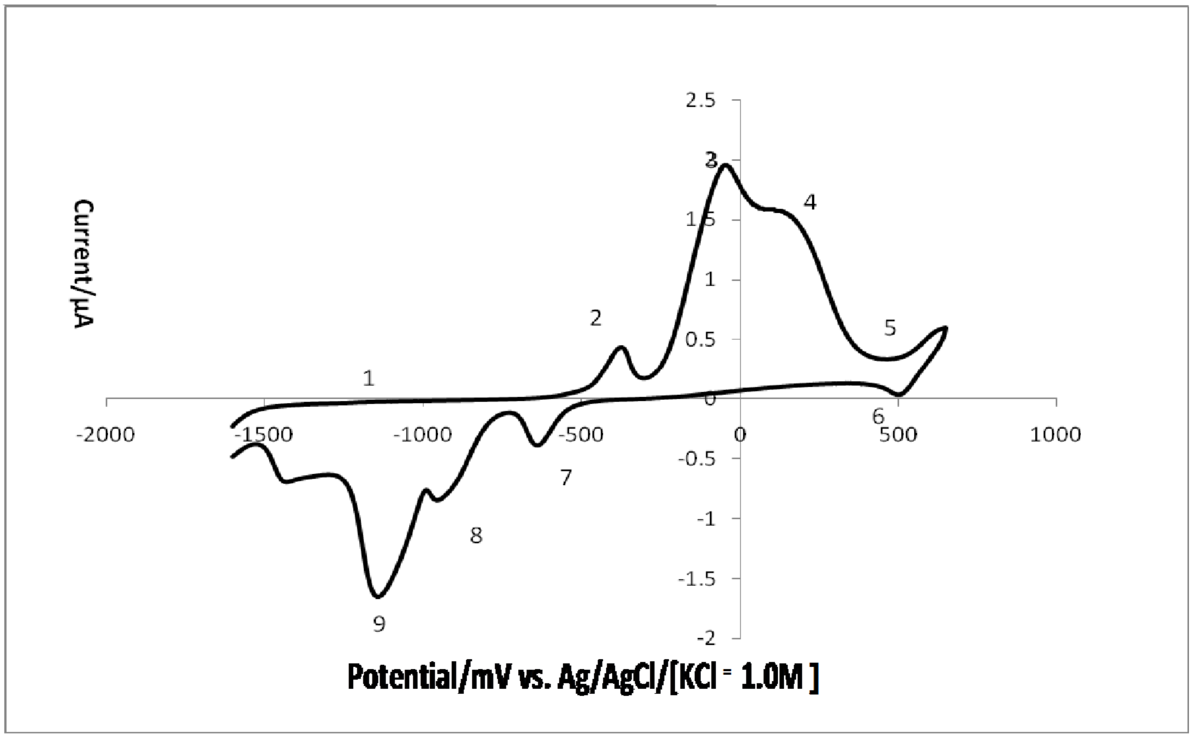


Figure 2: The cyclic voltammogram of polycrystalline copper electrodes in 1 M KOH recorded at a scan rate of 100 mV/ s.

1.5. Square wave potential regime:

Square wave amplitude means the difference between the Hi and Lo limits of the square wave. From the practical point of view, changing the amplitude of the square wave also changes the limits of the square wave, Hi and Lo values. Changing these values may shift the balance between oxidation and reduction during each cycle of the square wave. It may also affect the rates of nucleation and particle growth for the deposited particles. Figure (3) shows a scheme of square wave potential regime, the square wave amplitude 0.4 V at central any potential for example the potential central -0.2 V with square wave amplitude 0.4 V, the E_H = 0.00 V and E_L = -0.4 V values.

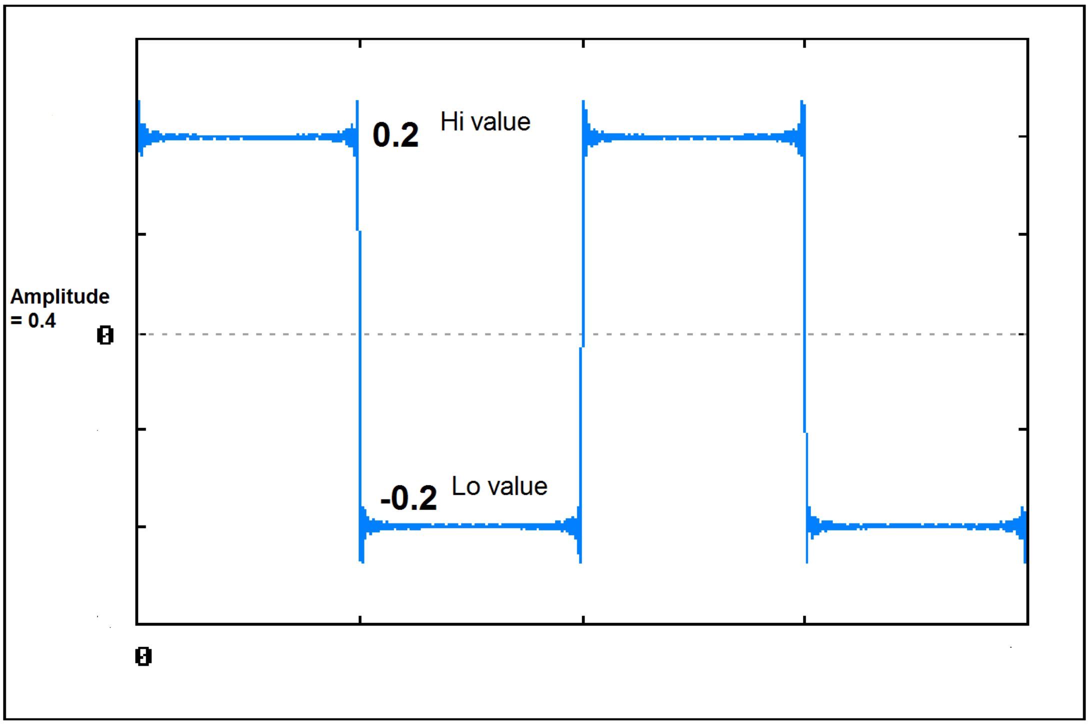


Figure 3: scheme of square wave potential regime.

1.6. Previous application of square wave to metallic surfaces:

Gold nanoparticles prepared by application square wave potential regime and their electroanalytical and electrocatalytic application. (Hamdan and Hourani, 2010).

A square wave potential regime was applied by Hourani and Wieckowski (1990) to prepare preferentially oriented (100) and (111) polycrystalline platinum electrodes. The faceted surfaces were then used for electrohydrogenation of ethylene. Reaction rates and mechanisms of electrohydrogenation of ethylene in aqueous solutions at the above-mentioned electrodes were proposed. This microengineering of surfaces by application of a square wave attests to the fact that cyclization of potential induces significant structural effects on surfaces by alternation of deposition and stripping of atoms (Hourani and Wieckowski, 1990).

A Ni/TiO2 nanocomposite was successfully prepared by a pulse electro-deposition (PED) technique. Highly ordered TiO_2 nanotube arrays fabricated by anodization were employed as a substrate and loaded with Ni nanoparticles by PED. The influence of pulse electrodeposition parameters was investigated on the morphology of nickel electrodeposits. The nanocomposite was characterized by field emission scanning electron microscopy (FESEM) and X-ray diffraction (XRD). Where they used pulse electro- deposition parameters on the morphology of Ni electrodeposition. (Yunhuai, Z. et al, 2009).

Synthesis of Fe‑Cr alloy nanoparticles by using a method which couples electrodeposition of metals with the employment of high power ultrasound. The production of alloyed nanoparticles was performed using a 20 kHz titanium alloy horn ultrasound generator, a “sonoelectrode” generating short current pulses (t_{ON}) triggered and followed immediately by ultrasonic pulses (t_{US}). A rest time (t_r) restores the initial conditions close to the sonoelectrode. The final product is a suspension of nanoparticles with high purity and high surface/volume ratio, which could be controlled by varying process parameters like time management and current density. (Yunhuai, Z. et al, 2009). Valentine, Z. and Manuele, D. (2009).

Electrodeposition of bismuth telluride films was carried out using pulsed method in order to improve morphology and electrode supply. A voltammetric study allowed determining the cathodic electrochemical behavior of the electrolyte and to establish the optimal deposition potential, which is around −250mV. The determination of the nucleation mode, obtained by potential step experiments, underlined a 3D instantaneous nucleation, although there are some derivations following the potential value. (Diliberto, S.etal, 2007).

Electrochemical interfaces provide fundamental advantages for the preparation of low-dimensional structures on metal and semiconducting substrates without irreversible modifications induced by the preparation process. Delocalized, and in particular localized electrodeposition using a scanning probe microscope tip as a nanoelectrode, allow a solely electrochemical bottom-up growth of nanostructures under defined nucleation and growth conditions. (Schindler, W.et al, 2005).

New galvanic technique was used to prepare tin nanoaggregates on insulating substrate by electrodeposition. The technique defined the electrodeposition operating conditions which correspond to a narrow window of parameters, and it helps to understand the activation prosperities of gold particles which had been used as nucleation sites (Devers, et al., 2003).

Cu_2S nanoparticles were electrosynthesized by cyclic voltammetry in the presence of polyvinylalcohol (PVA) as stabilizer. The studied the structures and nature of the products. (Fotouhi, L. and Rezaei, M., 2009).

1.7. Cyclic Voltammetry:

Cyclic voltammetry was first reported in 1938 and described theoretically in 1948 by Randalls Sevcik, Nicholson, Shain, Saveant and Viannelo. Those authors were able to develop the basis for understanding of the I-E cyclic voltammetric curves. (Nicholson, 1965 ; Christensen and Hamnett, 1994).

Cyclic voltammetry is the most widely used technique for acquiring qualitative information about electrochemical reaction, and it's the first experiment performed in an electroanalytical study. It offers a rapid detection of electroactive species, and convenient evaluation of the effect of media on the redox process (wang, 2006).

Cyclic voltammetry (CV) is perhaps the most versatile electroanalytical technique for the study of electroactive species and surface electrochemical investigations (Kounaves, 1997). Its versatility and the ease of measurements have resulted in extensive use of cyclic voltammetry in the fields of electrochemistry, inorganic chemistry, organic chemistry, and biochemistry. (Sawyer et al., 1984, Alper et al., 2004).

The power of cyclic voltammetry results from its ability to rapidly provide considerable information about the thermodynamics and reversibility of redox processes, the kinetics of heterogeneous electron transfer reactions and on coupled chemical reactions or adsorption (Holze, 2009).

The CV technique is usually the first experiment performed by an electro-chemist for exploration of the presence of electroactive species in solution or at the electrode surface. Indeed it is a fundamental tool for diagnostic studies that provide qualitative information about electrochemical processes under various conditions. (Brad and Faulkner, 1980; Skoog et al., 1998; Wang, 2000).

The Potentiostat controls the potential and measures the current in a three -electrode electrochemical cell like the one shown in Figure 4, and the response is the cyclic voltammogram shown in Figure 4. (Gosser, 1993; Wang 2000).

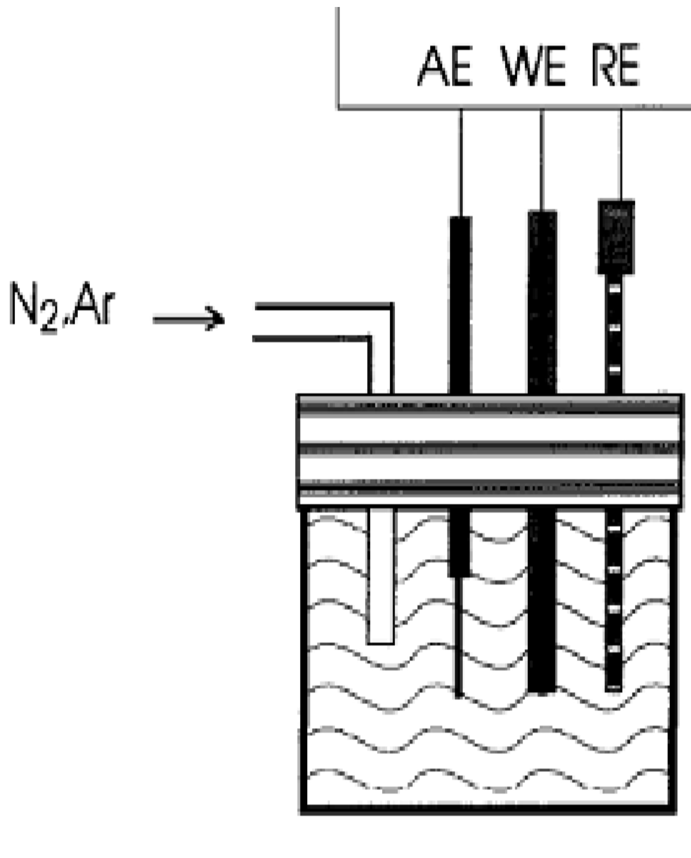


Figure 4: Overview of the cyclic voltammetry experiment, where AE is the auxiliary electrode RE is the reference electrode and WE is the working electrode. (Gosser, 1993).

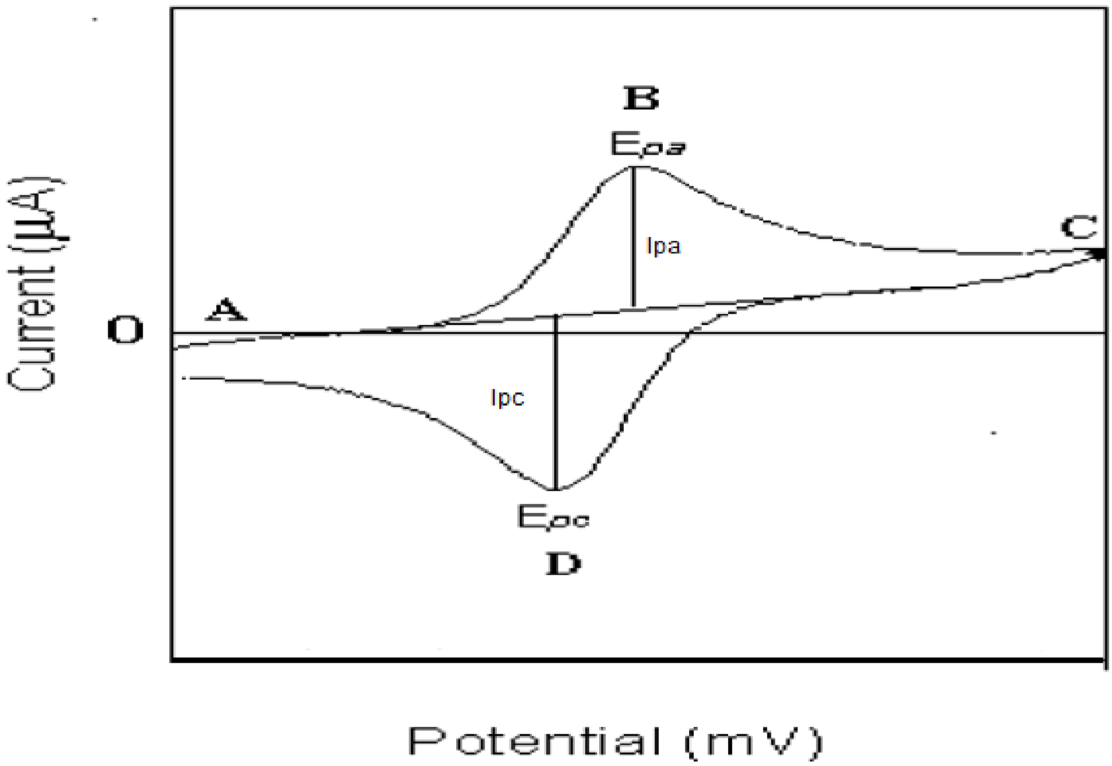


Figure 5: Cyclic voltammogram for a reversible system.

i_{pc}: peak of cathodic current; i_{pa} : peak of anodic current .

Cyclic voltammetry can also be used for surface characterization. The peak potential, multiplicities, relative intensities, and sharpness are indicators for the electronic state of the surface and their crystallographic orientations. Figure 5 illustrates the shape of a cyclic voltammogram with an electrode of fixed area. The voltammogram is characterized by a peak potential E_p, at which the current reaches a maximum value and by the value of the current i_p (Sawyer, et al., 1995).

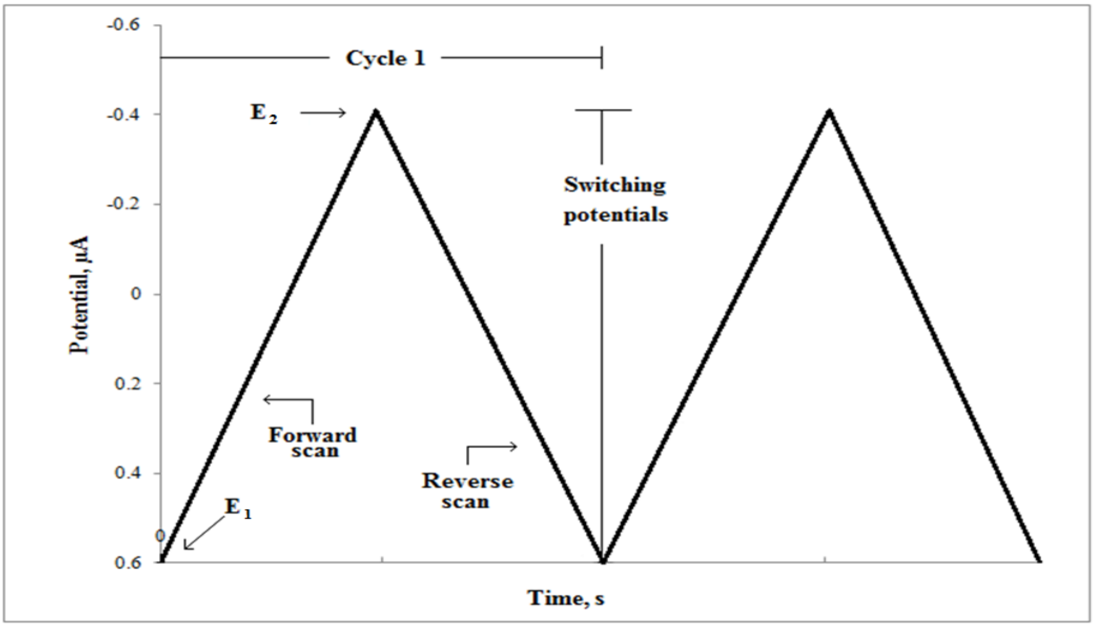


Figure 6: Potential-time excitation signal in cyclic voltammetric experiment

Cyclic voltammetry is an extension of linear sweep voltammetry with the potential applied is varied linearly between potentials E_1 and E_2, being a potential more positive (for oxidation) or negative (for reduction**)** than the peak maximum observed for the oxidation/reduction reaction concerned. At E_2 the voltage scan is reversed back to E_1 (Westbroek, *et al.*, 2005).

The power of cyclic voltammetry results from its ability to rapidly provide considerable information on the thermodynamics and reversibility of redox processes, the kinetics of heterogeneous electron transfer reactions and on coupled chemical reactions or adsorption processes (Holze, 2009).

1.8. Application of square wave:

By the application of an electrochemical regime to a solution containing of a nitrite, nitrate, and hydrazine leads to exhaustive oxidation/ reduction of these compounds. (Hourani, M., and waleed, B. (2010)).

The exploitation of an electrochemical perturbation for the destruction of a sulfur-containing organic compound to produced harmless inorganic has been investigated. It has been proved that application of an electrochemical perturbation could be used for desulfurization of sulfur compound. (Hourani, M., 1993).

(100) and (111) preferentially oriented platinum electrodes were obtained electrochemical surface orientation. These surfaces, along with polycrystalline and ordered single crystal Pt electrodes, were used to study rates and mechanisms of electrohydrogenation of ethylene in aqueous solutions. The Pt(100) preferentially oriented electrode was the most active of the surfaces which were examined with respect to the system kinetics, and an enhancement of 70% between Pt(111) and Pt(100) preferentially oriented surfaces was found. While the catalytic enhancement effects were not very high, they were distinctive and encouraging enough to conclude that further research with electrochemically oriented surfaces is worth pursuing. (Wieckowski, A. and Hourani, M, 1989).

Preparation of metallic and bimetallic of nanoaggregate electrodes by application of square wave potential regime and their electroanalytical and electrocatalytic applications. (Hourani, M., and Hamdan, T., 2010).

1.9. Importance and Objectives of the present work

The present work derives its importance of nanotechnology and its wide applications:

The present study aims at the following objectives:

1-Preparation of nanoparticles by electrodeposition using a square wave potential regime.

2- Investigation of the effect of experimental conditions on the size and the properties of the produced particles.

3-Characterization of the obtained particles by investigation of their cyclic voltammetric behavior and utilizing scanning electron microscopy, energy dispersive X-ray microscopy and other techniques.

2-EXPERIMENTAL

2.1- Instruments:

A Potentiostat (A 273 Princeton Applied Research) interfaced to a computer through GPIB interface along with Echem® software is used for electronic control, cyclic voltammetry and liner scan experiments.

The square wave with the chosen high and low values was generated from a function generator (Simpson, A 420) and was fed to the potentiostat at the external input. The desired lower and higher limits of square wave value were obtained by adjusting the applied potential.

The frequency of the square wave was also varied between 10 and 1 kHz to explore the influence of variation of frequency on the formed particles. The new electrode surface was investigated after deposition by cyclic voltammetry and SEM.

Optimal conditions for preparation of the gold, silver and copper nanostructures were explored, and then the nanostructured electrodes were investigated after deposition by cyclic voltammetry, SEM and EDX. All of the experiments were performed at ambient temperatures.

2.2. Cell and Electrodes:

A conventional H- shape three-electrode cell was used for cyclic voltammetric measurements, these are working electrode, reference electrode and a platinum auxiliary electrode. The electrochemical cell was equipped with a multiple inlet system for admission of supporting electrolyte, purging and blanketing the solution with oxygen-free nitrogen (Figure 7). The reference electrode was an Ag/AgCl/ [KCl 1.0M] and all the potentials reported in this thesis are referenced to this electrode. The working electrode was a 1.0 mm diameter tantalum electrode (99.99% pure, Johnson Matthy, U.S.A).

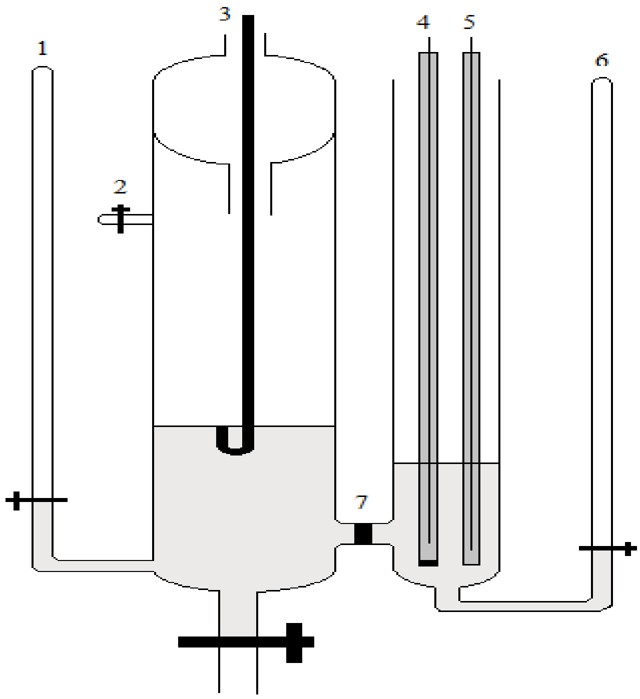


Figure 7: Three electrode cell setup

1: Purging inlet, 2: Blanketing inlet, 3: Working electrode, 4: Reference electrode, 5: Auxiliary electrode, 6: Purging inlet, 7: Fine frit

2.3. Materials:

All reagents used were highly pure certified analytical reagent (A.R.) chemicals and used as received from the suppliers without further purification. The working electrode was made of tantalum and the auxiliary electrode as made of platinum (Johnson Matthy, 99.99% purity).

The purging nitrogen was supplied by the National Gas Company and coupled with Oxisorb® cartridge (Suplico) to remove traces of oxygen. All experiments were carried out in deoxygenated aqueous solutions.

All solutions were made from the above mentioned reagents dissolved in triply distilled water where the second distillation was carried out from basic potassium permanganate solution to get rid of any traces of organic impurities. All glassware used in this work were cleaned with chromic acid solution and washed with triply distilled water.

2.4. The deposition cell:

Another cell was used for electrodeposition of gold, silver or copper nanostructures at the tantalum surface. The cell was the SMDE electrode where the electronics of the SMDE were bypassed and the electrodes were connected directly to the potentiostat.



Figure 8: The deposition cell.

2.5. Procedures

2.5.1. Surface pretreatment

Surfaces are never clean which demands a special pretreatment to obtain the clean surface. Almost every metal has its own special procedure for cleaning.

A. Preparation tantalum electrode

The electrode surface was mechanically polished, with alumina powder to obtain a smooth surface. The electrode surface was then chemically polished in a solution of 5:2:2 (v/v/v) 98% H_2SO_4, 65% HNO_3 and 48% HF .followed by immersion in 48% HF For a few minutes and finally rinsed with triply distilled water . After this pretreatment of the metal surface was ready for electrodeposition.

A.1. Cyclic voltammogram of polycrystalline Tantalum electrode

Figure 9, shows a typical voltammogram of tantalum in 0.5 M H_2SO_4. The first voltammetric cycle shows the commencement of oxidation of tantalum at about -450 mV. The oxidation potential peak at -200 mV then assumes a constant value after that. On the second cycle, the oxidation threshold starts at a much more positive potential (+400 mV) because tantalum electrode changes from tantalum to tantalum oxide surface.

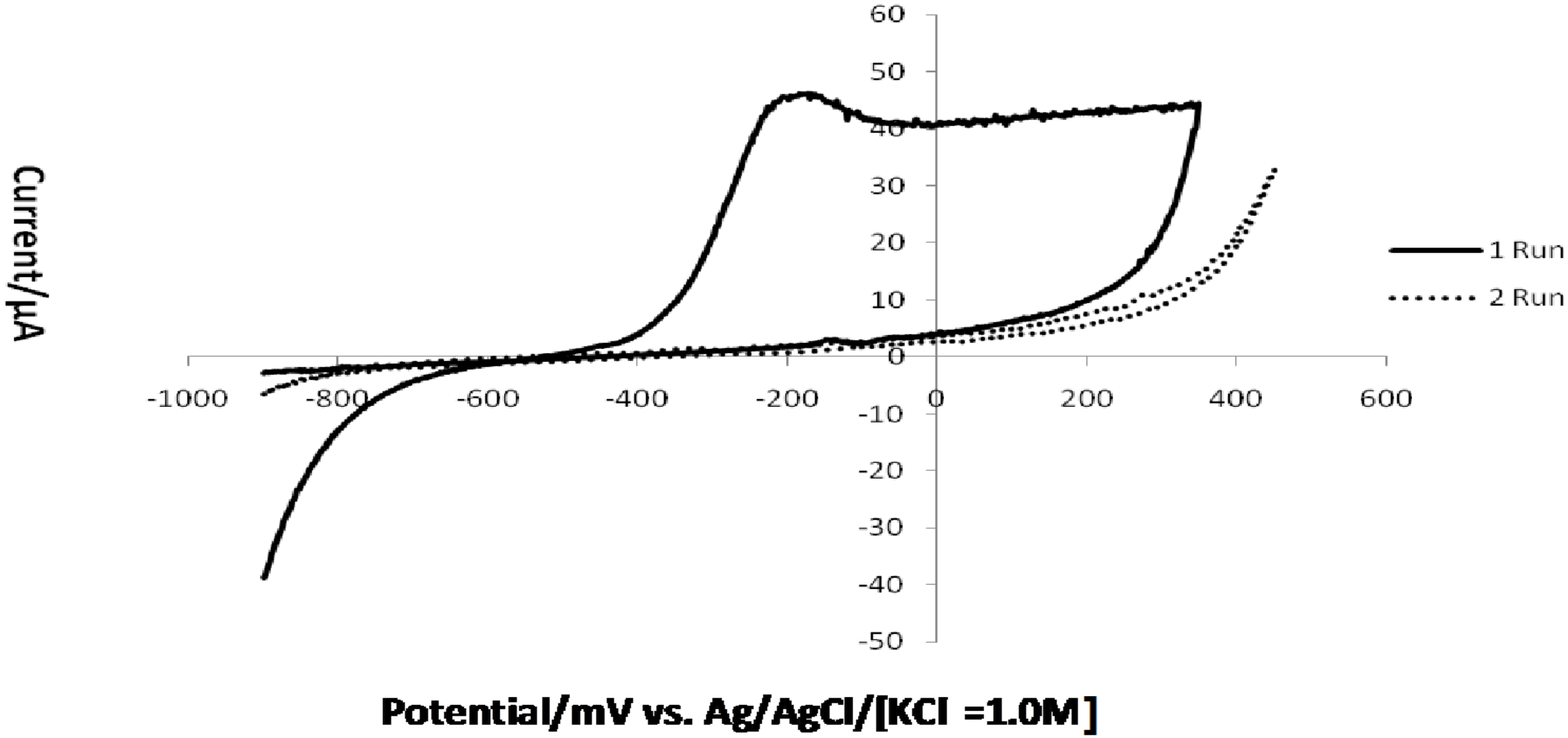


Figure 9: The voltammogram of polycrystalline tantalum electrode in 0.5 M H_2SO_4 recorded at a scan rate 100 mV/ s.

A.2. The voltammogram of the hydrogen region of Tantalum electrode

The electrode was conditioned by cycling the potential for in the hydrogen region only to ensure the identity of the electrode surface tantalum metal or more clearly, oxygen free tantalum surface. Tantalum the oxidation threshold potential was never exceeded to avoid oxide formation.

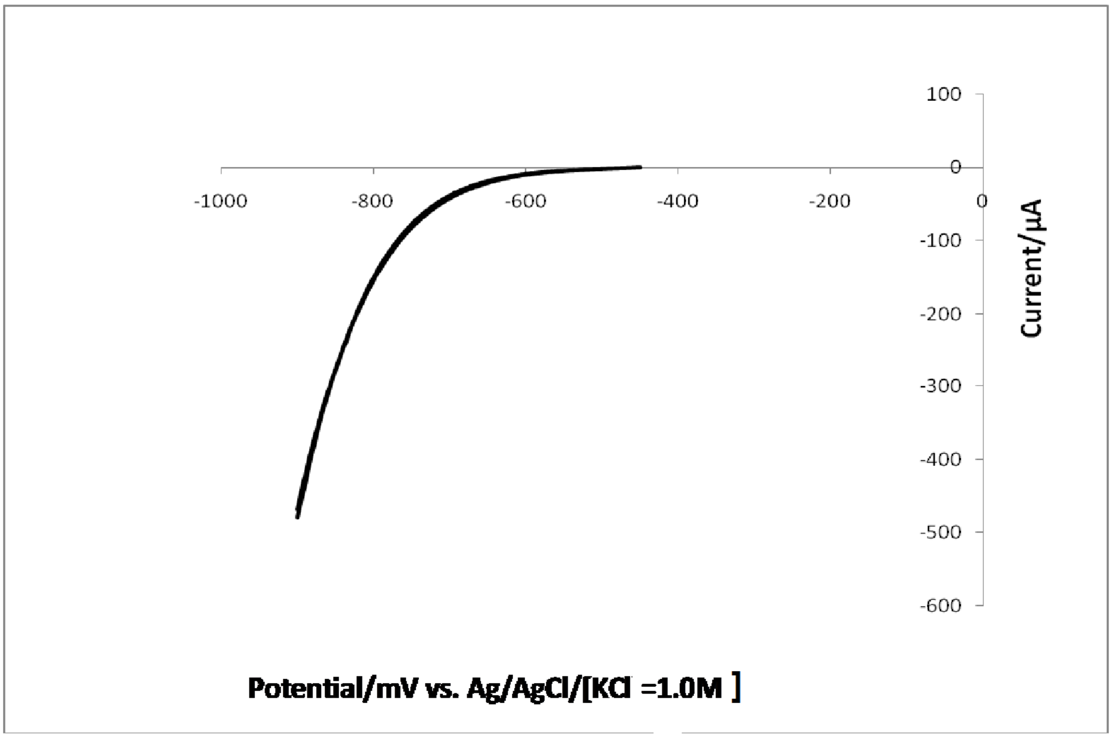


Figure 10: The voltammogram of polycrystalline showing the hydrogen evolution tantalum electrode in 0.5 H_2SO_4 M recorded at a scan rate 100 mV/ s.

B- Preparation of copper Electrode

Initially, copper surface was polished by alumina powder, and then the metal surface was chemically etched in 20% HNO_3 for 5 seconds and rinsed with triply distilled water. Then the electrode was mounted in the cell that contained a purged 0.5 mol L^{-1} H_2SO_4 or 1 mol L^{-1} KOH. The I-E potentiodynamic curve was recorded and taken as a criterion for surface cleanliness for further work or investigations.

B.1. Cyclic voltammogram of polycrystalline Cu (II) electrode in acidic media

The electrode was conditioned by cycling the potential between the hydrogen evolution and oxygen evolution limits (-1.2and 0. 5 V) until the regular voltammogram of polycrystalline cupper was produced in acidic media as shown in Figure 11.

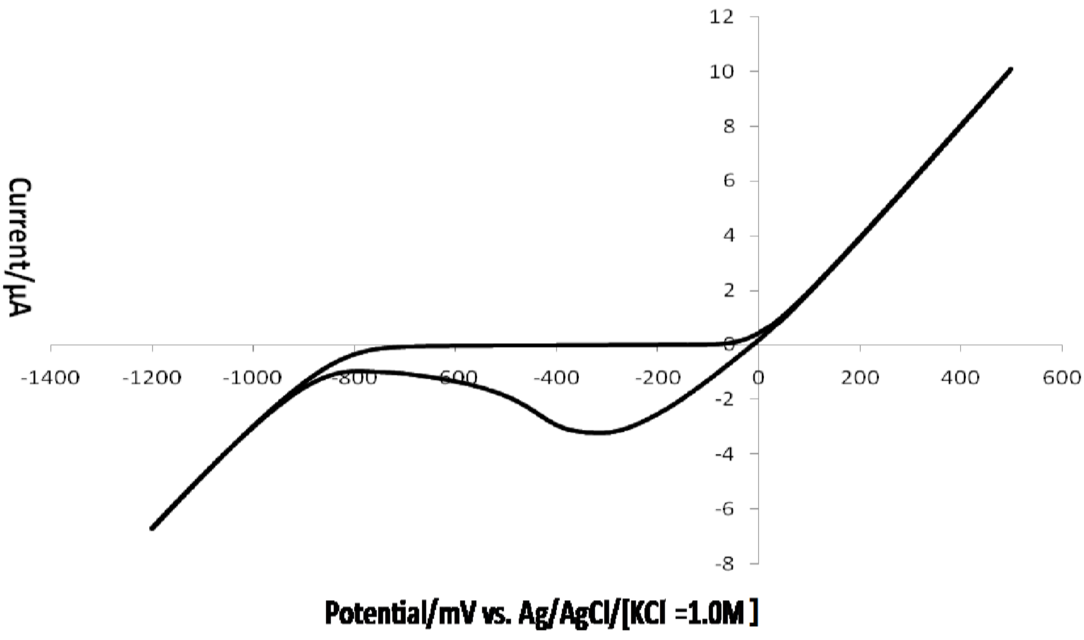


Figure 11: The voltammogram of polycrystalline Cu electrode in 0.5 M H_2SO_4 recorded at a scan rate of 100 mV/ s.

B.2. Cyclic voltammogram of polycrystalline Cu (II) electrode in basic media

The electrode was conditioned by cycling the potential between the hydrogen evolution and oxygen evolution limits (-1.7and 0. 55 V) until the regular voltammogram of polycrystalline copper electrode was reproduced in basic medium (Figure 12).

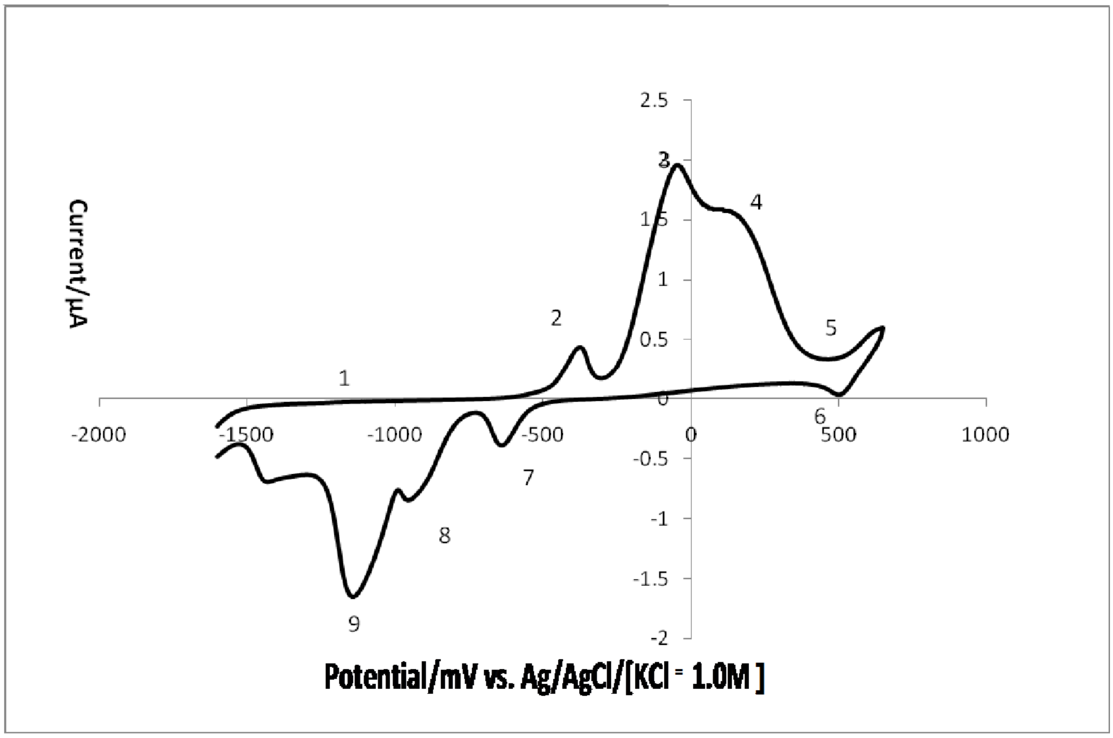


Figure 12: The cyclic voltammogram of polycrystalline copper electrodes in 1 M KOH recorded at a scan rate of 100 mV/ s.

C- Silver electrode:

Initially, silver surface was mechanically polished by alumina powder, and then the metal surface was treated with formic acid, citric acid and sodium thiosulfate respectively. The electrode was conditioned by cycling the potential between the hydrogen evolution and oxygen evolution limits (-0.55 and 0.25 V) until the regular voltammogram of polycrystalline silver electrode was reproduced in acidic medium figure (13).

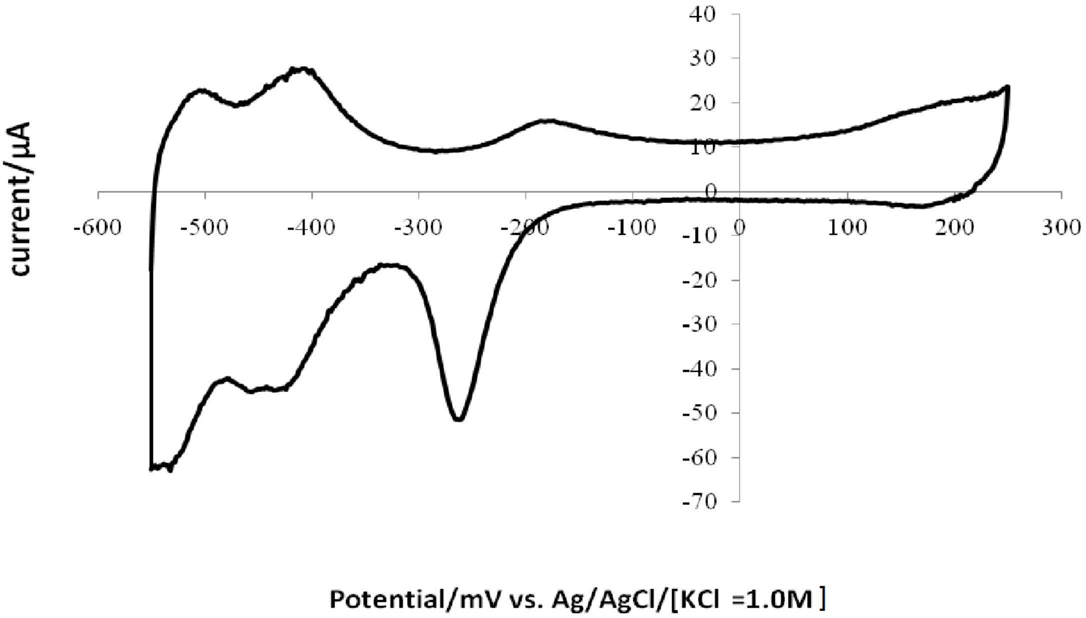


Figure13: Cyclic voltammogram of polycrystalline Ag electrodes in 0.5 M H_2SO_4 recorded at a scan rate of 100 mV/ s.

2.5.2. Preparation of solutions used in the preparation of nanometallic structures

2.5.2.1. Gold:

A gold stock solution 1.9 × 10^{-3} M was prepared by dissolving gold metal in aqua regia. Then from the stock solution, three more concentrations (10^{-2}, 10^{-3}, and 10^{-4}) M were prepared in 0.5 M sulfuric acid.

2.5.2.2. Silver:

Silver solutions were prepared from silver perchlorate hydrate $AgClO_4$. X H_2O Three concentrations (10^{-2}, 10^{-3}, and 10^{-4}) M Ag^+ in 0.5 M H_2SO_4 were prepared.

2.5.2.3. Copper:

Copper solutions were prepared from copper (II) perchlorate hexahydrate ($Cu(ClO_4)_2.6H_2O$). Initially a stock solution was prepared from which (10^{-2}, 10^{-3}, and10^{-4}) M Cu^{+2} solutions in 0.5 M H_2SO_4 were prepared.

3- Results and Discussion

3.1. Gold nanostructures

3.1.1. The effect of Hi and Lo limits of the square wave on the deposited nanoparticles

Figure 14 shows two I-E curves for two nanostructured deposited particles. The first was produced by application of 0.4 V amplitude square waves while the other was produced by application of a 1.0 V amplitude square wave. The first conclusion that can be made from investigation of these voltammograms is that these voltammograms are identical with the well-known voltammetric features of gold electrodes which positively prove the identity of the gold nanoparticles.

Further investigation of the I-E curves shown in figure 14 demonstrates that the voltammetric features are enhanced for the electrode produced by application of 1.0 V square wave amplitude compared to that produced by application of a 0.4 V – amplitude square wave. The charge under oxygen stripping peak was taken as a quantitative measure of the total surface area of the deposited gold on tantalum surface. This concept relies on the fact that the voltammetric features are dependent on the surface area of the electrode.

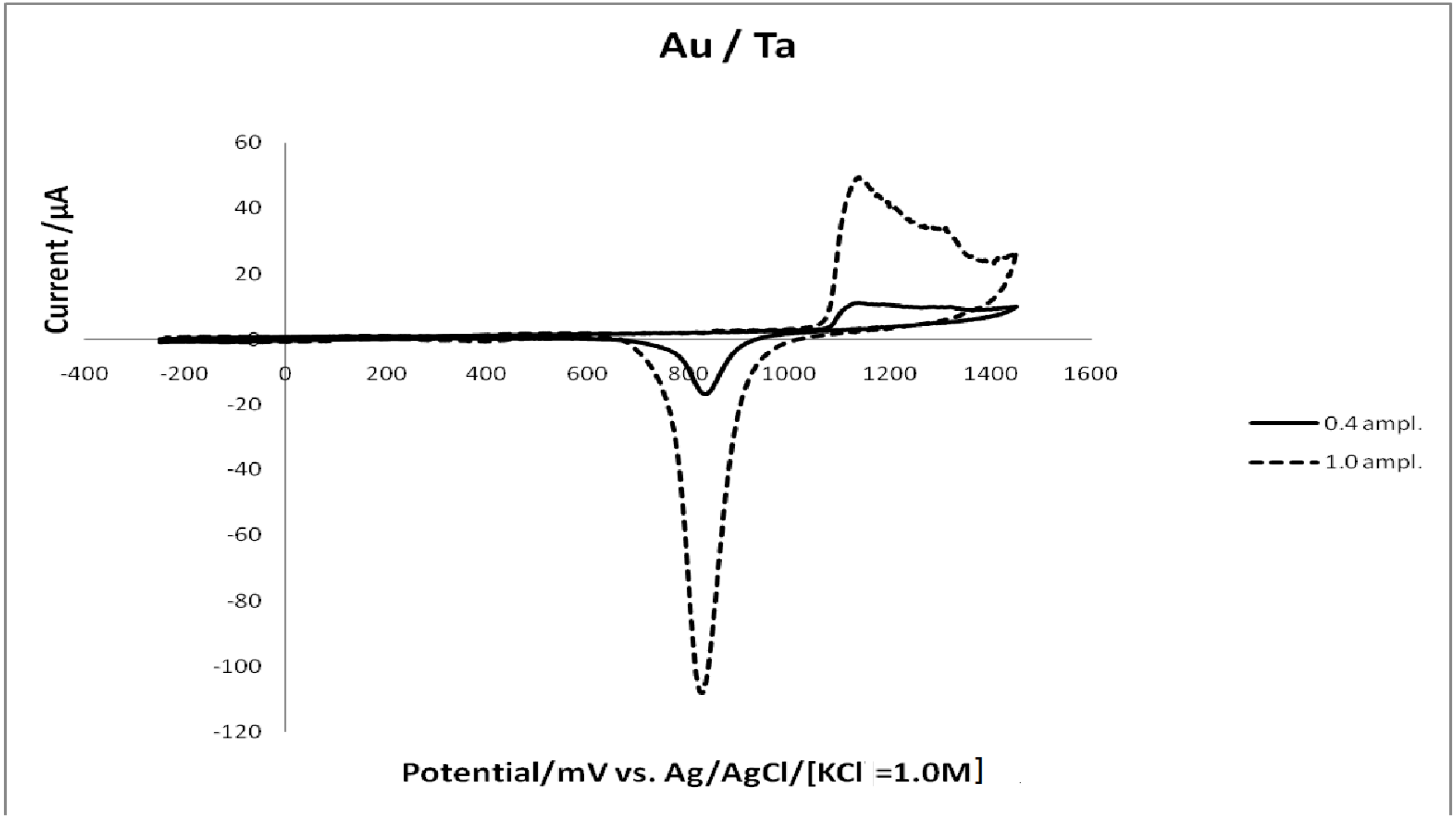


Figure 14: Cyclic voltammogram for gold nanostructures on a tantalum substrate produced at different amplitudes of the square wave. Parameters for both experiments were: deposition time= 120 s, E= -0.4 V, frequency =100 Hz, gold concentration = 10^{-3} M and scan rate = 100 mV/ s. (_____) 0.4 V amplitude and (------) 1.0 V amplitude.

Upon comparing the two I-E figure 14 shown the curves indicates that increasing the amplitude of the square wave enhances the deposition process as evidenced from the enlarged oxidation charge.

The proof for the identity of the gold deposited particles came from the EDX spectroscopy, in addition to the evidence which came from cyclic voltammetry.

This enlargement might be attributed to enhancement of deposition rate by moving towards lower negative potential, figure 14 shows, E_H +0.1 and E_L-0.9 V compared with E_H -0.2 and E_L -0.6 V.

Figures 15 and 16 show the SEM micrographs for the two surfaces produced by deposition of gold nanoparticles by application of square waves at 0.4 V and 1.0 V respectively. Both SEM micrographs show deposited gold nanoparticles as evidenced by the EDX spectra. Moreover, both SEM micrographs show enhanced deposition along the grain boundaries and a variation in particle size. The average particle size upon application of the 1.00 V square wave amplitude is apparently smaller that in case of application of the 0.4 V amplitude square wave. This in fact explains the larger surface area observed on the cyclic voltammograms of the two electrodes. The total surface area is larger for the smaller particle size nanostructures.

Investigation of the SEM micrographs and the results displayed in Table 1 shows that the particle size, shape and distribution on the surface are dependent on amplitude of the square wave.

Table 1: The effect of E_H and E_L square wave limits central at -0.4 V with 0.4 and 1.0 V amplitude on the size, shape and distribution of nanoparticles.

Experiments	E_L = -0.6, E_H = -0.2 V centered at -0.4 V, amplitude 0.4 V, concentration =10^{-3} M, frequency =100 Hz, time =120 seconds and scan rate of 100 mV/ s.	E_L = -0.6, E_H = -0.2 V centered at -0.4 V, amplitude 1.0 V, concentration =10^{-3} M, frequency =100 Hz, time =120 seconds and scan rate of 100 mV/ s.
Number of particles. (particle/cm^2)	8.80×10^9	7.40×10^9

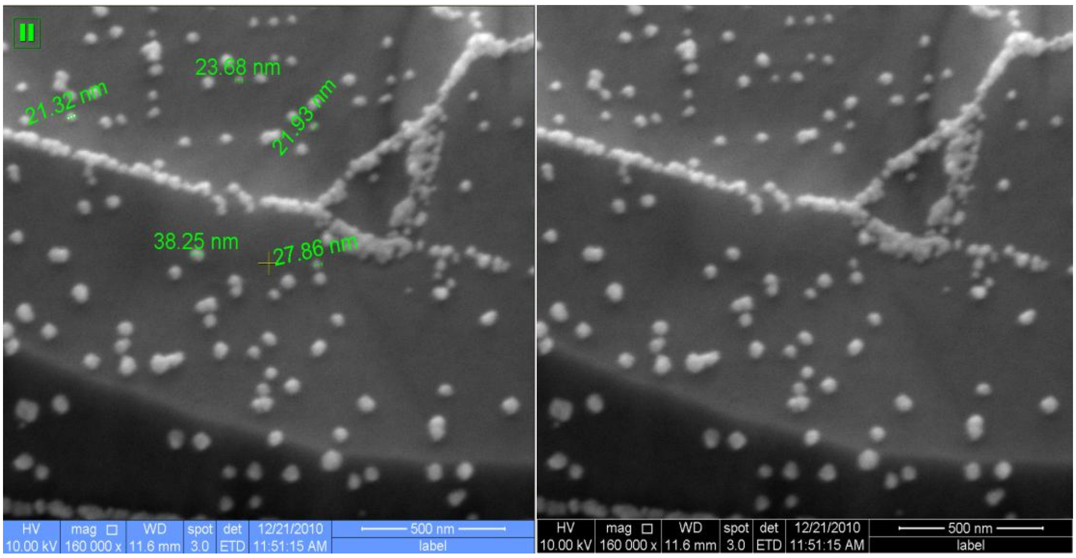


Figure 15: SEM images deposition gold nanostructures on tantalum. Parameters of the experiments E_L = -0.6, E_H = -0.2 V centered at -0.4 V, amplitude 0.4 V, concentration =10^{-3} M, frequency =100 Hz, time =120 seconds and scan rate of 100 mV/ s.

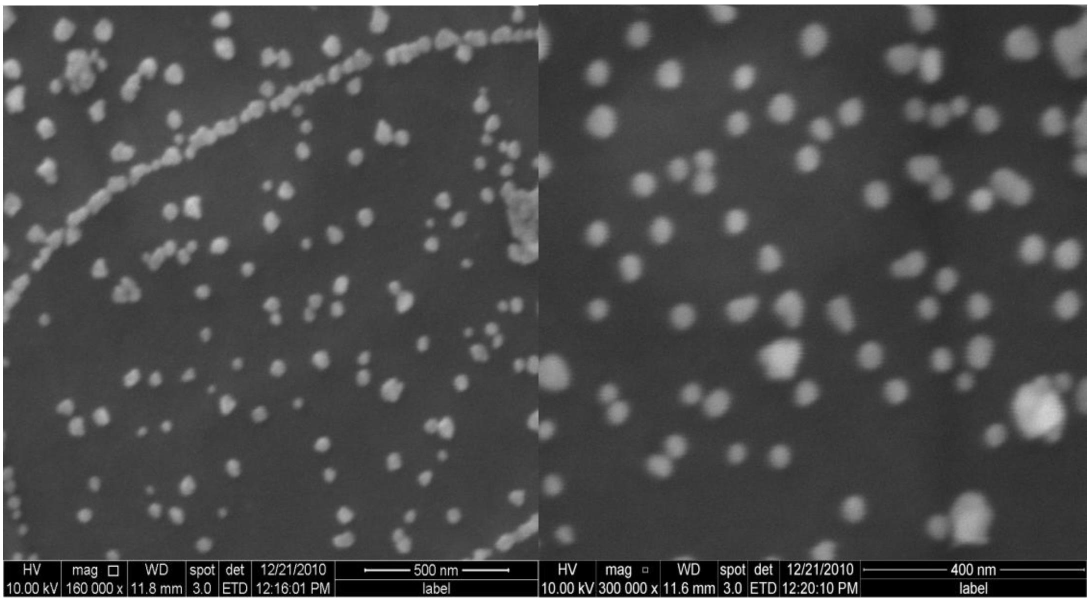


Figure 16: SEM images deposition gold nanostructures on tantalum. Parameters of the experiments E_L = -0.9, E_H = +0.1 V centered at -0.4 V, amplitude 1.0 V, concentration =10^{-3} M, frequency =100 Hz, time =120 seconds and scan rate of 100 mV/ s.

Figure 17 shows two I-E curves for two nanostructured gold electrodes produced at two different square wave amplitudes. Again the total surface area of deposited gold nanoparticles at 1.0 V square wave amplitude is higher than that produced for the nanostructured electrode produced at 0.4 V amplitude. This finding ensures the previous conclusion that increasing the square wave amplitude enhances the deposition process at one hand and has a crucial influence on the nature of the deposited particles which can be explored by electron scanning microscopy.

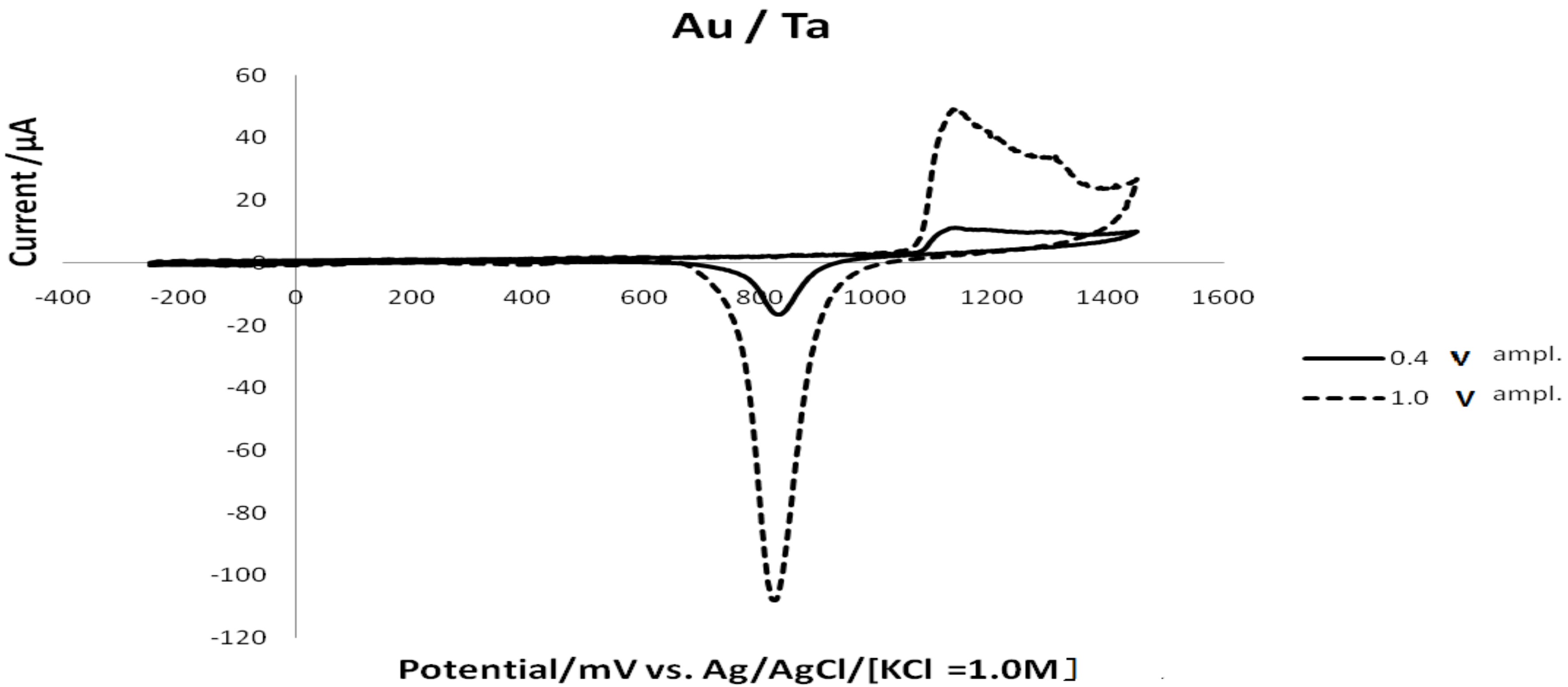


Figure 17: Cyclic voltammogram for gold nanostructures on a tantalum substrate produced at different amplitudes of the square wave. Parameters for both experiments were: deposition time= 120 s, E= -0.6 V, frequency =100 Hz, gold concentration = 10^{-3} M and scan rate = 100 mV/ s. (_____) 0.4 V amplitude and (------) 1.0 V amplitude.

Figures 18 and 19show two SEM representative micrographs for two nanogold structures produced by deposition of gold by application of a square wave centered at -0.6 V with different amplitudes; 0.4 V and 1.0 V. The SEM micrographs show that the gold nanoparticles vary in terms of size, shape and uniformity of distribution on the surface. The results are shown in Table 2.

Table 2: The effect of E_H and E_L square wave limits at central **-**0.6 V with 0.4 and 1.0 V amplitude on the size, shape and distribution of nanoparticles.

Experiments	E_L = -0.8, E_H = -0.2 V centered at -0.6 V, amplitude 0.4 V, concentration =10^{-3} M, frequency =100 Hz, time =120 seconds and scan rate of 100 mV/ s.	E_L = -0.8, E_H = -0.2 V centered at -0.6 V, amplitude 1.0 V, concentration =10^{-3} M, frequency =100 Hz, time =120 seconds and scan rate of 100 mV/ s.
Amounts of particles. (particle/cm^2)	9.60×10^9	6.40×10^9

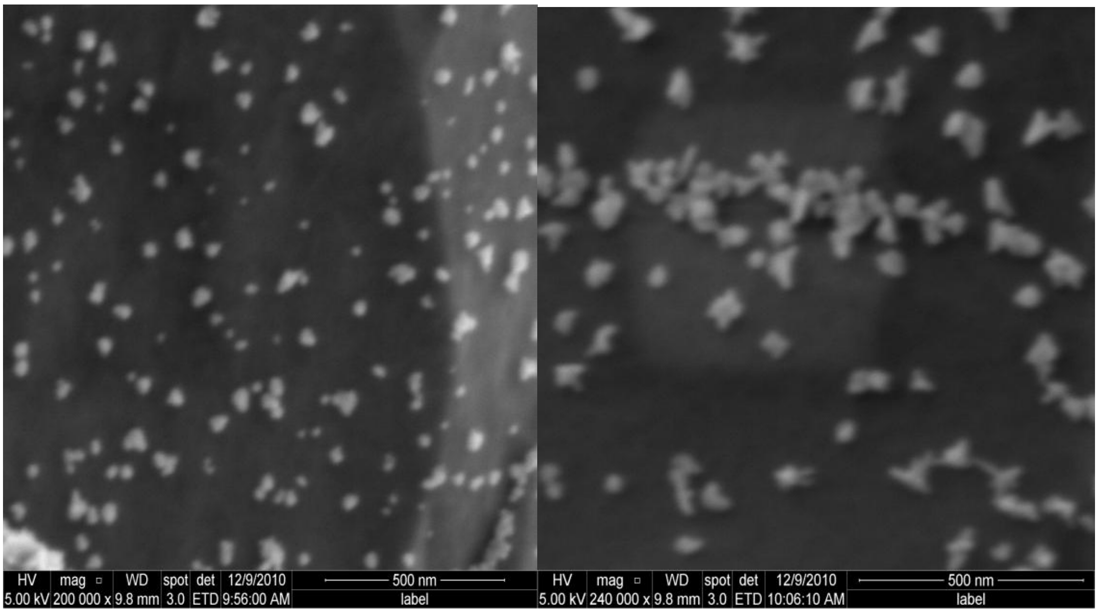


Figure 18: SEM images deposition gold nanostructures on tantalum. Parameters of the experiments E_L = -0.8, E_H = -0.2 V centered at -0.6 V, amplitude 0.4 V, concentration =10^{-3} M, frequency =100 Hz, time =120 seconds and scan rate of 100 mV/ s.

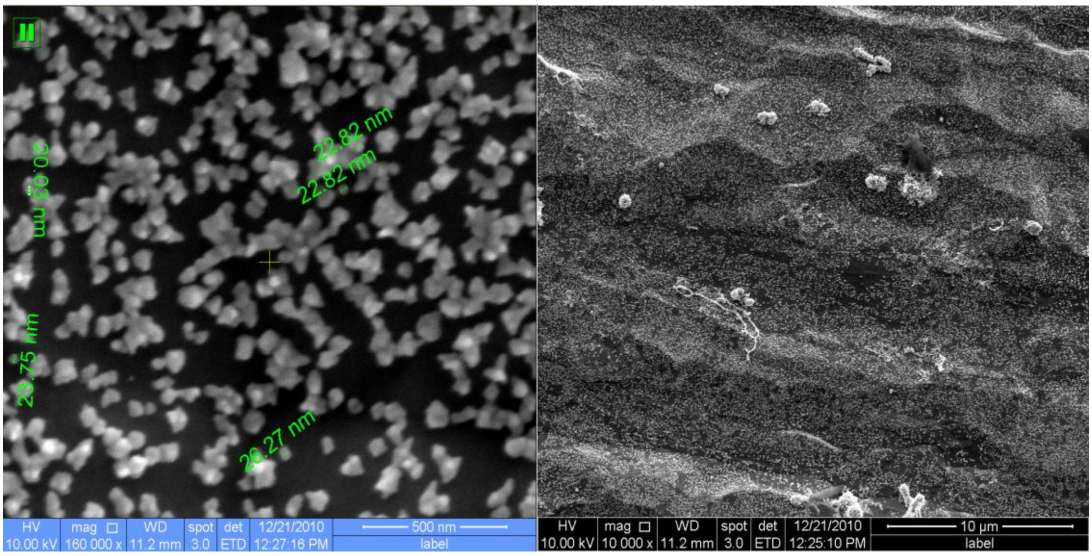


Figure 19: SEM images deposition gold nanostructures on tantalum. Parameters of the experiments E_L= -1.1, E_H = -0.1 V centered at -0.6 V, amplitude 1.0 V, concentration =10^{-3} M, frequency =100 Hz, time =120 seconds and scan rate of 100 mV/ s.

Figures 20 and 21 show the SEM micrographs of deposited gold nanostructures produced by application of square wave potential regime with different amplitudes 0.6 and 0.8 centered at -0.5 V.

Table 3: The effect of E_H and E_L limits values central at -0.5 with amplitude 0.6 and 0.8 V square wave amplitude on the size, shape and distribution of nanoparticles.

Experiment	E_L = -0.8, E_H = -0.2 V centered at -0.5 V, amplitude 0.6 V, concentration =10^{-3} M, frequency =100 Hz, time =120 seconds and scan rate of 100 mV/ s	E_L = -0.8, E_H = -0.2 V centered at -0.5 V, amplitude 0.8 V, concentration =10^{-3} M, frequency =100 Hz, time =120 seconds and scan rate of 100 mV/ s
Number of particles (particle/cm^2)	7.92×10^9	6.40×10^9

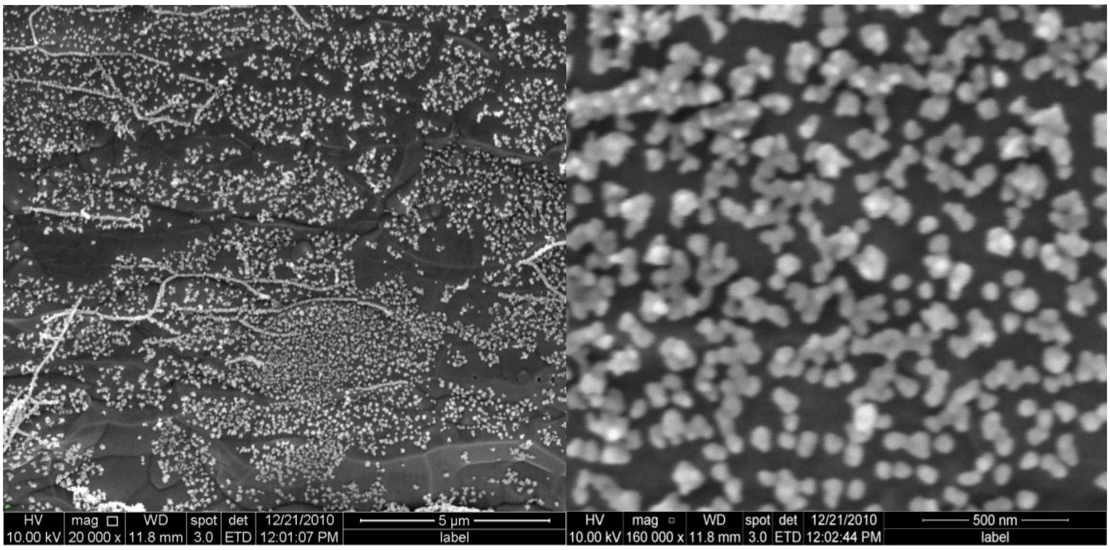


Figure 20: SEM images deposition gold nanostructures on tantalum. Parameters of the experiments E_L = -0.8, E_H = -0.2 V centered at -0.5 V, amplitude 0.6 V, concentration =10^{-3} M, frequency =100 Hz, time =120 seconds and scan rate of 100 mV/ s.

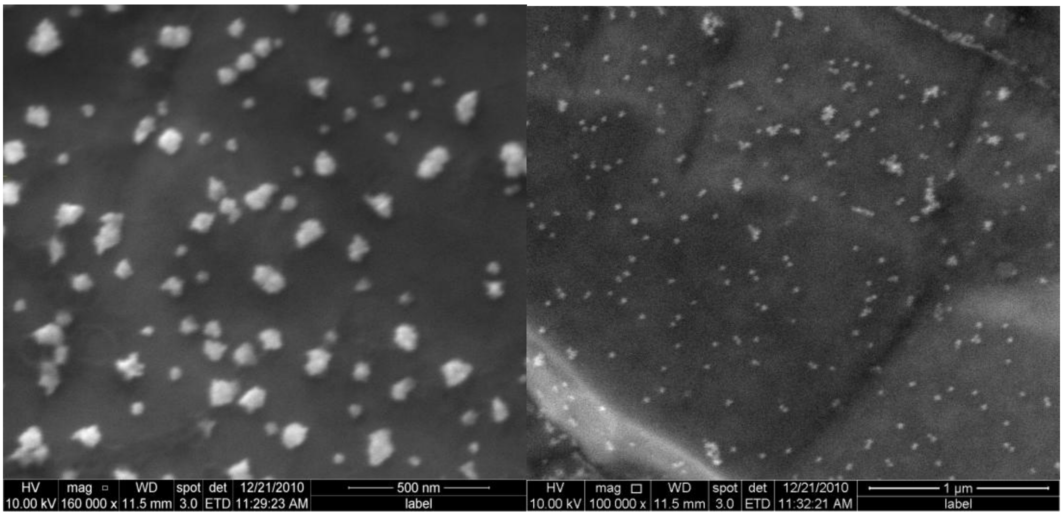


Figure 21: SEM images deposition gold nanostructures on tantalum. Parameters of the experiments E_L = -0.9, E_H = -0.1 V centered at -0.5 V, amplitude 0.8 V, concentration =10^{-3} M, frequency =100 Hz, time =120 seconds and at a scan rate of 100 mV/ s.

Figure 22 shows the relation between the total surface area from SEM micrographs and the potential at centered amplitude square wave 0.6 V. the total surface area increased upon decreased the potential from -0.1 to -0.3. The maximum area was at -0.3 V where it decreased going to -0.4 V.

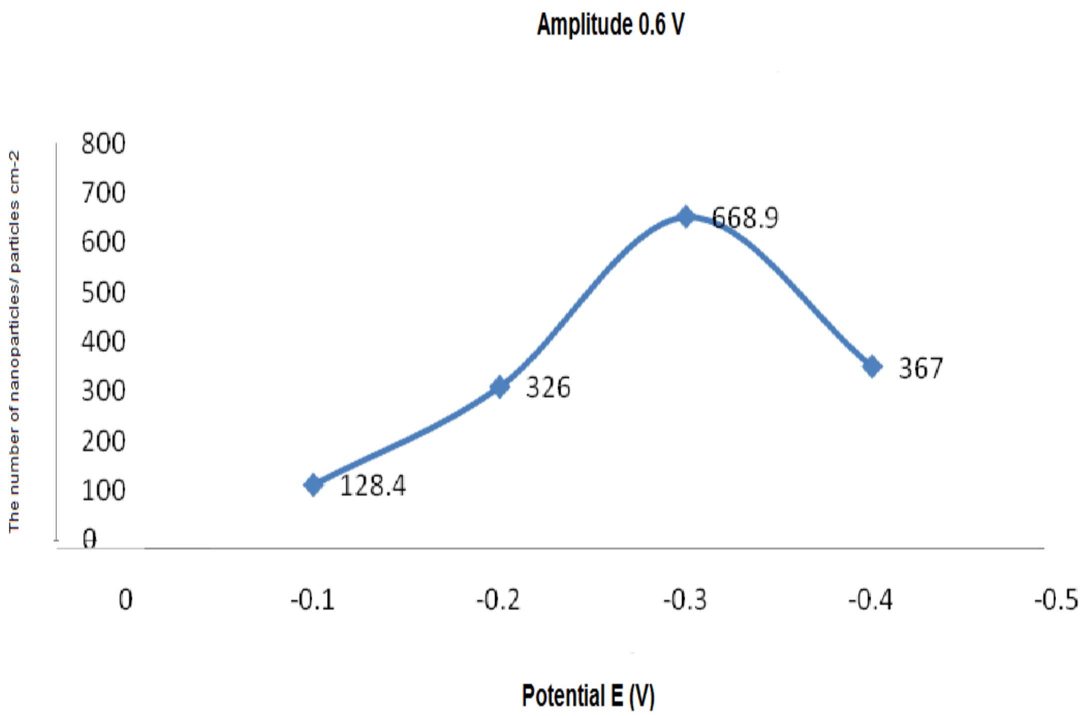


Figure 22: a plot the number of particles × 10^7 (particles/cm^2) vs. potential E. parameters of experiments gold solution= 10^{-3} M, time=60s and frequency=100 Hz

Figure 23 shows the relation between the total surface area from the cyclic voltammograms and potential at frequencies 10 and 50 Hz. At potential -0.3 V the larger total surface area than other potential at frequency 10 and 50 Hz.

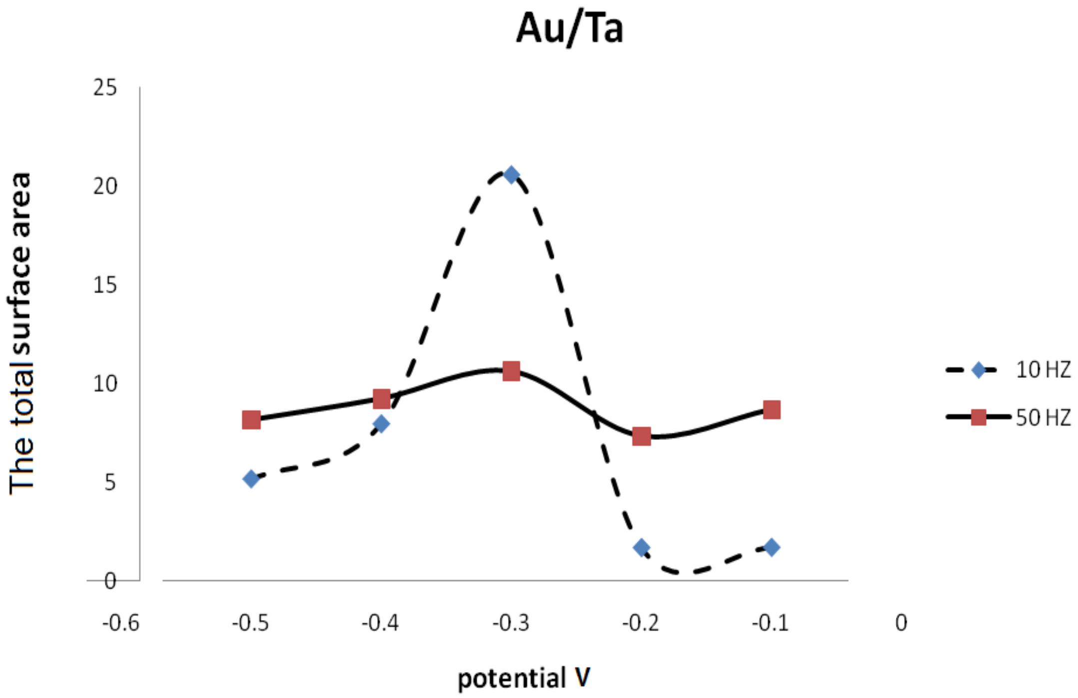


Figure 23: a plot the surface area vs. potential E. parameters of experiments gold solution= 10^{-3} M, time=60s and amplitude = 0.6V.

The shape, uniformity and distribution of the nanostructures were formed to depend on the experimental parameters of deposition. The following factors were addressed in the present work.

3.1.1.2 The effect of deposition time

Figure 24 shows the cyclic voltammograms of deposited gold nanostructures produced by application of square wave potential regime on tantalum electrode with different deposition times.

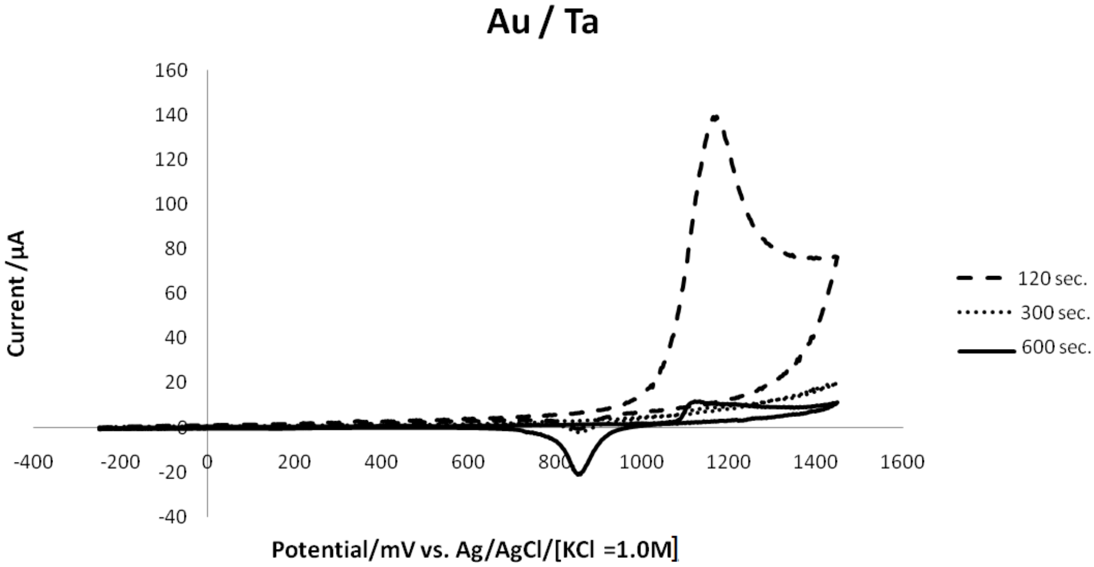


Figure 24: Cyclic voltammogram of Au/Ta deposition gold nanostructures on tantalum. Parameters of the experiments E_L = -0.3, E_H = +0.1 V, amplitude 0.4 centered at -0.1 V, concentration10^{-3} M, freqancy100 Hz and at a scan rate of 100 mV/ s

The charge underneath oxygen desorption from gold surface is proportional to the surface area of gold. This conclusion is supported by the fact that there is no counter peak for desorption of oxygen from tantalum surface. This positively ensures the expected conclusion that increasing the deposition time increases the amount of deposited gold.

The effect of deposition time on size, shape and uniformity of distribution of nanoparticles on the tantalum surface. Figures 25 – 27 show the effect of deposition time on the deposited nanoparticles. Figure 25 shows the SEM micrograph for the deposited gold nanoparticles produced at 60 s deposition time. The nanoparticles are separately scattered on the tantalum surface with a high degree of uniformity.

Figure 25 show the SEM micrographs of deposited gold nanostructures produced by application of square wave potential regime at 60 s time. A rough estimate of nanoparticles amounts to a value of 6.69×10^9 particle/cm^2.

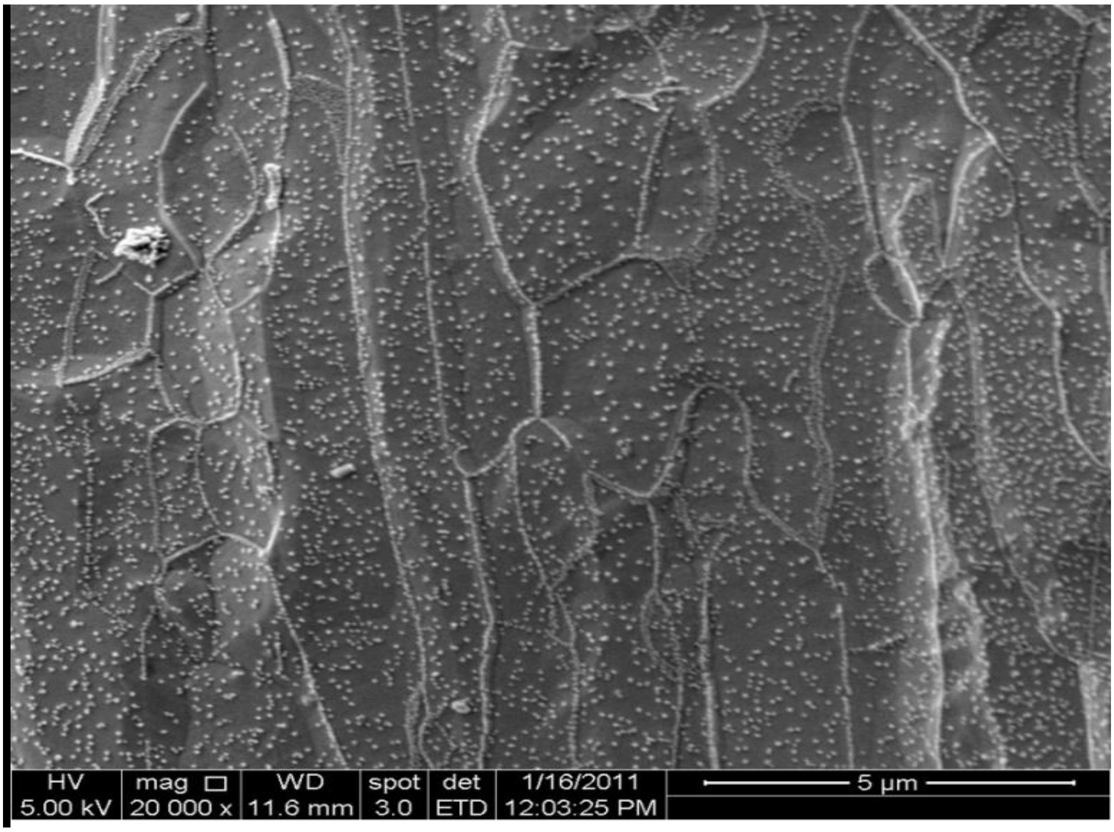


Figure 25: SEM images deposition gold nanostructures on tantalum. Parameters of the experiment E_L = -0.3, E_H = +0.1 V, amplitude = 0.4 centered at -0.4 V concentration = 10^{-3} M, frequency = 100 Hz, time = 60 seconds and scan rate of 100 mV/ s.

Figure 26 shows the SEM micrograph for the deposited gold nanoparticles obtained at a deposition time of 120s. Further investigation of the deposited nanoparticles indicates that the obtained particles are larger with an average size of about 37 nm and with an average distribution of 3.21×10^9 particles/cm^2.

The SEM micrograph displayed in Figure 27 shows a thick crust of deposited layers of gold particles on tantalum surface. This thick crust shows poor adherence to the tantalum substrate and was pealed of at some edges.

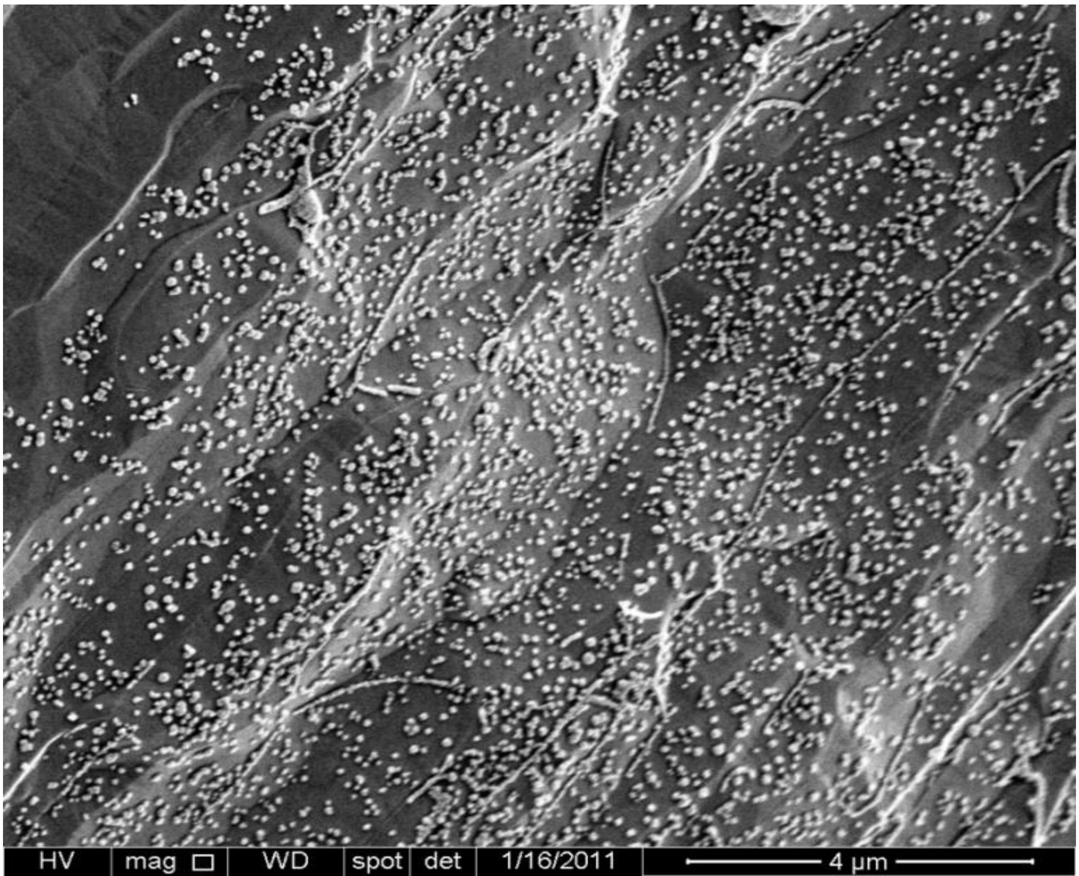


Figure 26: SEM images deposition gold nanostructures on tantalum. Parameters of the experiment E_L = -0.3, E_H = +0.1 V, amplitude = 0.4 centered at -0.4 V concentration = 10^{-3} M, frequency = 100 Hz, time = 120 seconds and scan rate of 100 mV/ s.

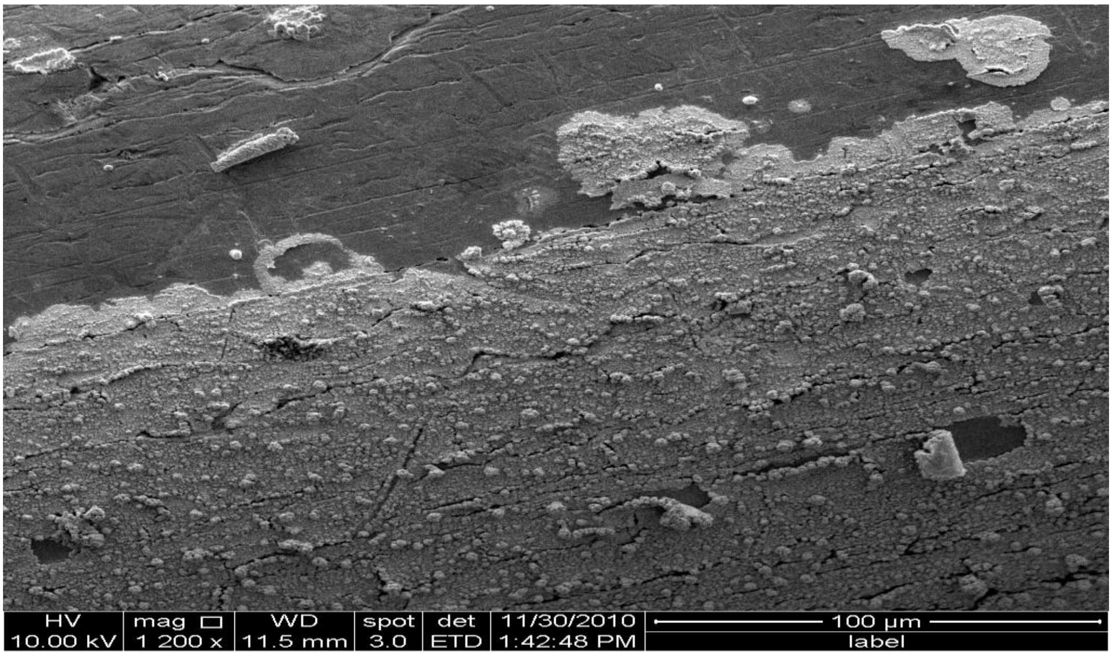


Figure 27: SEM images deposition gold nanostructures on tantalum. Parameters of the experiment E_L= -0.3, E_H = +0.1 V, amplitude = 0.4V centered at -0.4 V concentration = 10^{-3} M, frequency = 100 Hz, time = 300 seconds and scan rate of 100 mV/ s.

These findings indicate the importance of deposition time in producing nanoparticles in the first place. Deposition time is important as expected in formation of nanoparticles and their size and distribution at the surface.

Figure 28 shows the relation btween the total surface area caculated from SEM micrographs and deposition time. Increasing the deposition time decreases the total covered surface area. It 120s deposition time achieved we get the larger total surface area.

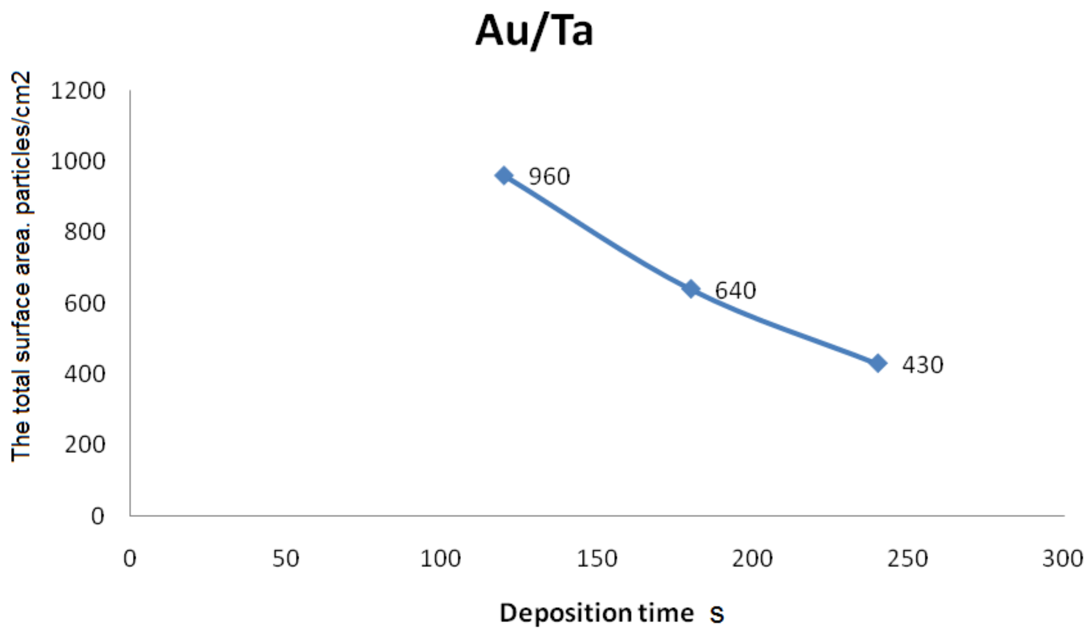


Figure28: a plot the number of particles × 10^7 (particles/cm^2) vs. time (s).parameters of the experiments potential = -0.6, amplitude = 0.4 V, frequency = 100 HZ and different time 120, 180 and 240 seconds.

3.1.1.3. The effect of frequency of the square wave on the deposited nanoparticles

Figures 29 shows the results extracted from cyclic voltammograms of the deposited gold nanostructured prepared at different frequencies of the square wave potential regime. These results indicate that the charge underneath the oxygen desorption peak is dependent on the frequency of the square wave. In fact, the charge underneath the curve is proportional to the total surface area of the deposited nanoparticles. The total surface area is dependent on the number and size of deposited particles.

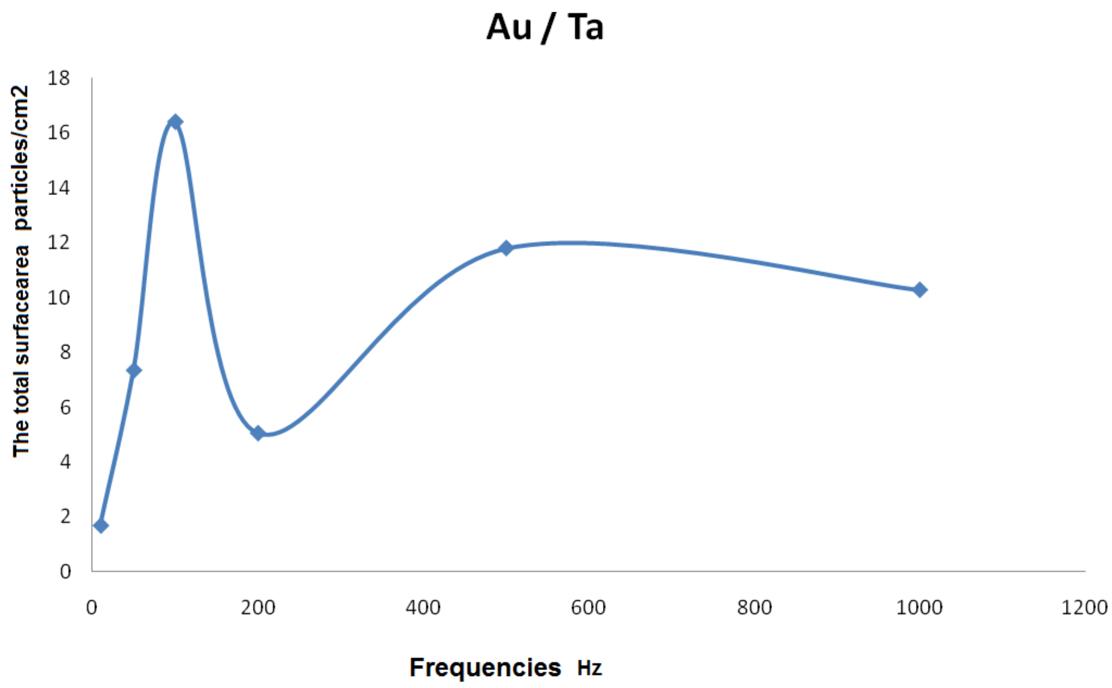


Figure 29: a plot the total surface are vs. frequency of Au/Ta deposition gold nanostructures on tantalum. Parameters of the experiments E_L = -0.8, E_H = -0.2 V, amplitude = 0.6 centered at -0.5 V, concentration = 10^{-3} M, time = 60 seconds and scan rate of 100 mV/s.

Figure 29 shows a complex relationship between the frequency of the applied square wave and the total surface area of the deposited particles where the curve chose a maximum at 100 Hz and a minimum at 200 Hz. This behavior was found to be consistent at some other amplitude values of the square wave. SEM micrographs indicated that larger numbers of nanoparticles were obtained at 100 Hz frequency (to be discussed letter). However, on our voltammetric data, however, we can safely conclude that the frequency affects the nature of the deposited nanoparticles.

Figures 30-32 show the SEM micrographs of deposited gold nanostructures produced by application of square wave potential regime on tantalum electrode at the frequencies, 50, 100 and 1000 Hz respectively.

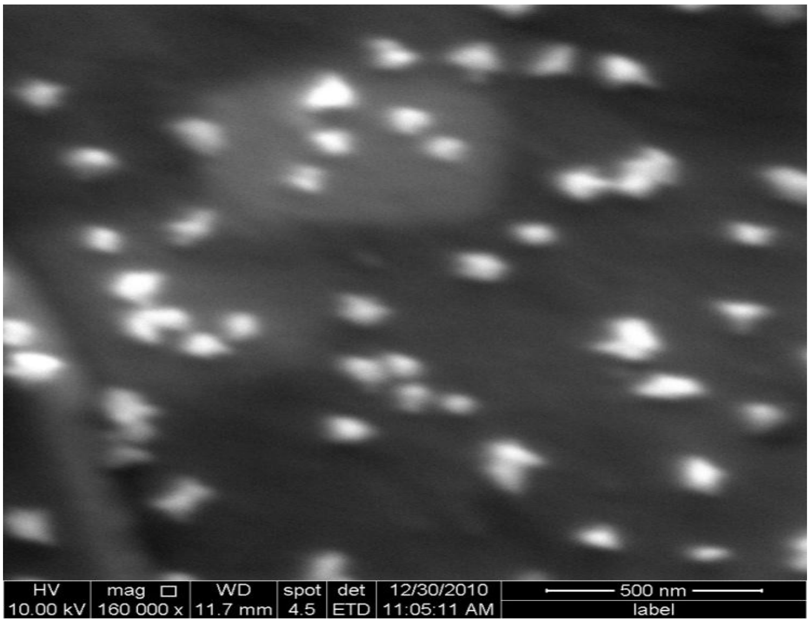


Figure 30: SEM images of deposition gold nanostructures on tantalum. Parameters of the experiment E_L = -0.8, E_H = -0.2 V centered at = -0.5 V, amplitude = 0.6V, frequency = 50 Hz, concentration = 10^{-3} M, time = 60 seconds and scan rate of 100 mV/ s.

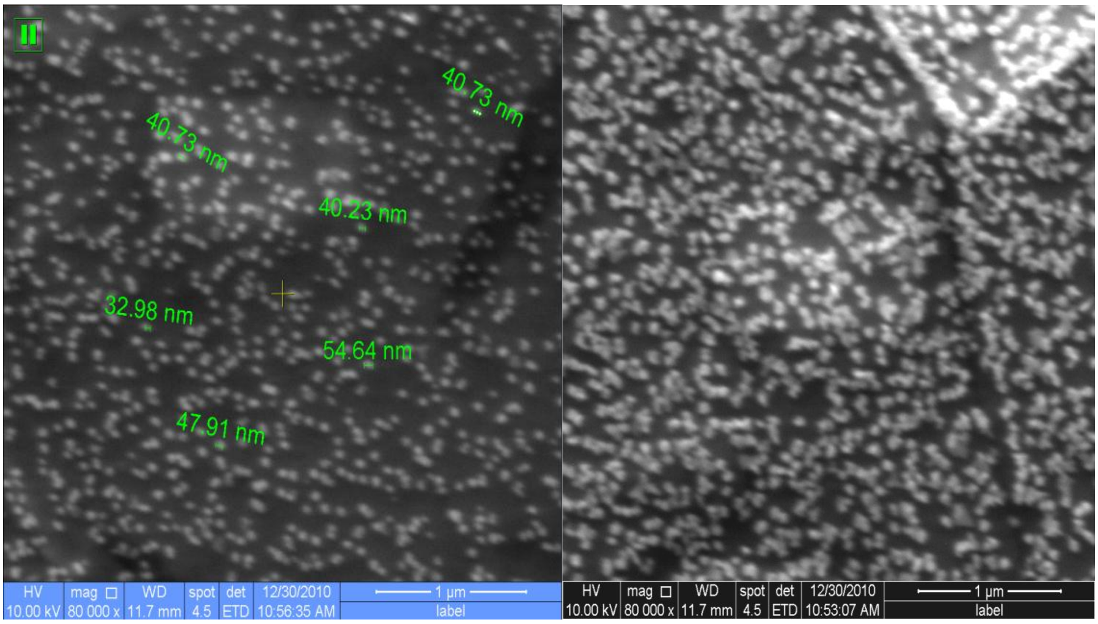


Figure 31: SEM images deposition gold nanostructures on tantalum. Parameters of the experiment E_L = -0.8, E_H = -0.2 V centered at = -0.5 V, amplitude = 0.6V, concentration = 10^{-3} M, time = 60 seconds, frequency = 100 Hz and scan rate of 100 mV/ s.

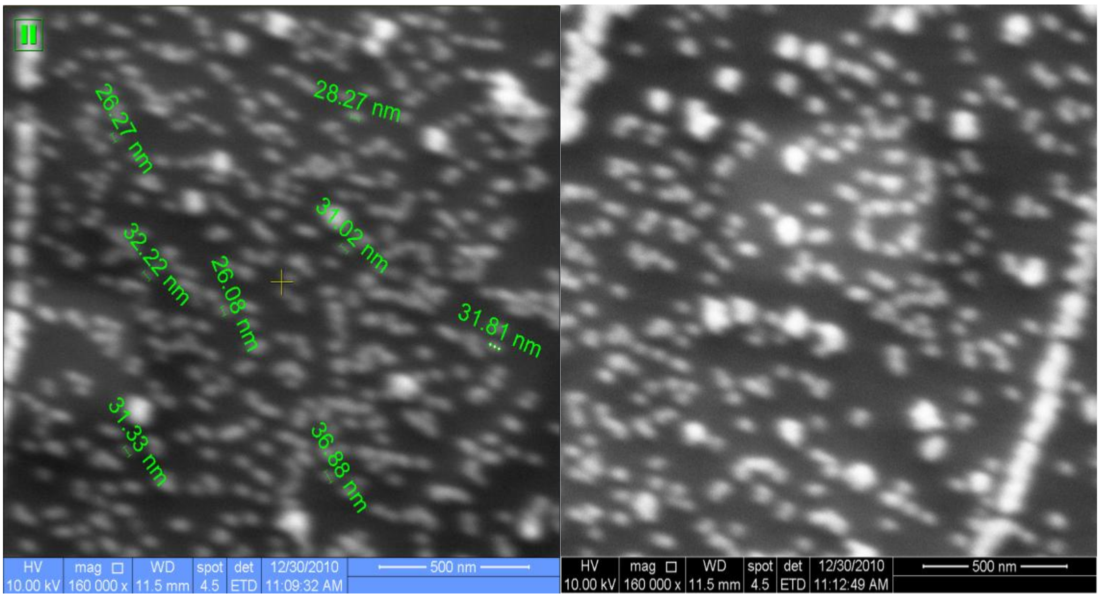


Figure 32: SEM images deposition gold nanostructures on tantalum. Parameters of the experiment E_L = -0.8, E_H = -0.2 V centered at = -0.5 V, amplitude = 0.6V, concentration = 10^{-3} M, time = 60 seconds, frequency = 1 kHz and scan rate of 100 mV/ s.

Figure 30 shows the SEM micrograph of deposited gold nanostructures produced by application of square wave potential regime at frequency of 50 Hz. A rough estimate of nanoparticles amounts give a value of 2.40×10^9 particles/cm^2. The average size of the deposited nanoparticles is about 32.5 nm. The figure 29 shows the nanostructures at 50 Hz with flake-like shape.

Figure 31 shows the SEM micrograph for the deposited nanoparticles obtained at frequency of 100 Hz used in deposition. Further investigation of the deposited nanoparticles indicate that the obtained particles are larger with an average size of about 42.81 nm and with an average number of 6.20×10^9 particles/cm^2.

At the frequency of 100 Hz shape, size, uniformity and distribution on the surface on a regular basis and nanophysics or nanocrystalline gold can be classified as three-dimensional structures and shows the nanostructures at 100 Hz with spherical shape.

Figure 32 shows the SEM micrograph for the deposited nanoparticles obtained at the frequency of 1 K Hz. Further investigation of the deposited nanoparticles indicate that the obtained particles are larger than about the experiments carried out at 50 and Hz with an average size of about 30.45 nm and with an average number of 1.24×10^9 particles/cm^2. The figure 32 shows the nanostructures at 1K Hz are of spherical shape.

Application of the same producer for the deposition of nanoparticles at amplitude of 0.6 V for the square wave centered at -0.5 V also showed the same trend (Figure 33). At frequency 100 Hz the total surface area calculated from SEM micrographs is the larger than the frequencies 50 and 1000 Hz.

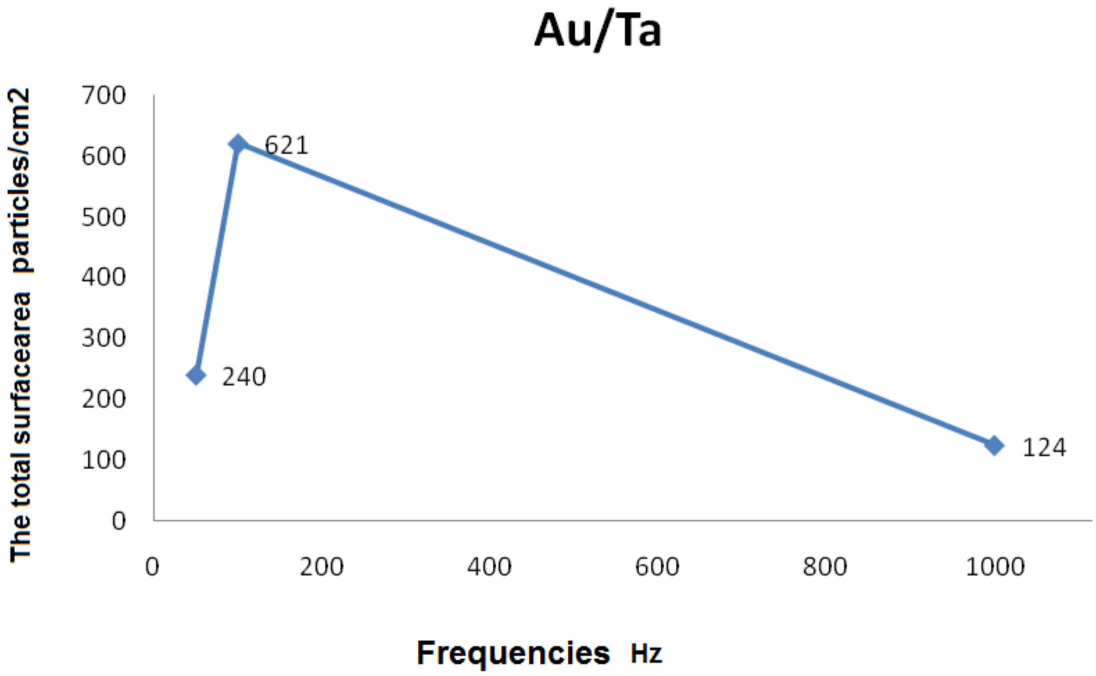


Figure 33: a plot the number of particles × 10^7 (particles/cm^2) vs. frequencies 50, 100 and 1000 Hz. parameters of the experiments potential = -0.5V, amplitude = 0.6 V, time= 60s and different frequency 50, 100 and 1000 Hz.

Figure 34 shows the relation between the total surface area calculated from cyclic voltammograms and frequencies (10 to 1000 Hz) at different central potential (-0.1,-0.2, -0.3,-0.4 and -0.5) V at half-amplitude of the square wave with a total amplitude of 0.6 V. Frequency at 100 Hz give the optimum of all potentials used in this experiments at centered amplitude square wave 0.6 V.

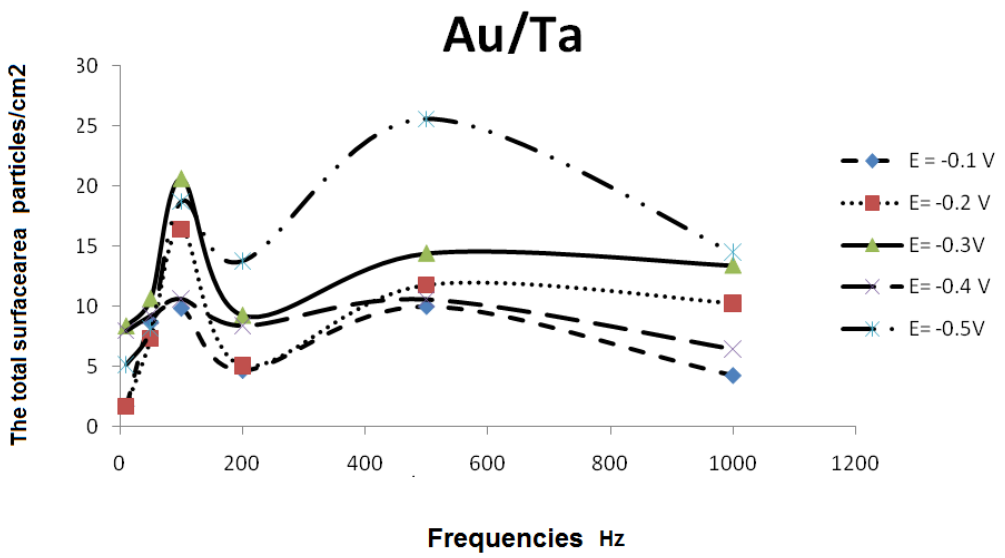


Figure 34: a plot the total surface area vs. frequency, deposited gold on tantlum substrate . Parameters of experiments different potential at centered amplitude = 0.6 V, time= 60s and different frequency 10, 50, 100, 200, 500 and 1 K Hz

3.1.1.4. The effect of concentration of gold solution on the deposited nanoparticles:

Figure 35 shows the total surface area underneath the oxygen desorption peak extracted from cyclic voltammogram of the deposited gold nanoparticles. This figure shows that a larger total surface area is produced at higher concentration of gold in the solution figure 35 shows. This can be explained on the fact that both mechanisms of deposition; nucleation and particle growth are dependent on the concentration of gold solution.

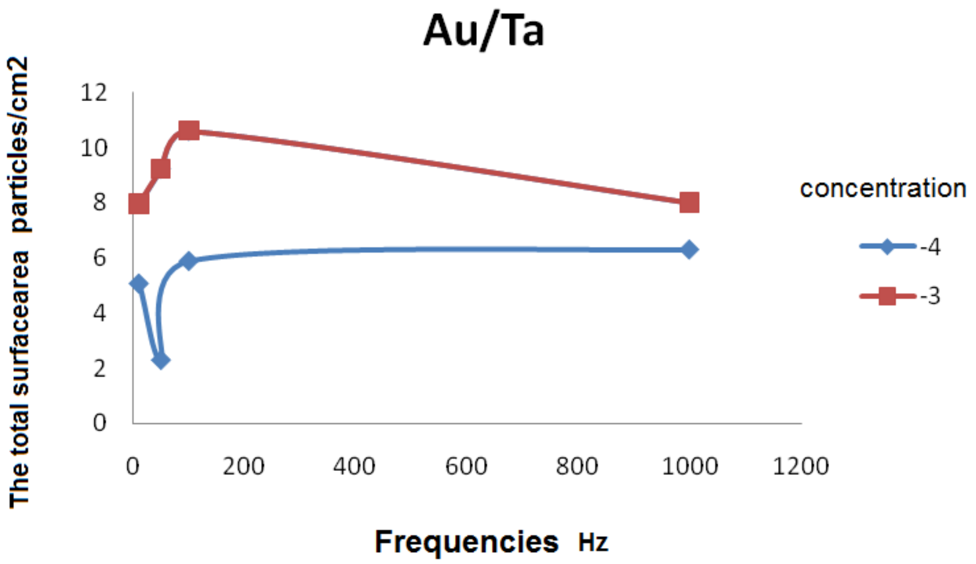
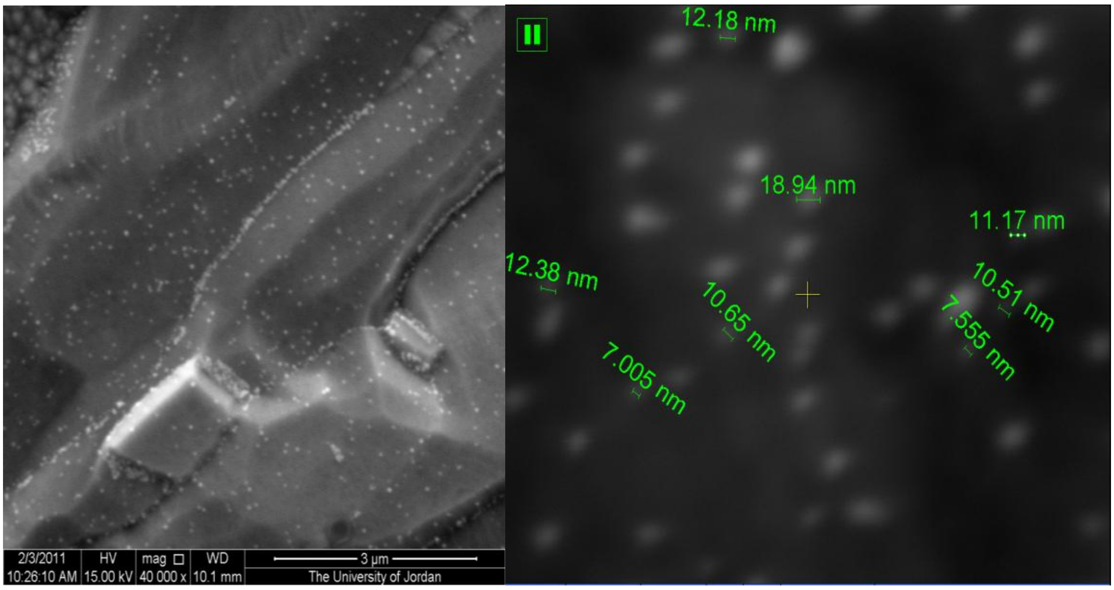


Figure 35: a plot of total surface area vs. frequencies of Au/Ta deposition of gold nanostructures on tantalum. Parameters of the experiments E_L= -0.6, E_H =- 0.2 V, amplitude =0.4V centered at -0.4 V, time 60 seconds and a scan rate of 100 mV/ s.

Figures 36 and 37 show the SEM micrographs of deposited gold nanostructures produced by application of square wave potential regime on tantalum electrode with different concentrations of (10^{-3} and 10^{-4}) M respectively.

Figure 36 shows the SEM micrograph for the deposited nanoparticles obtained at 10^{-3} M gold concentration. Further investigation of the deposited nanoparticles indicates that the obtained particles are larger than the total surface area deposited on surface at used 10^{-4} M solution gold with an average size of about 11.3 nm and with an average distribution of 4.40×10^{9} particles/cm^{2}.



a b

Figure 36: SEM images (a and b) deposition gold nanostructures on tantalum. Parameters of the experiment E_L= -0.7, E_H = +0.1 V centered at = -0.3V, amplitude = 0.6V, frequency = 100 Hz, gold concentration = 10^{-3} M, time = 30 seconds and scan rate of 100 mV/ s.

Figure 37 shows the SEM micrograph for the deposited nanoparticles obtained at 10^{-4} M gold concentration. Further investigation of the deposited nanoparticles indicates that the obtained particles are smaller than concentration 10^{-3} M used in deposited gold with an average distribution of 3.00×10^{9} particles/cm^2.

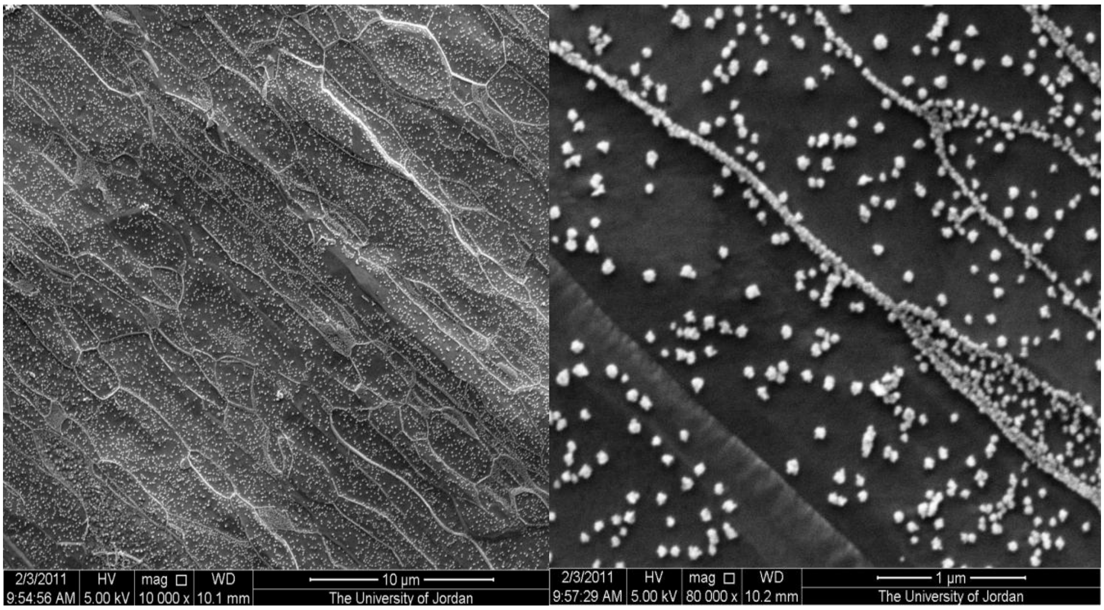


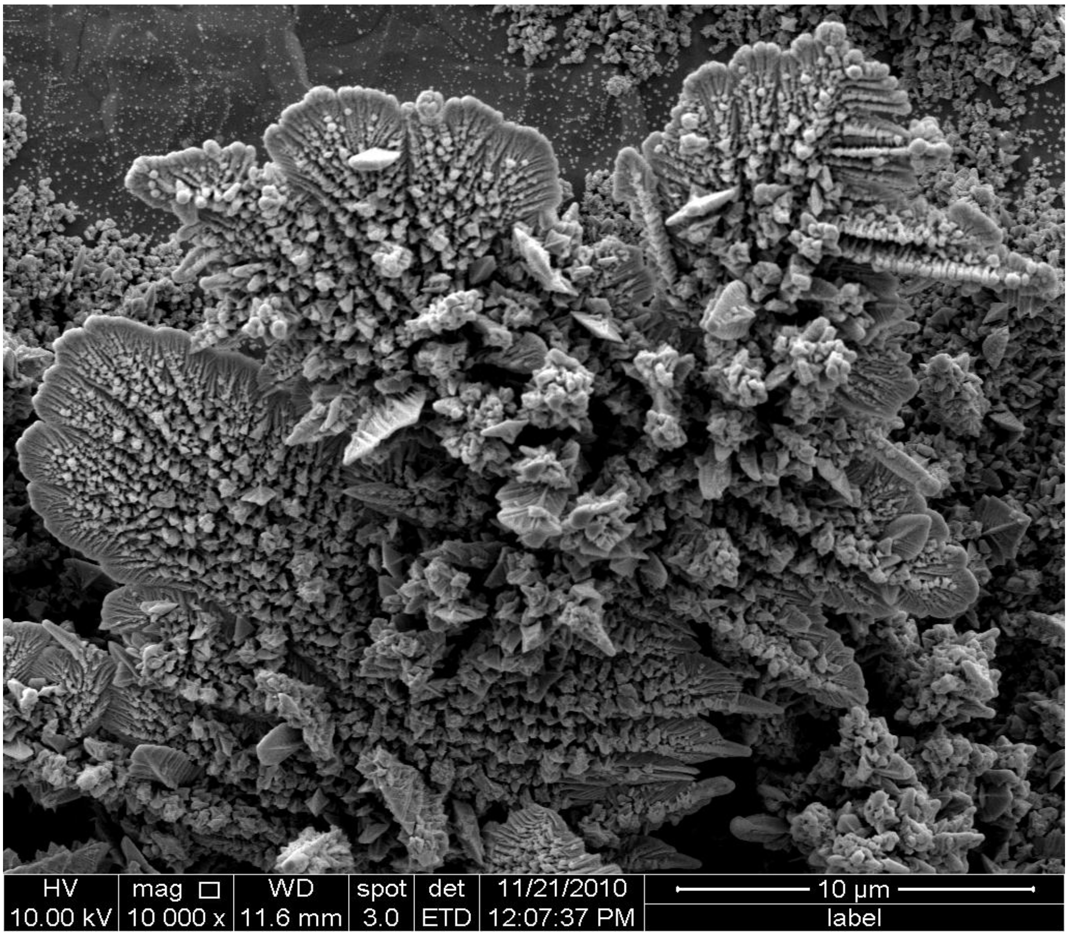
Figure 37: SEM images deposition gold nanostructures on tantalum. Parameters of the experiment E_l = -0.7, E_h = +0.1 V centered at = -0.3V, amplitude = 0.6V, frequency = 100 Hz, gold concentration = 10^{-4} M, time = 30 seconds and scan rate of 100 mV/ s.

Comparing the two SEM micrographs in figures 36 and 37 shows that smaller size particles and larger the total surface area were obtained at higher concentration 10^{-3} M. This result is not unexpected since the deposition kinetic is dependent on the concentration of the deposited atoms.

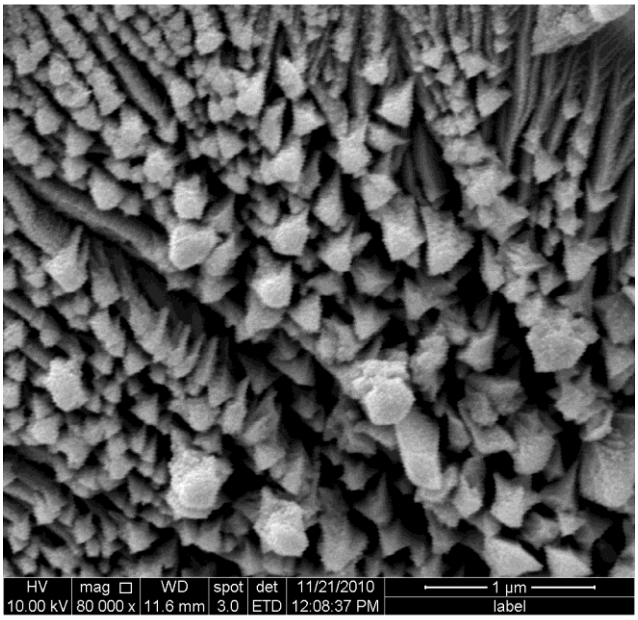
3.1.2. Microstructures of deposited gold at longer deposition time:

Figures 38-40 show the SEM micrographs of deposited gold nanostructures produced by application of square wave potential regime at different times (900,300,120 seconds).

Figure 38-a shows the SEM image for the deposited gold produced at 900 s deposition time. It shows flower-like gold formation at 10^{-3} M higher concentration and longer deposition time. The flower-like gold was is not distributed over on the entire surface.



a

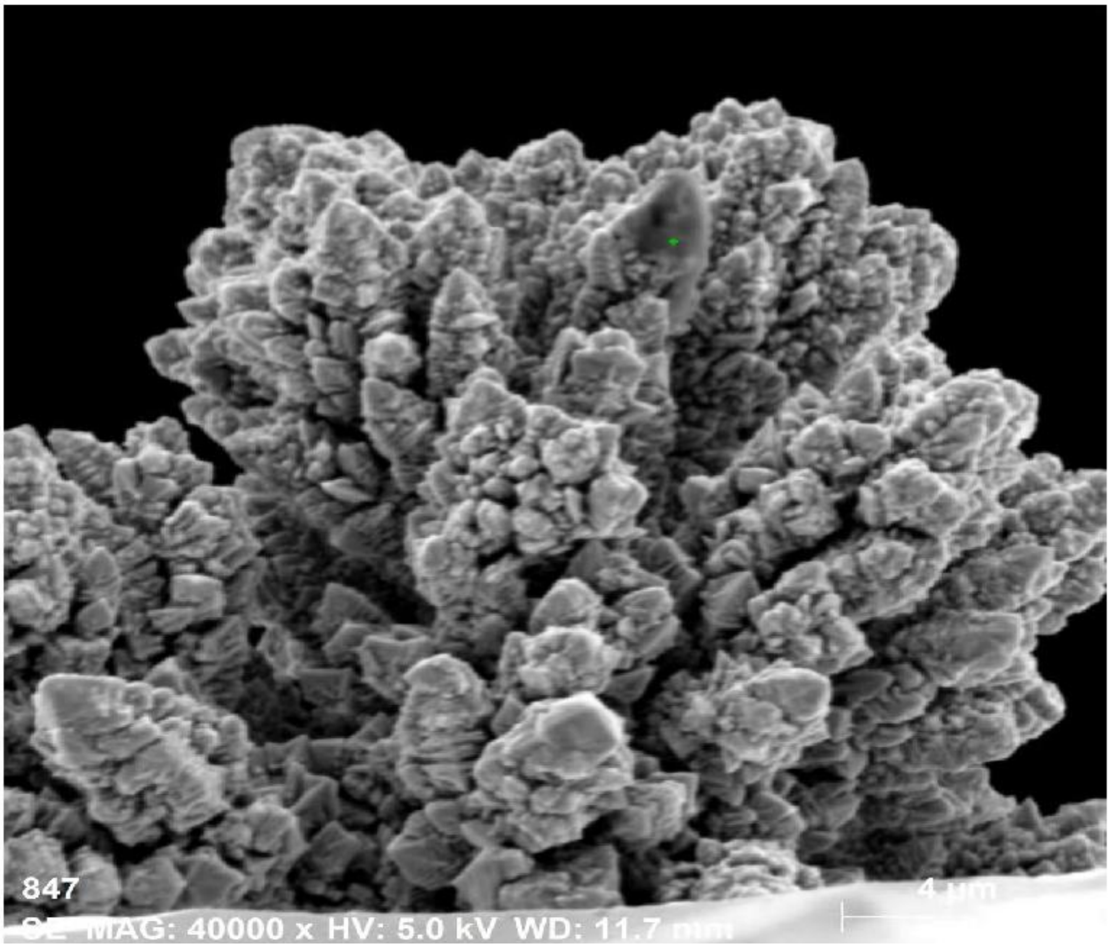


b

Figure 38: SEM images (a and b) deposition gold nanostructures on tantalum. Parameters of the experiment E_l = -0.3, E_h = +0.1 V centered at = -0.1V, amplitude = 0.4V, frequency = 100 Hz, gold concentration = 10^{-3} M, time = 900 seconds and scan rate of 100 mV/ s.

Figure 38-b shows the SEM micrographs of the surface on flower-like gold. Enlarging the surface of flower showing the composition of epitaxial growth and distribution on surface of flower.

Figure 39-a shows the SEM image for the deposited gold produced at 600 s deposition time; flower-like gold formation at higher concentration 10^{-3} M and longer deposition time. The flower-like gold was not distributed over the entire surface.



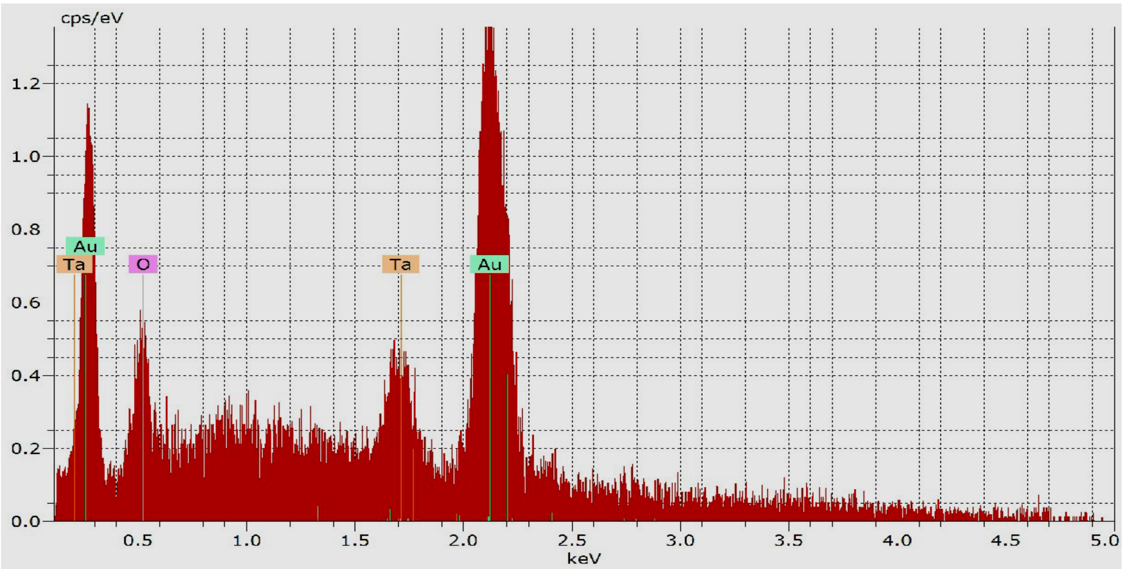
a

Figure 39: (a): SEM images deposition gold nanostructures on tantalum. Parameters of the experiment E_l = -0.8, E_h = -0.4 V centered at = -0.6V, amplitude = 0.4V, frequency = 100 Hz, gold concentration = 10^{-3} M, time = 300 seconds and scan rate of 100 mV/ s.

Figure 39-b shows the EDX spectra of the analysis of flower-like gold which proves that the product is gold.

Spectrum: Acquisition 757

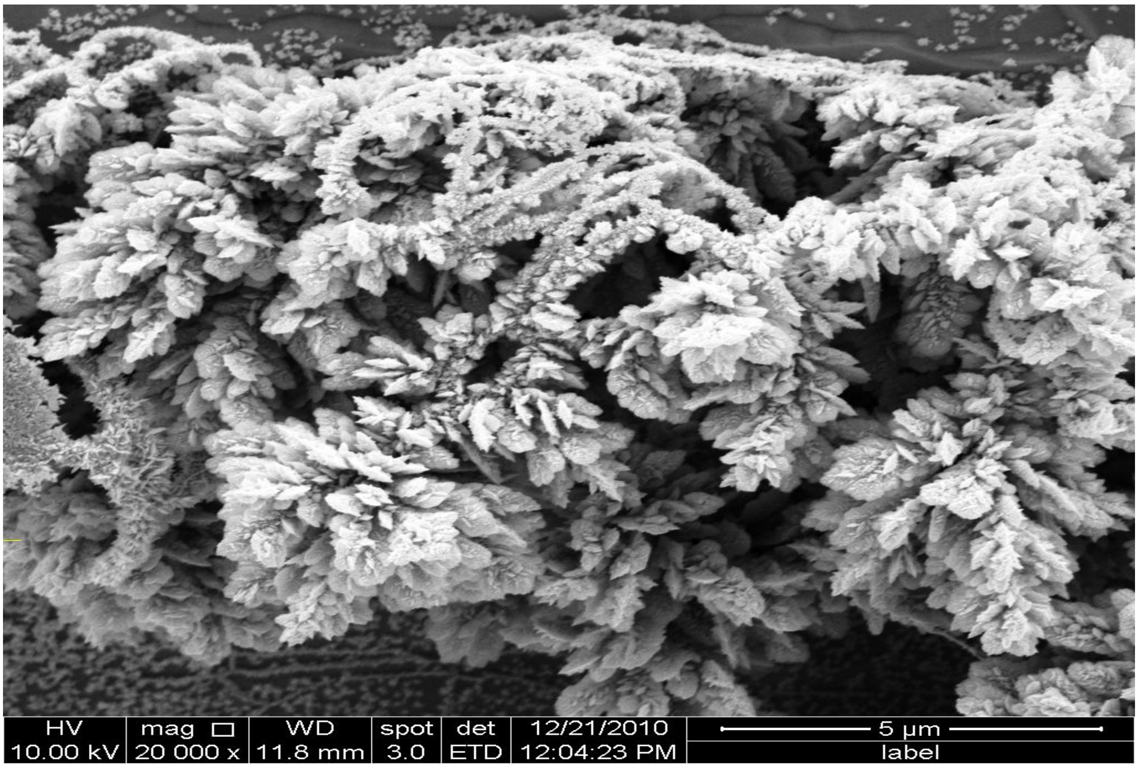
El	AN	Series	unn. C [wt.%]	norm. C [wt.%]	Atom. C [at.%]	Error [%]
O	8	K-series	6.91	6.42	45.57	1.6
Ta	73	M-series	10.40	9.67	6.07	0.8
Au	79	M-series	90.22	83.91	48.36	4.9
		Total:	107.53	100.00	100.00	



b

Figure 39(b): EDX spectra of flower gold microstructures deposited on tantalum substrate. Parameters of the experiment E_l = -0.8, E_h = -0.4 V centered at = -0.6V, amplitude = 0.4V, frequency = 100 Hz, gold concentration = 10^{-3} M, time = 300 seconds and scan rate of 100 mV/ s.

Figure 40 shows the SEM image for the deposited gold produced at 120 s deposition time; flower-like gold formation at higher concentration and longer deposition time. The flower-like gold not distributed the entire surface. Growth of flower-like gold microcrystals at ambient temperatures on tantalum electrode. Figure 40-b shows the EDX spectra the analysis of flower-like gold and proves that the product is gold.

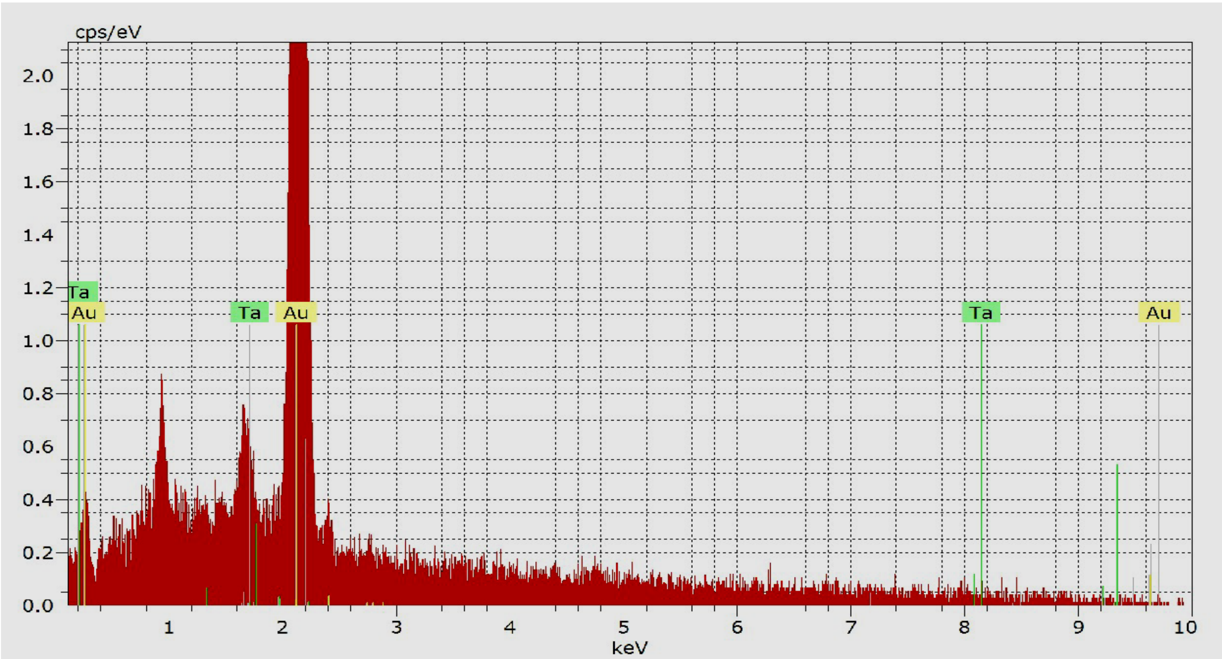


a

Figure 40 -a SEM images deposition gold nanostructures on tantalum. Parameters of the experiment E_L = -0.6, E_H = 0.00 V centered at = -0.3V, amplitude = 0.6V, frequency = 100 Hz, gold concentration = 10^{-3} M, time = 120 seconds and scan rate of 100 mV/ s.

Spectrum: Acquisition 803

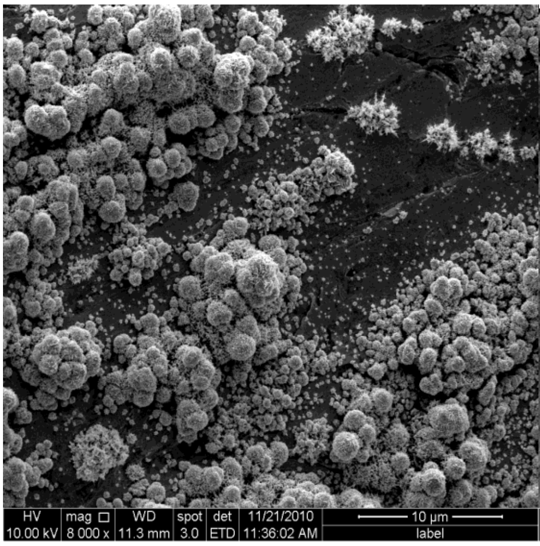
El	AN	Series	unn. C [wt.%]	norm. C [wt.%]	Atom. C [at.%]	Error [%]
Ta	73	M-series	2.91	3.19	3.47	0.3
Au	79	M-series	88.40	96.81	96.53	3.5
		Total:	91.32	100.00	100.00	



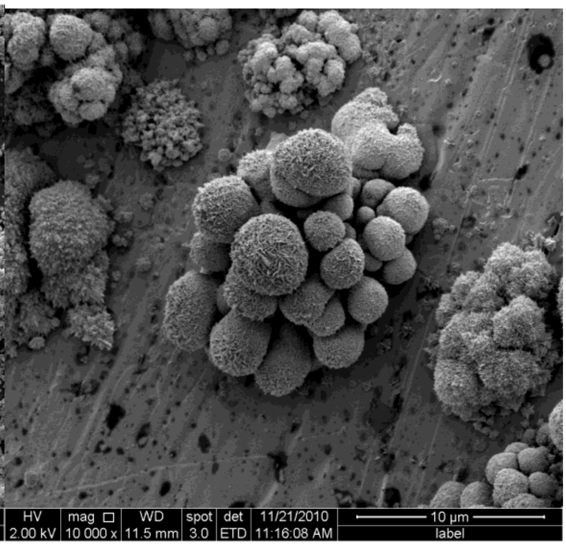
b

Figure 40-b EDX spectra of flower gold deposited on tantalum substrate. Parameters of the experiment E_L = -0.6, E_H = 0.00 V centered at = -0.3V, amplitude = 0.6V, frequency = 100 Hz, gold concentration = 10^{-3} M, time = 120 seconds and scan rate of 100 mV/ s. (b)

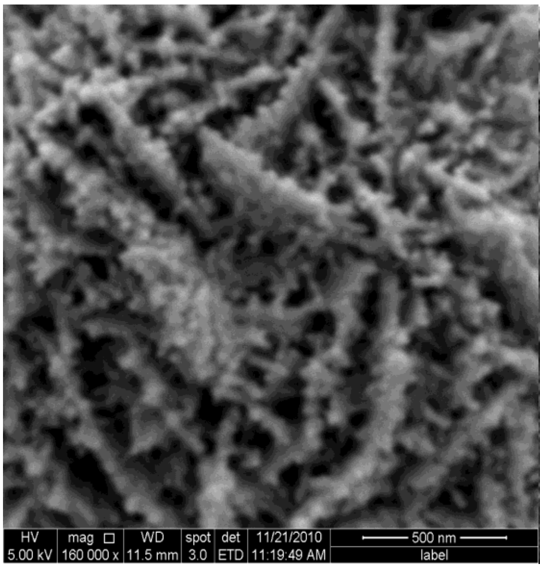
Figure 41 shows the SEM image are prepared thorn-flower like gold at 900 s deposition time with square wave amplitude 0.6 V; flower-like gold formation at higher concentration 10^{-3} M and longer deposition time. The thorn-flower like gold is was not distributed over the entire surface. Growth of thorn-flower like gold microcrystals at ambient temperatures on tantalum wire.



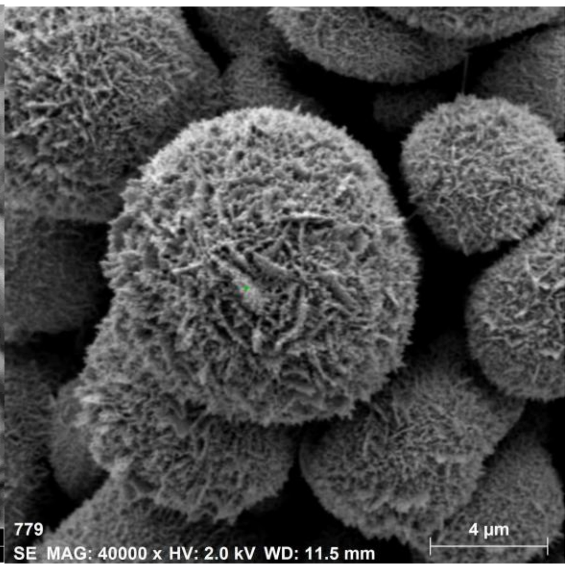
41-a



41-b



41-c



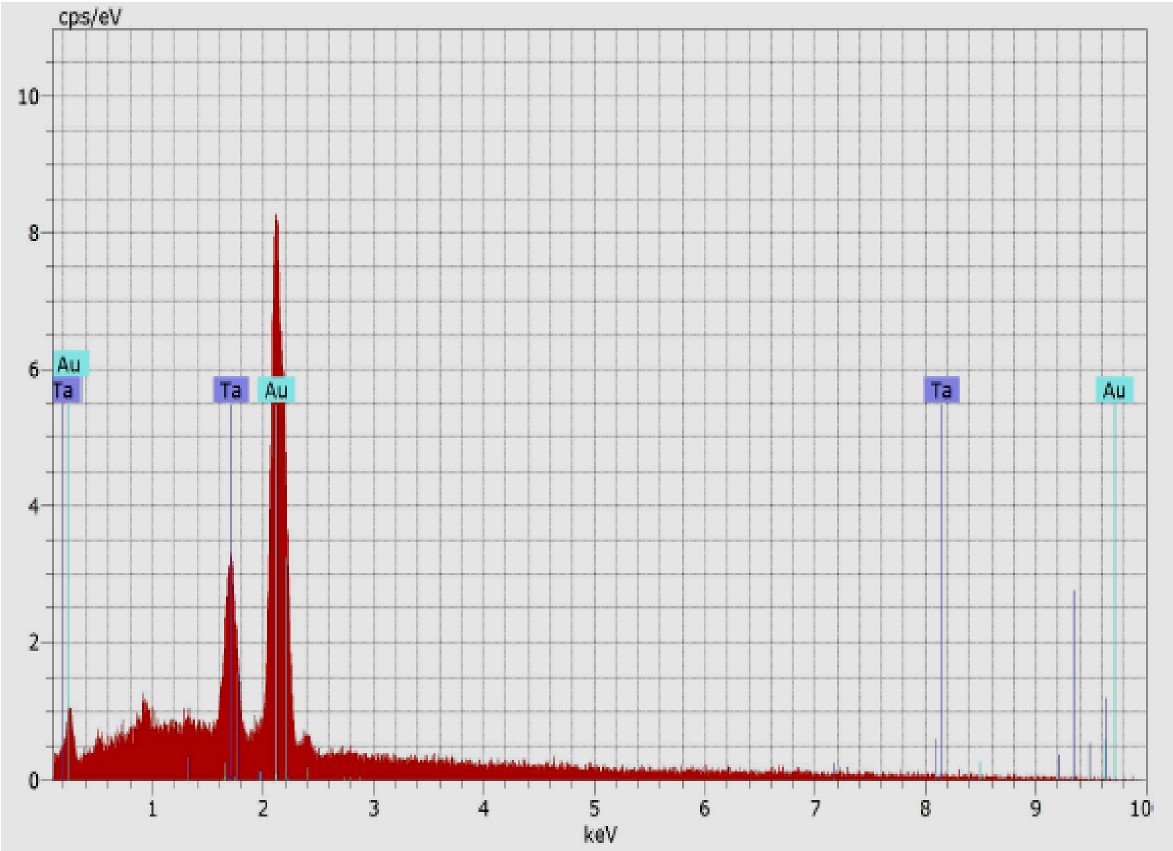
41-d

Figure 41-(a-d): SEM images deposition gold nanostructures on tantalum. Parameters of the experiment E_L = -0.6, E_H = 0.00 V centered at = -0.3V, amplitude = 0.6V, frequency = 100 Hz, gold concentration = 10^{-3} M, time = 900 seconds and at a scan rate of 100 mV/ s

Figure 41-b shows the EDX spectra, the analysis of flower-like gold and proves that the product is gold.

Spectrum: Acquisition 684

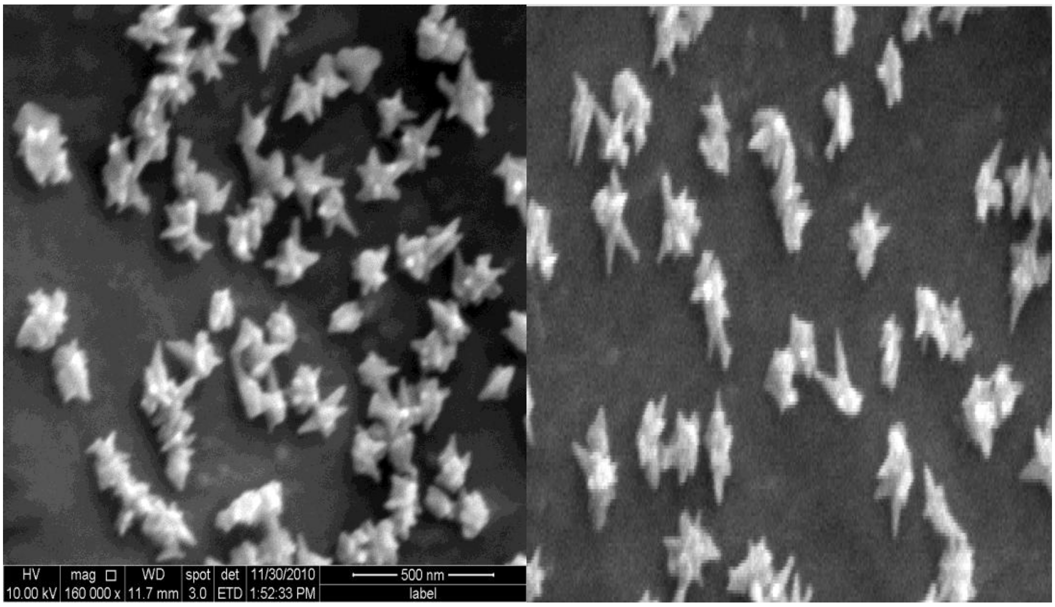
El	AN	Series	unn. C [wt.%]	norm. C [wt.%]	Atom. C [at.%]	Error [%]
Ta	73	M-series	21.73	11.95	12.87	1.2
Au	79	M-series	160.14	88.05	87.13	7.7
		Total:	181.87	100.00	100.00	



e

Figure 41-e EDX spectra of flower gold deposited on tantalum substrate. Parameters of the experiment E_L = -0.6, E_H = 0.00 V centered at = -0.3V, amplitude = 0.6V, frequency = 100 Hz, gold concentration = 10^{-3} M, time = 900 seconds and at a scan rate of 100 mV/ s.

Figure 42 shows the SEM micrograph prepared thorn-like gold nanoparticles that were obtained at 10^{-3} M gold concentration. Further investigation of the deposited nanoparticles indicates that the obtained particles are larger with an average size of about 42 nm and with an average distribution of 4.00×10^{9} particles/cm^{2}. The figure 42 shows the nanostructures thorn shape has formed a layer. Figure 42-c shows of the EDX spectra the analysis of thorn-like gold and proves that the product is gold.



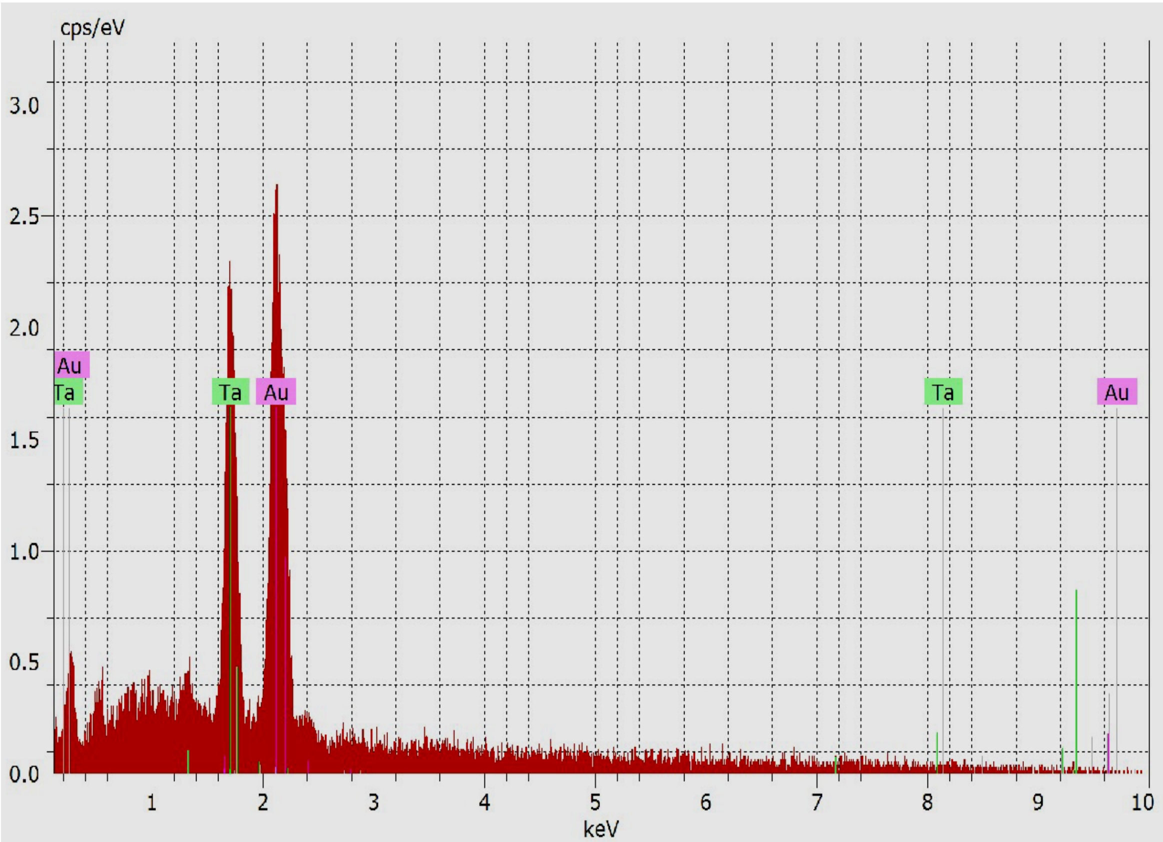
42- a

42- b

Figure 42: SEM images (a and b) deposition gold nanostructures on tantalum. Parameters of the experiment E_L = -0.6, E_H = -0.2 V centered at = -0.4V, amplitude = 0.4V, frequency = 100 Hz, gold concentration = 10^{-3} M, deposition time = 300 seconds and scan rate of 100 mV/ s.(

Spectrum: Acquisition 751

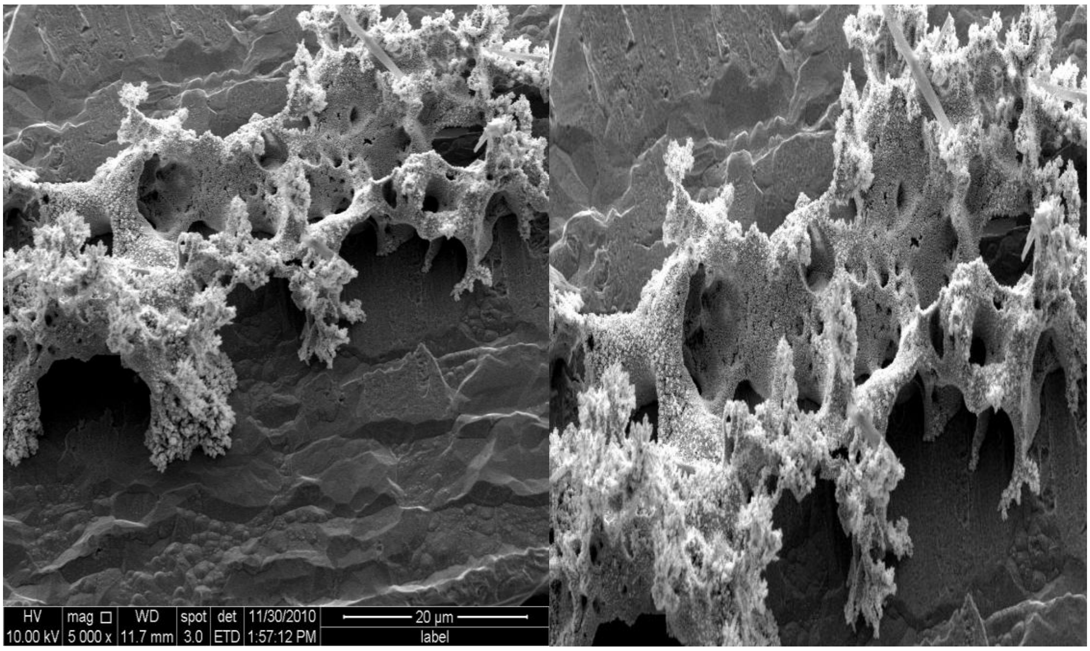
El	AN	Series	unn. C [wt.%]	norm. C [wt.%]	Atom. C [at.%]	Error [%]
Ta	73	M-series	27.79	29.53	31.33	1.4
Au	79	M-series	66.31	70.47	68.67	2.8
		Total:	94.10	100.00	100.00	



c

Figure 42 :(c) EDX spectra of thorn gold deposited on tantalum substrate. Parameters of the experiment E_L = -0.6, E_H = -0.2 V centered at = -0.4V, amplitude = 0.4V, frequency = 100 Hz, gold concentration = 10^{-3} M, deposition time = 300 seconds and scan rate of 100 mV/ s

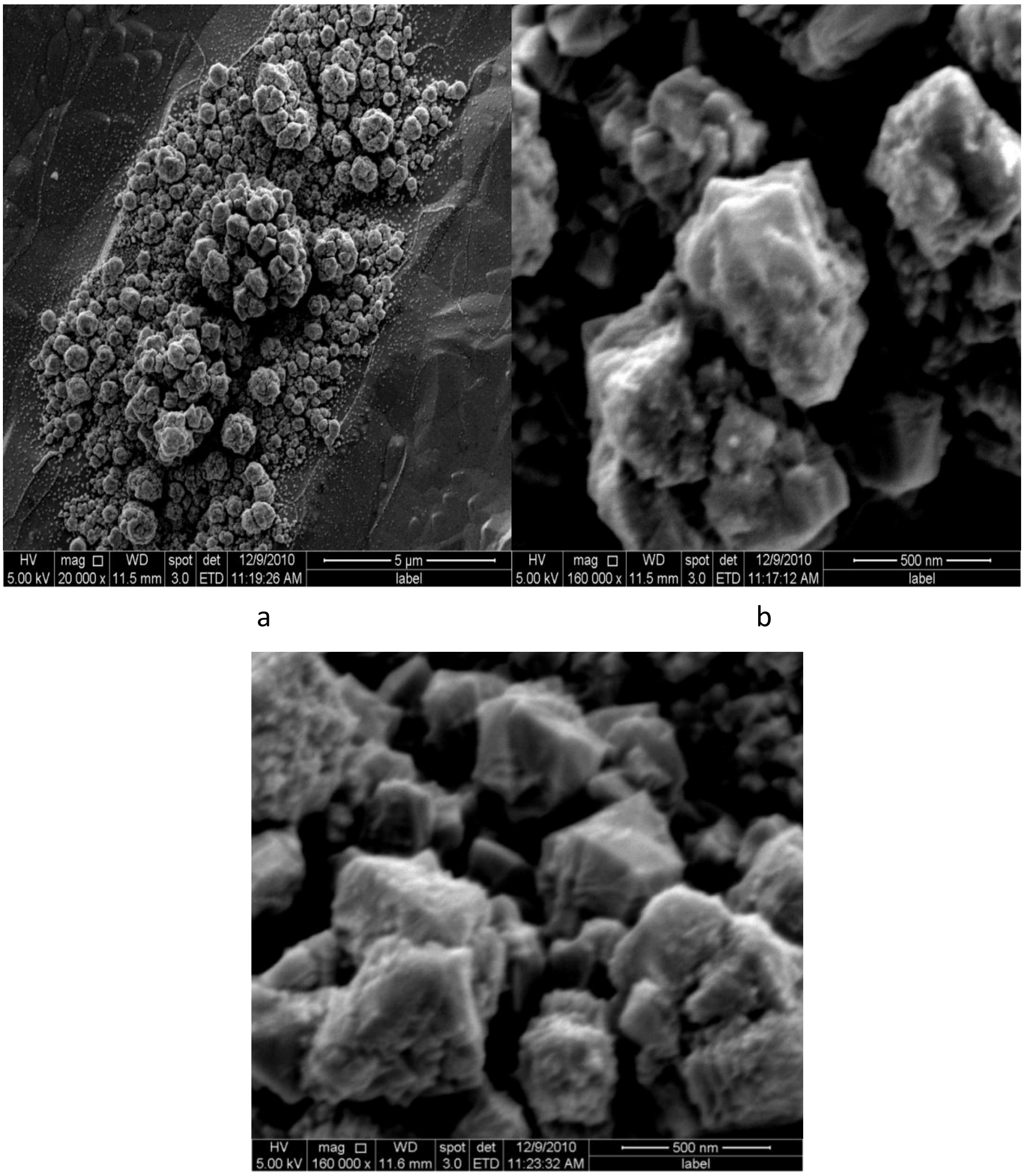
Figure 43 shows the SEM micrographs are prepared spongy- like gold at 300s deposition time; the sponge-like gold is formed on a tantalum surface at 10^{-3} M gold solution concentration with long deposition time. The sponge-like gold was not distributed over the entire surface.



a b

Figure 43: SEM images (a and b) deposition gold nanostructures on tantalum. Parameters of the experiment E_L = -0.6, E_H = -0.2 V centered at = -0.4V, amplitude = 0.4V, frequency = 100 Hz, gold concentration = 10^{-3} M, time = 300 seconds and scan rate of 100 mV/ s.

Figure 44 shows the SEM image which prepared as twinned- like gold at 180 s deposition time. The twinned-like gold has formed at 10^{-3} M gold solution and long deposition time. The twinned-flower like gold is distributed on the surface.

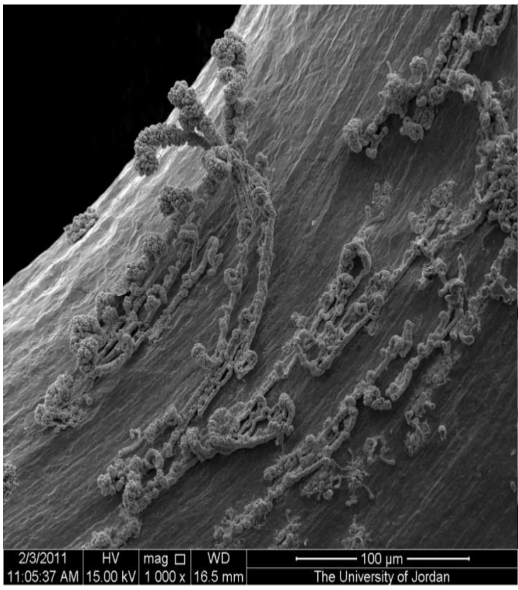


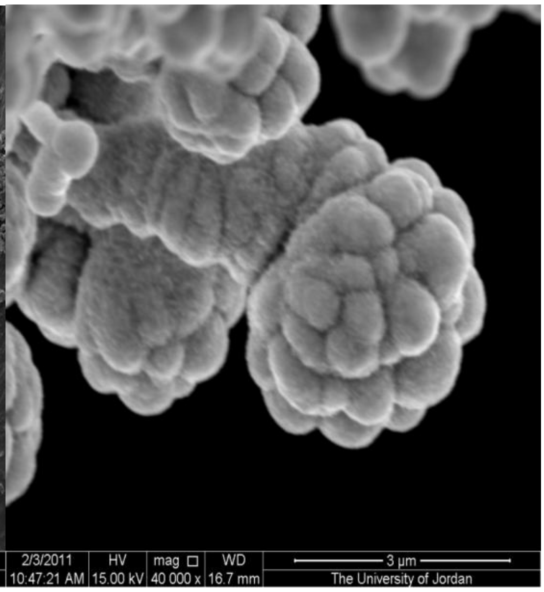
a b

c

Figure 44: SEM images (a, b and c) deposition gold nanostructures on tantalum. Parameters of the experiment E_L = -0.7, E_H = -0.3 V centered at = -0.5V, amplitude = 0.4V, frequency = 100 Hz, gold concentration = 10^{-3} M, time = 180 seconds and scan rate of 100 mV/ s.

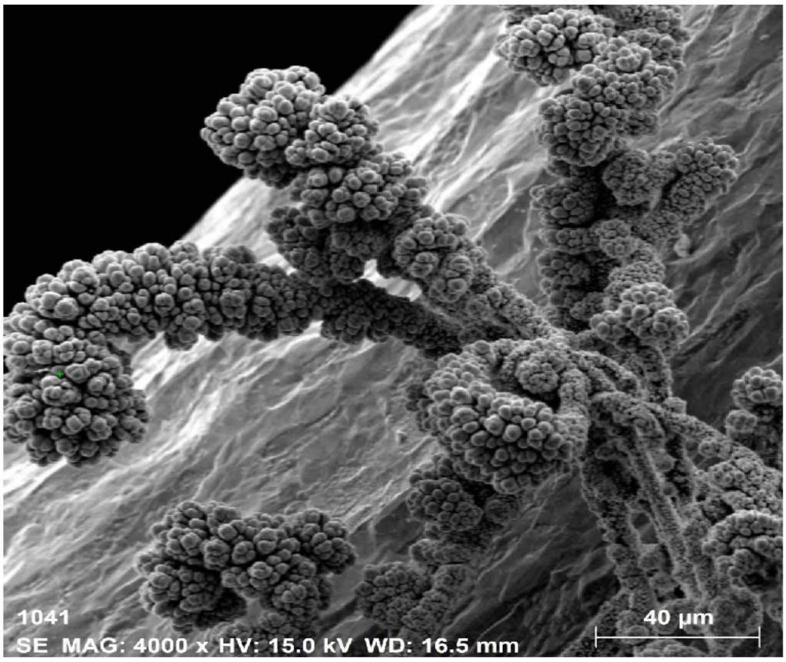
Figure 45 a-c show the SEM image are prepared epitaxial growth gold at 30s deposition time; epitaxial growth gold formation at higher concentration and little deposition time. The epitaxial growth gold distribution on the surface.





45- a

45- b



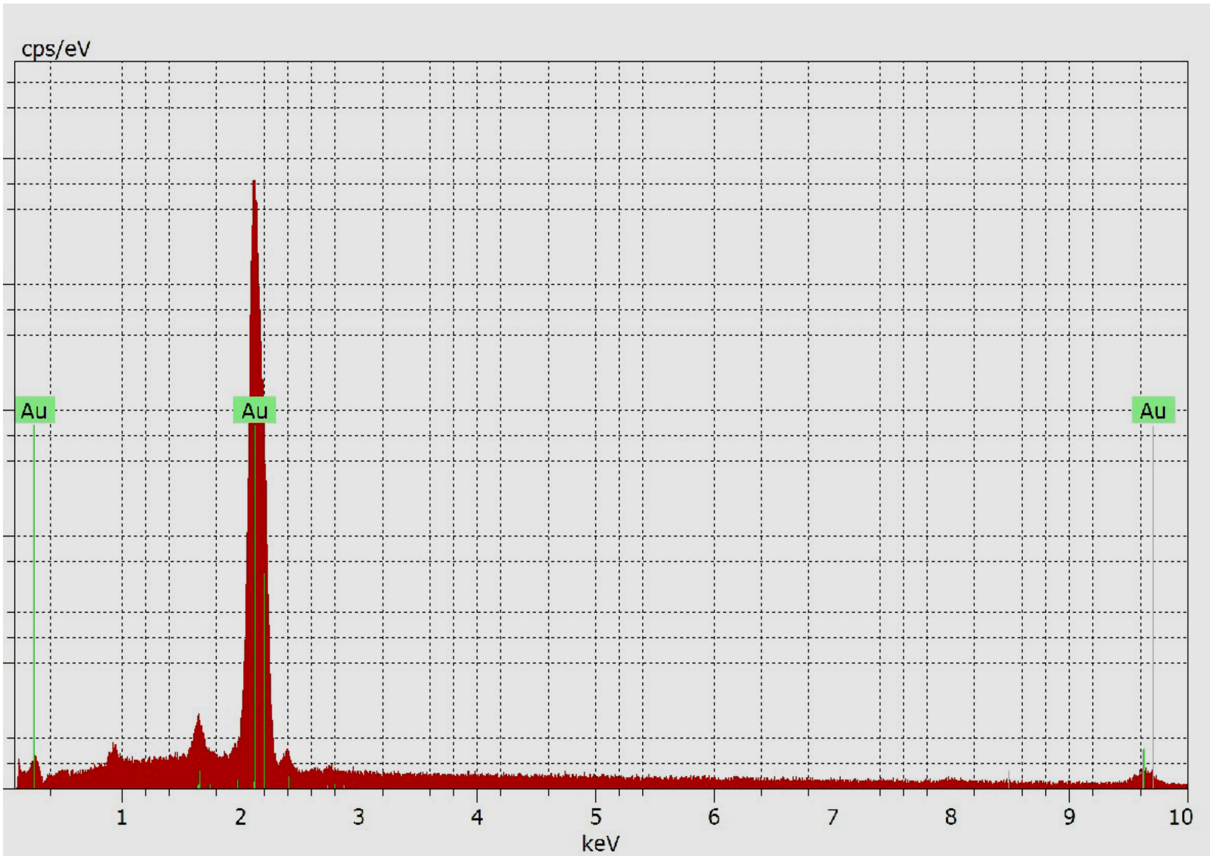
45- c

Figure 45: SEM images (a-c) deposition gold nanostructures on tantalum. Parameters of the experiment E_L= -0.6, E_H= 0.0 V centered at = -0.3V, amplitude = 0.6V, frequency = 100 Hz, gold concentration = 10^{-2} M, time = 30 seconds and scan rate of 100 mV/ s

Figure 45-d shows the EDX spectra the analysis of epitaxial growth gold and proves that the product is gold.

Spectrum: Acquisition 954

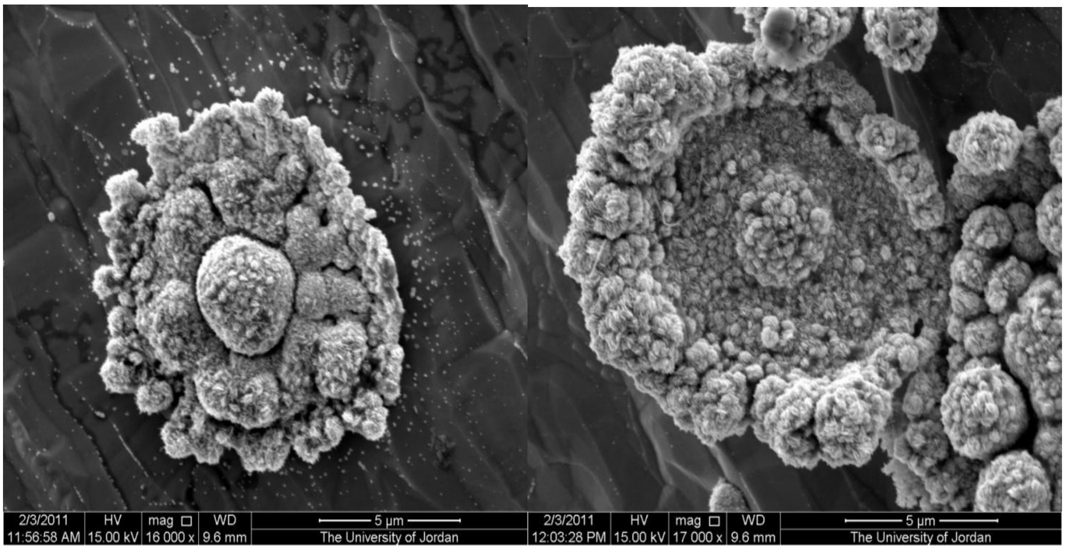
El	AN	Series	unn. C [wt.%]	norm. C [wt.%]	Atom. C [at.%]	Error [%]
Au	79	M-series	93.01	100.00	100.00	3.5
		Total:	93.01	100.00	100.00	



d

Figure 45: (d) EDX deposition of gold nanostructures on tantalum. Parameters of the experiment E_L= -0.6, E_H= 0.0 V centered at = -0.3V, amplitude = 0.6V, frequency = 100 Hz, gold concentration = 10^{-2} M, time = 30 seconds and scan rate of 100 mV/ s.

Figures 46-48 show SEM image are prepared co-flower- like gold at different potential values of -0.1 and -0.4 V centered at amplitude square wave 0.6 V and 60s deposition time. Figures 46 and 47 shows the SEM micrographs the co-flower like gold formation at potential -0.1V at centered amplitude 0.6V, higher concentration 10^{-2}M and little deposition time. The co-flower like gold was distributed on the surface with different sizes. Figure 47-c shows the EDX a spectrum proves the analysis of the co-flower gold and does not contain any impurities.



a b

Figure 46: SEM images (a and b) deposition gold nanostructures on tantalum. Parameters of the experiment E_L = -0.4, E_H = +0.2 V centered at = -0.1V, amplitude = 0.6V, frequency = 500 Hz, gold concentration = 10^{-2} M, time = 60 seconds and scan rate of 100 mV/ s.

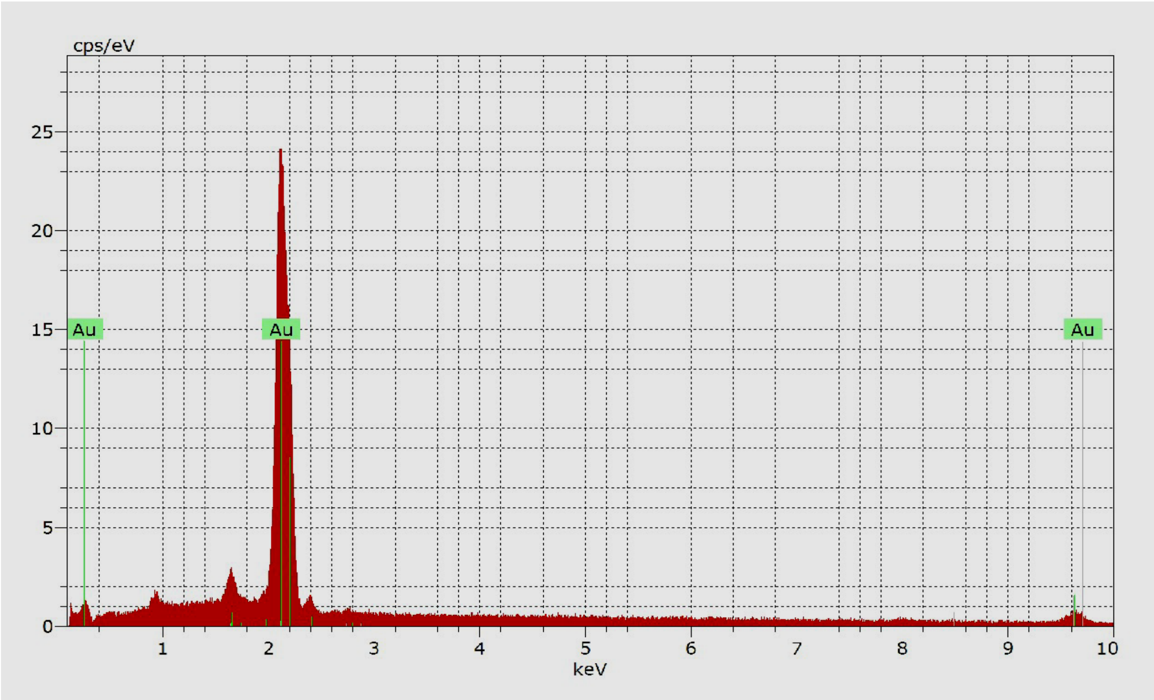


a

Figure 47: SEM images (a) deposition gold nanostructure on tantalum. Parameters of the experiment E_L = -0.4, E_H = +0.2 V centered at = -0.1V, amplitude = 0.6V, frequency = 100 Hz, gold concentration = 10^{-2} M, time = 60 seconds and scan rate of 100 mV/ s.

Spectrum: Acquisition 954

El	AN	Series	unn. C [wt.%]	norm. C [wt.%]	Atom. C [at.%]	Error [%]
Au	79	M-series	93.01	100.00	100.00	3.5
		Total:	93.01	100.00	100.00	



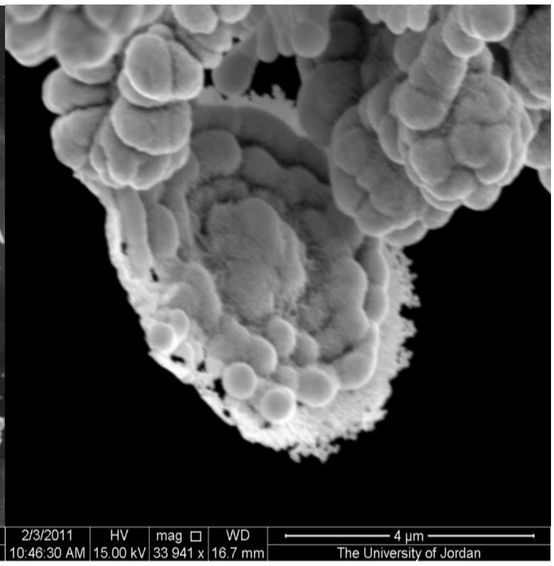
b

Figure 47: (b) EDX spectra of co-flower growth of gold deposited on tantalum substrate. Parameters of the experiment E_L = -0.4, E_H = +0.2 V centered at = -0.1V, amplitude = 0.6V, frequency = 100 Hz, gold concentration = 10^{-2} M, time = 60 seconds and scan rate of 100 mV/ s.

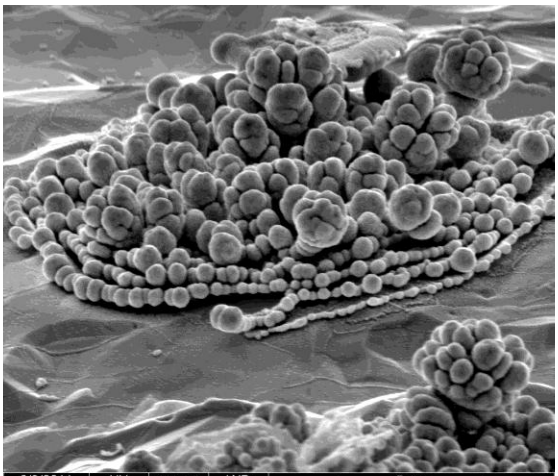
Figure 48 shows the SEM micrographs the co-flower like gold formation at potential of -0.4V at centered amplitude of 0.6V, higher concentration 10^{-2} M and 60s deposition time. Figure 48- c shows the SEM micrographs of co-flower gold, and show the epitaxial growth.



a



b



c

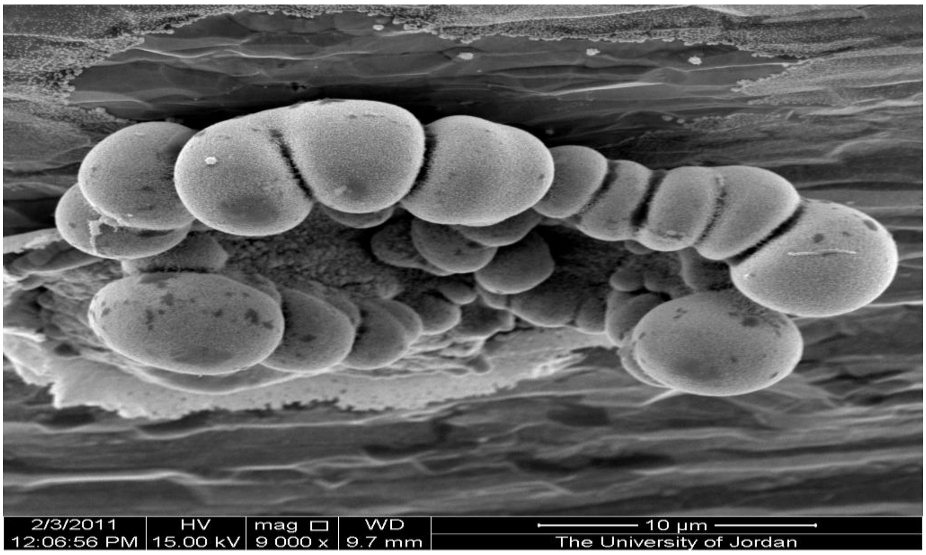
Figure 48a-c SEM images deposition of gold nanostructures on tantalum. Parameters of the experiment E_L = -0.7, E_H = -0.1 V centered at = -0.4V, amplitude = 0.6V, frequency = 100 Hz, gold concentration = 10^{-2} M, time = 60 seconds and scan rate of 100 mV/ s.

Figure 48 shows the SEM micrographs the co-flower like gold formation at potential of -0.4V at centered amplitude of 0.6V, higher concentration 10^{-2} M and 60s deposition time.



d

Figure 48-d: SEM images deposition gold nanostructures on tantalum. Parameters of the experiment E_L = -0.7, E_H = -0.1 V centered at = -0.4V, amplitude = 0.6V, frequency = 100 Hz, gold concentration = 10^{-2} M, time = 60 seconds and scan rate of 100 mV/ s.



e

Figure 48-e: SEM images deposition of gold nanostructures on tantalum. Parameters of the experiment E_L = -0.7, E_H = -0.1 V centered at = -0.4V, amplitude = 0.6V, frequency = 500 Hz, gold concentration = 10^{-2} M, time = 60 seconds and scan rate of 100 mV/ s.

Figure 49 shows the SEM micrographs of needles gold which are prepared at higher concentration and low deposition time. The figure 49 shows formation of needles on the surface of co-flower gold.

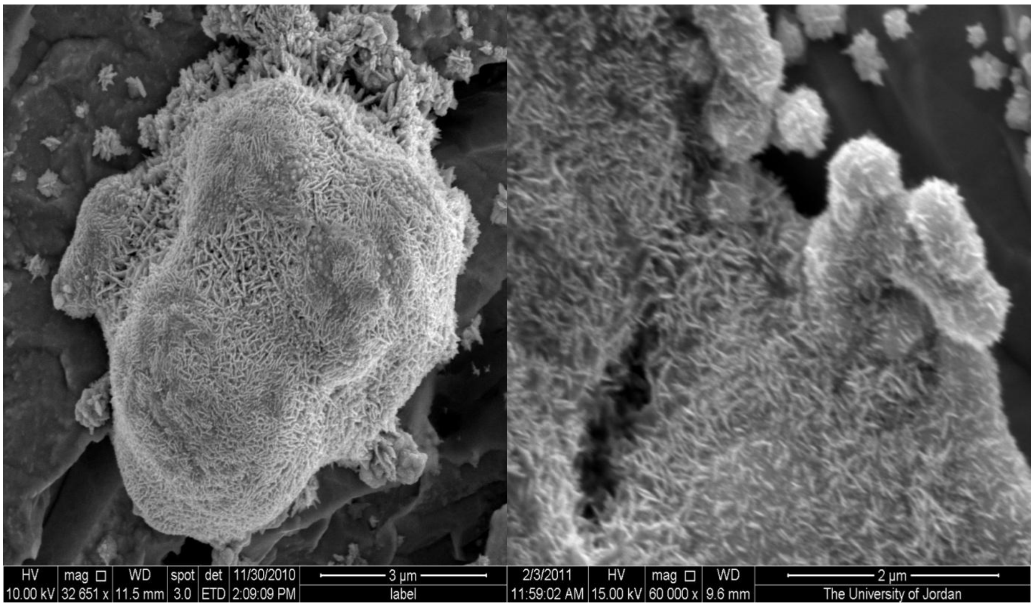


Figure 49: SEM images deposition of gold nanostructures on tantalum. Parameters of the experiment E_L = -0.4, E_H = +0.2 V centered at = -0.1V, amplitude = 0.6V, frequency = 100 Hz, gold concentration = 10^{-2} M, time = 60 seconds and scan rate of 100 mV/ s.

Figure 50 show the SEM micrographs of deposited gold nanostructures produced by application of square wave potential regime with different parameters. Strongly influenced by the properties of materials by the presence of grain boundaries. Low-angle grain boundaries consist of rows of separate disorders crystals separate from a slightly different direction. The disintegration of the first model proposed for the low-angle grain boundaries Taylor.

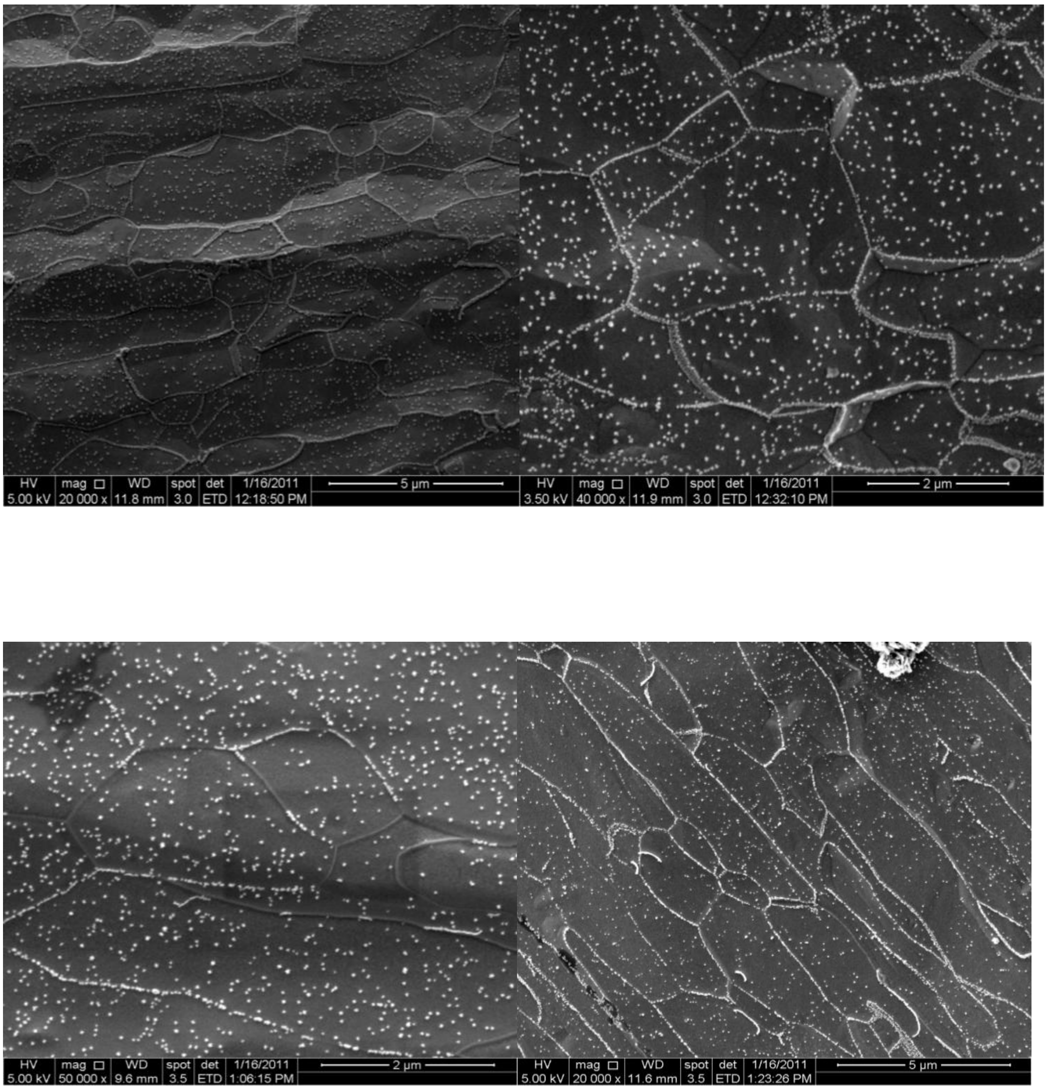


Figure 50: SEM image the grain boundaries of nanometric gold deposited on tantalum substrate at different conditions used in deposited gold

Table (4-a): comparing between all experiments of gold deposited.

Metal	CV figure	SEM figure	EDX figure	E_H V	E_L V	Center V	Amplitude V	Frequency Hz	Concentration M	Time seconds	Scan rate mV/s	Size nm	Area Particles cm^{-2}
gold	14(----)	15	----	-0.2	-0.6	-0.4	0.4	100	10^{-3}	120	100	26.6	8.80×10^9
gold	14(-----)	16	-----	+0.1	-0.9	-0.4	1.0	100	10^{-3}	120	100	------	7.40×10^9
gold	17(-----)	18	-----	-0.4	-0.8	-0.6	0.4	100	10^{-3}	120	100	------	9.60×10^9
gold	17(-----)	19	-----	-0.1	-1.1	-0.6	1.0	100	10^{-3}	120	100	------	6.40×10^9
gold	-------	20	-----	-0.2	-0.8	-0.5	0.6	100	10^{-3}	120	100	------	7.92×10^9
gold	-------	21	-----	-0.1	-0.9	-0.5	0.8	100	10^{-3}	120	100	------	6.40×10^9
gold	24	-----	-----	+0.1	-0.3	-0.1	0.4	100	10^{-3}	120,300 and 600	100	------	--------
gold	-----	25	-----	-0.2	-0.6	-0.4	0.4	100	10^{-3}	60	100	-----	6.69×10^9
gold	-----	26	-----	-0.2	-0.6	-0.4	0.4	100	10^{-3}	120	100	-----	3.21×10^9
gold	-----	27	----	-0.2	-0.6	-0.4	0.4	100	10^{-3}	300	100	-----	-------
gold	------	30	-----	-0.2	-0.8	-0.5	0.6	50	10^{-3}	60	100	32.5	2.40×10^9

Table (4-b): comparing between all experiments of gold deposited.

Metal	CV figure	SEM figure	EDX figure	E_H V	E_L V	Center V	Amplitude V	Frequency Hz	Concentration M	Time seconds	Scan rate mV/s	Size nm	Area Particles cm^{-2}
gold	------	31	-----	-0.2	-0.8	-0.5	0.6	100	10^{-3}	60	100	42.8	6.20×10^{9}
gold	------	32	-----	-0.2	-0.8	-0.5	0.6	1000	10^{-3}	60	100	30.45	1.24×10^{9}
gold	--------	36	----	+0.1	-0.7	-0.3	0.6	100	10^{-3}	30	100	11.3	4.40×10^{9}
gold	--------	37	-----	+0.1	-0.7	-0.3	0.6	100	10^{-4}	30	100	------	3.00×10^{9}
gold	-------	38	-----	+0.1	-0.3	-0.1	0.4	100	10^{-3}	900	100	------	----------
gold	-------	40-a	40-b	0.00	-0.6	-0.3	0.6	100	10^{-3}	120	100	------	-----------
gold	-------	41(a-d)	41-e	0.00	-0.6	-0.3	0.6	100	10^{-3}	900	100	------	-----------
gold	-------	42(a-b)	42-c	-0.2	-0.6	-0.4	0.4	100	10^{-3}	300	100	------	4.00×10^{9}
gold	-------	43	-------	-0.2	-0.6	-0.4	0.4	100	10^{-3}	300	100	------	----------

Table (4-c): comparing between all experiments of gold deposited.

Metal	CV figure	SEM figure	EDX figure	E_H V	E_L V	Center V	Amplitude V	Frequency Hz	Concentration M	Time seconds	Scan rate mV/s	Size nm	Area Particles cm^{-2}
gold	-------	44	------	-0.3	-0.7	-0.5	0.4	100	10^{-3}	180	100	------	-----------
gold	-------	45(a-c)	45-d	0.00	-0.6	-0.3	0.6	100	10^{-2}	30	100	------	-----------
gold	-------	47-a	47-b	-0.2	-0.4	-0.1	0.6	100	10^{-2}	60	100	-------	-----------
gold	-------	48(a-C)	-------	-0.1	-0.7	-0.4	0.6	100	10^{-2}	60	100	-------	----------
gold	------	49	-------	-0.2	-0.5	-0.1	0.6	100	10^{-2}	60	100	-------	----------

3.2. Silver nanometallic structures

3.2.1. The factors effect of nanostructures of silver

3.2.1.1. The effect of Hi and Lo values limited of square wave on the deposited nanoparticles

Figures 51-53 show the results extracted from the cyclic voltammogram of the deposited silver nanostructures produced by application of square wave potential regime with different amplitude centered at -0.2 V.

Square wave amplitude means the difference between the Hi and Lo of the square wave. In practice, changing the amplitude square wave also change the limits of the square wave, Hi and Lo values. Changing these values may shift the balance between oxidation and reduction during each cycle of the square wave. It may also affect the rates of particle nucleation and growth of the deposited particles.

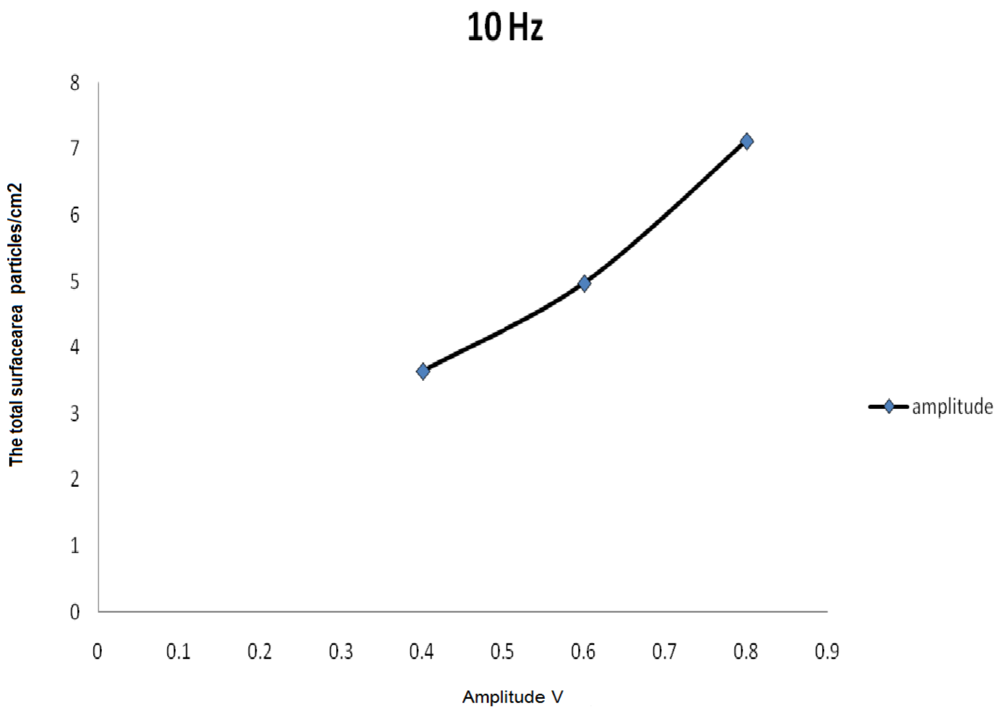


Figure 51: a plot of surface area vs. E_L and E_H values of Ag/Ta deposition silver nanostructures on tantalum. Parameters of the experiments amplitude 0.4, 0.6 and 0.8 V centered at = -0.2 V, frequency = 10 Hz, time = 60 seconds, silver concentration = 10^{-3} M and scan rate of 100 mV/ s.

Figure 51 shows that increasing the difference between E_H and E_LV values increases the amount of silver nanostructures deposited on surface.

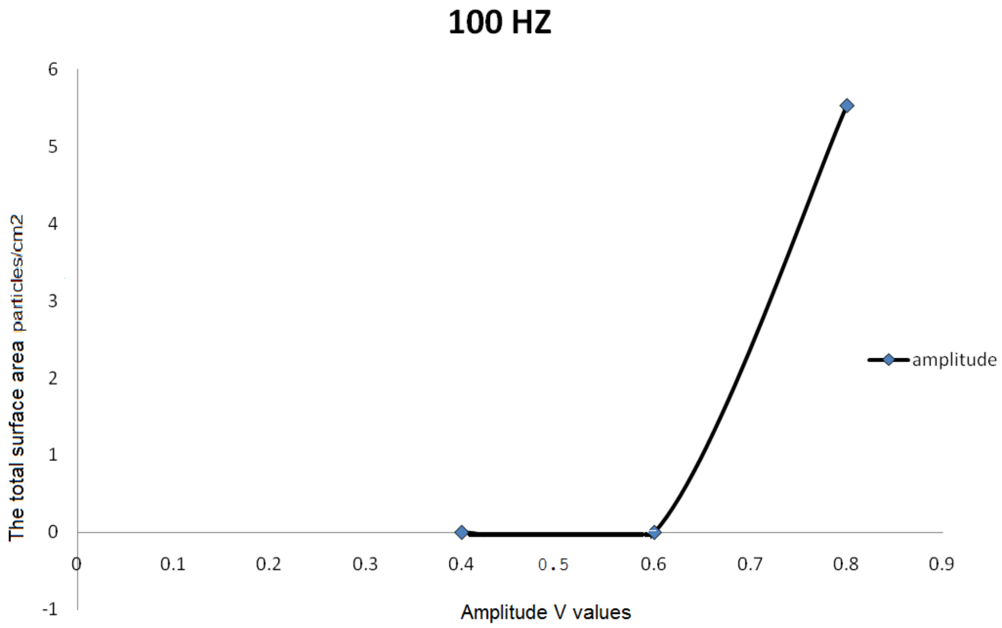


Figure 52: a plot surface area vs. E_L and E_H values of Ag/Ta deposition silver nanostructures on tantalum. Parameters of the experiments amplitude 0.4, 0.6 and 0.8 V centered at = -0.2 V, frequency = 100 Hz, time = 60 seconds, silver concentration = 10^{-3} M and scan rate of 100 mV/ s.

In figure 52 and 53, the surface areas from cyclic voltammogram at square wave at the amplitude 0.4 and 0.6 V are zero, but the 0.8 V amplitude shows the presence of silver deposited on tantalum substrate and a large amount of a large amount of silver deposited.

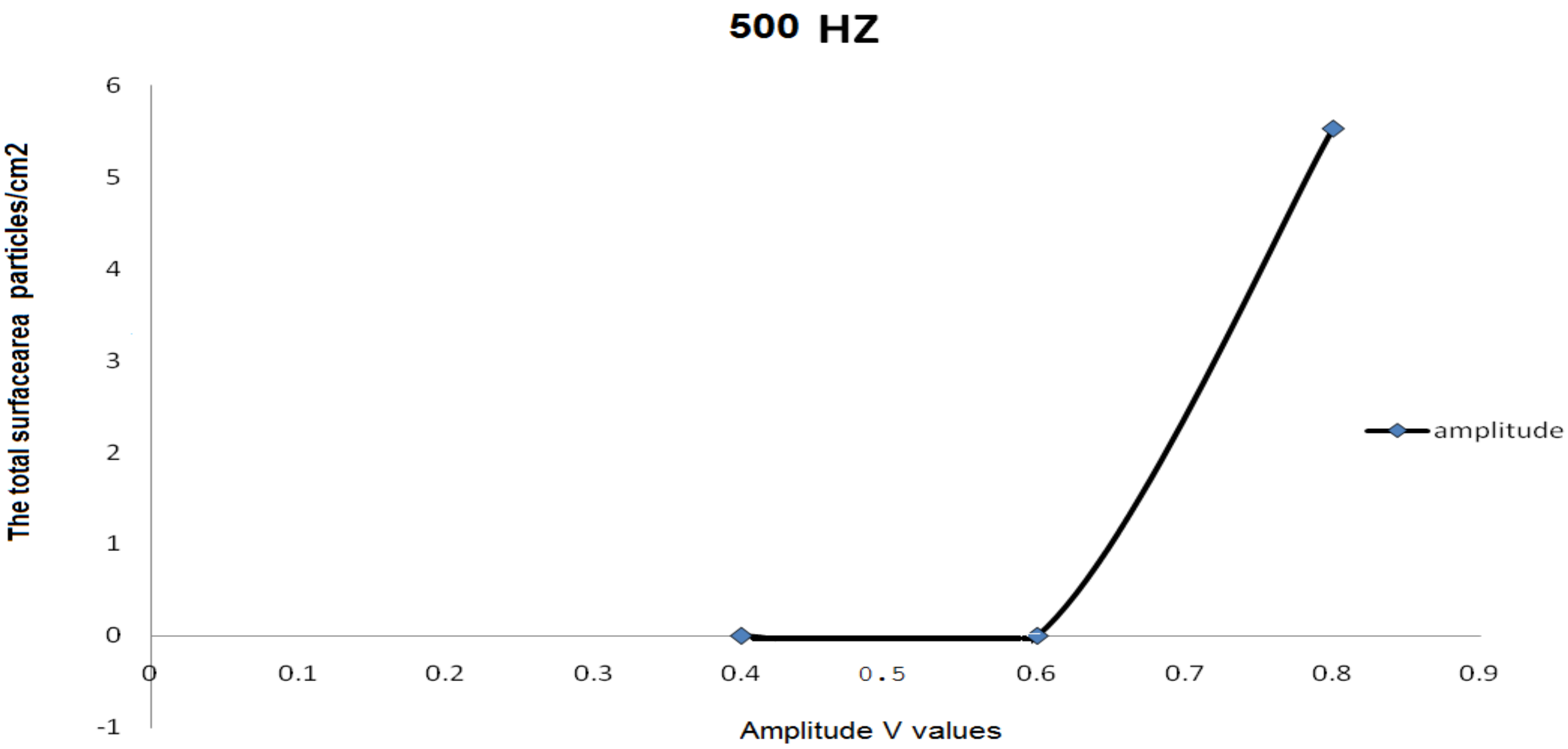


Figure 53: a plot surface area vs. EL and EH values of Ag/Ta deposition silver nanostructures on tantalum. Parameters of the experiments amplitude 0.4, 0.6 and 0.8 V centered at = -0.2 V, frequency = 500 Hz, time = 60 seconds, silver concentration = 10^{-3} M and scan rate of 100 mV/ s.

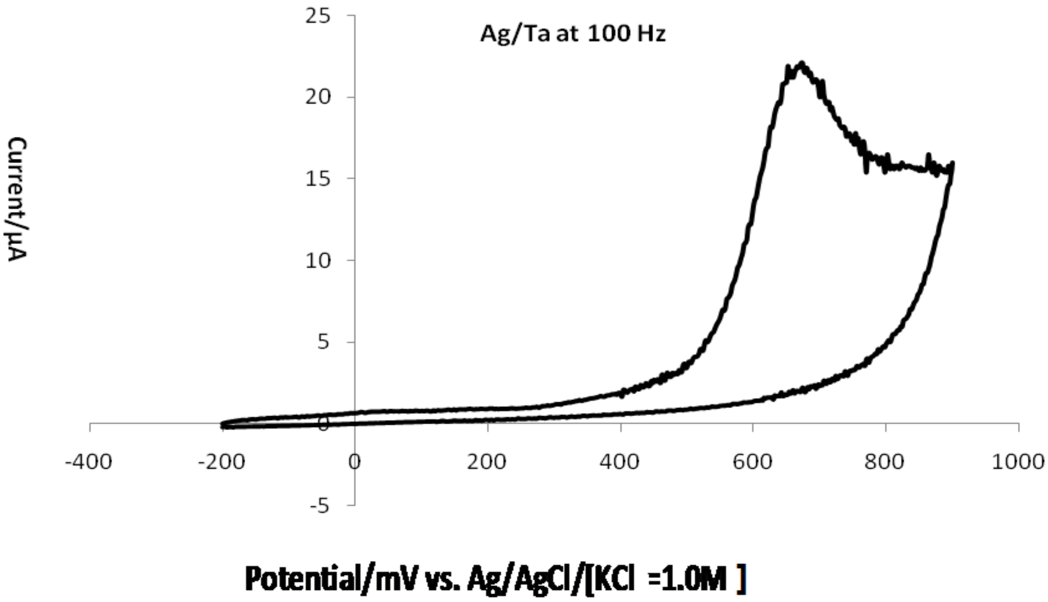


Figure 54: Cyclic voltammetry of Ag/Ta deposition silver nanostructures on tantalum. Parameters of the experiments E_H= 0.00 and E_L= -0.4 V with amplitude 0.4 V centered at = -0.2 V, frequency = 100 Hz, time = 60 seconds, silver concentration = 10^{-3} M and scan rate of 100 mV/ s.

Figure 54 proved that there is no deposition of silver nanostructures at square wave amplitude of 0.4 V. But the SEM micrograph proves that deposition of silver nanostructures on the surface; show figure 55 SEM images of silver nanostructures.

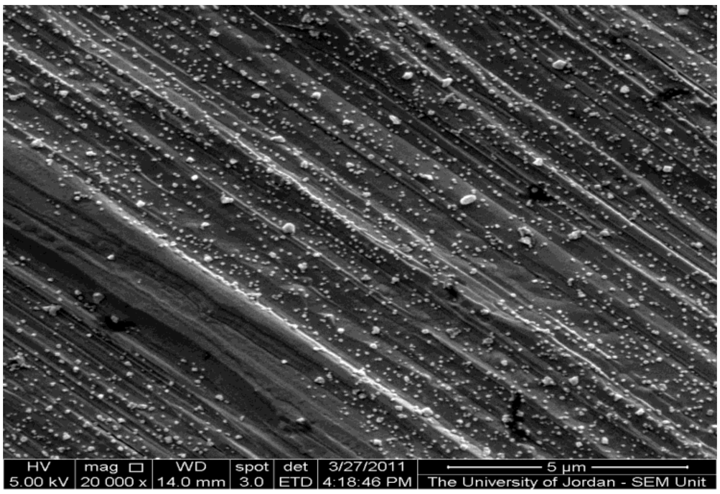


Figure 55: SEM image deposition of silver nanostructures on tantalum. Parameters of the experiment E_L = -0.4, E_H = 0.00 V centered at -0.2 V, amplitude 0.4V, 100 Hz, concentration 10^{-3} M, 60 seconds and at a scan rate of 100 mV/ s.

Figures 56 - 58 show the SEM micrographs for the deposited nanoparticles obtained with different amplitude of 0.6, 0.8 and 1.0 V. Figure 56 shows that the obtained particles at 0.6 V amplitude are small with an average distribution of 2.43× 10^9 particles/cm^2 and shows that the shape of particles is spherical silver nanostructures.

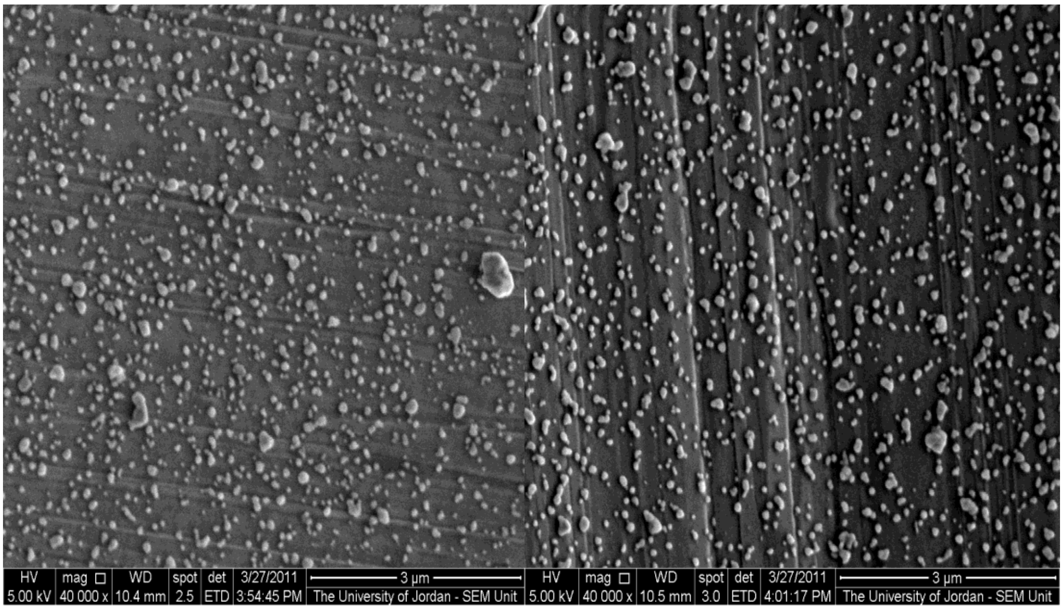


Figure 56: SEM images deposition silver nanostructures on tantalum. Parameters of the experiment E_L= -0.6, E_H = -0.1 V at centered -0.4, amplitude 0.6V, 50 Hz, concentration 10^{-3} M, 60 seconds and at a scan rate of 100 mV/ s.

Figure 57 and 58 shows the SEM micrograph for the deposited nanoparticles obtained with different amplitude 0.8 and 1.0V.Figure 57 shows the nanostructures at 0.8 amplitude with spherical shape. Further investigation of the deposited nanoparticles indicates that the obtained particles are smaller than nanoparticles are formed at square wave amplitude 0.6 and 0.8 V; with an average distribution of 4.30 × 10^9 particles/cm^2.

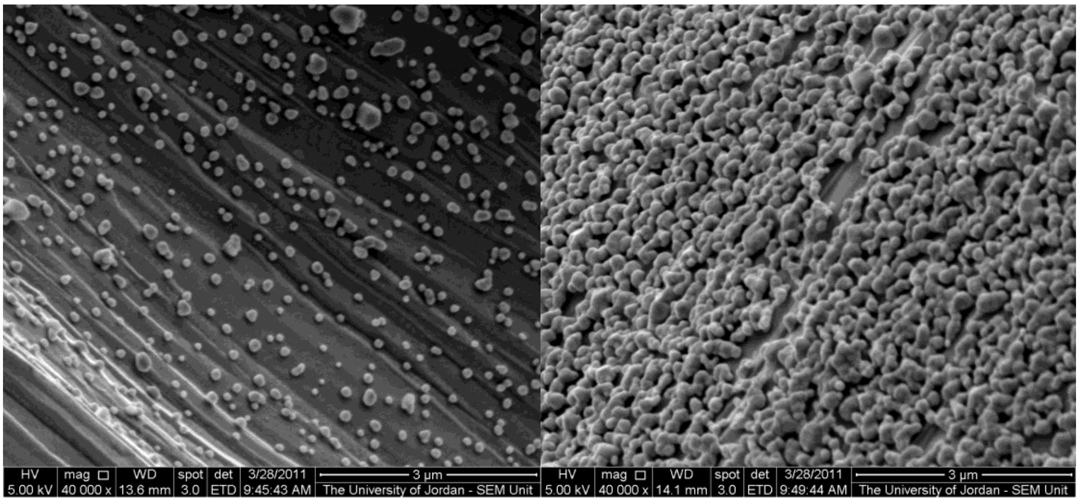


Figure 57: SEM images deposition of silver nanostructures on tantalum. Parameters of the experiment E_L= -0.8, E_H = 0.00 V at centered -0.4V, amplitude 0.8V, 50 Hz, concentration 10^{-3} M, 60 seconds and at a scan rate of 100 mV/ s.

Figure 58 shows the SEM micrographs of silver nanostructures at 1.0 V amplitude with different shape formed as a layer and different size of nanoparticles. Further investigation of the deposited nanoparticles indicates that the obtained particles are large than nanoparticles were formed at 0.4 and 0.6V amplitude square wave with an average distribution of 7.00×10^9 particles/cm^2.

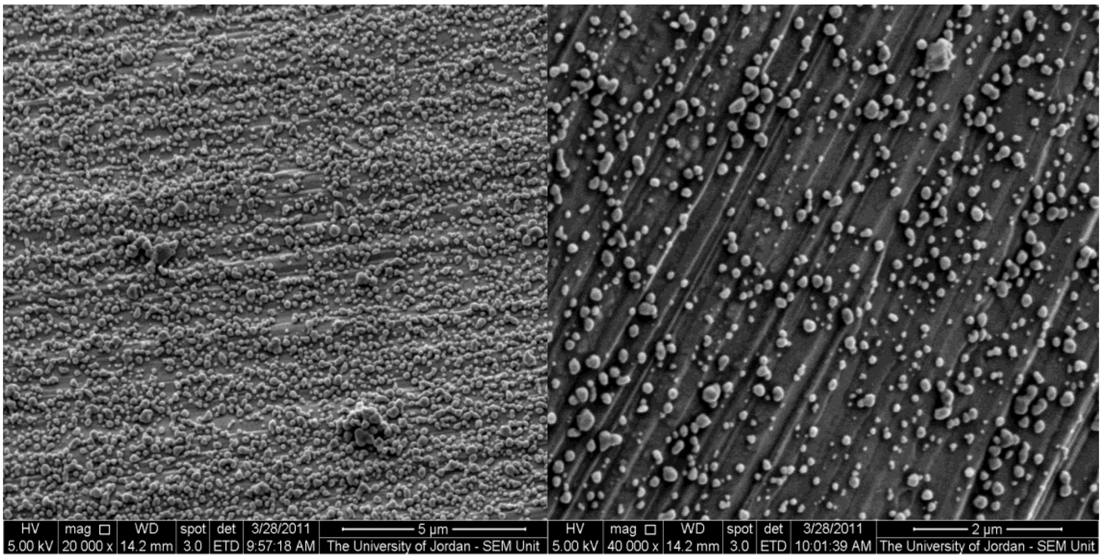


Figure 58: SEM images deposition of silver nanostructures on tantalum. Parameters of the experiment E_L = -0.9, E_h = +0.1 V centered at = -0.4V, amplitude = 1.0V, frequency = 50 Hz, silver concentration 10^{-3} M, time = 60 seconds and scan rate of 100 mV/ s.

3.2.1.2. The effect of deposition time:

Figures 59 and 60 show the SEM micrographs of deposited silver nano-structures produced by application of square wave potential regime with different time of 120 and 60 seconds. Figure 59 shows the SEM micrographs for the surface produced by deposition of silver nanoparticles by application of square wave with 60s deposition time. Figure 59 shows SEM micrographs deposited silver nanoparticles as evidenced by the EDX spectra. Moreover, both SEM micrographs show enhanced deposition along the nanodendrites and a variation in particle size. The long deposition time allow a growth of nanoparticles and thus leads to the formation of nanodendrites. The average particle size upon 120s deposition time is apparently larger that in case of 60s deposition time. The total surface area is larger for the smaller particle size nanostructures at a little deposition time.

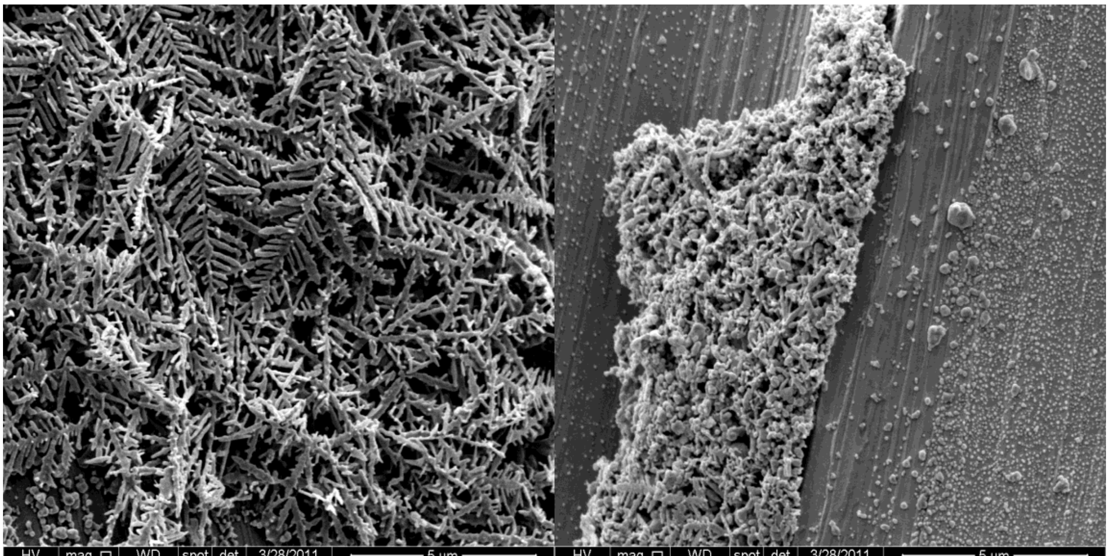


Figure 59: SEM images deposition of silver nanostructures on tantalum. Parameters of the experiment E_L = -0.6, E_H = 0.00 V centered at = -0.3V, amplitude = 0.6V, frequency = 100 Hz, silver concentration 10^{-3} M, time = 120 seconds and scan rate of 100 mV/ s.

Figure 60 shows the nanostructures at 60s deposition time with uniformly shape layer, equal size of nanoparticles and distribution on the surface. Further investigation of the deposited nanoparticles indicates that the obtained particles are smaller and with an average distribution of 3.50 × 10^9 particles/cm^2.the better uniformity, homogeneity and spherical shape on the surface.

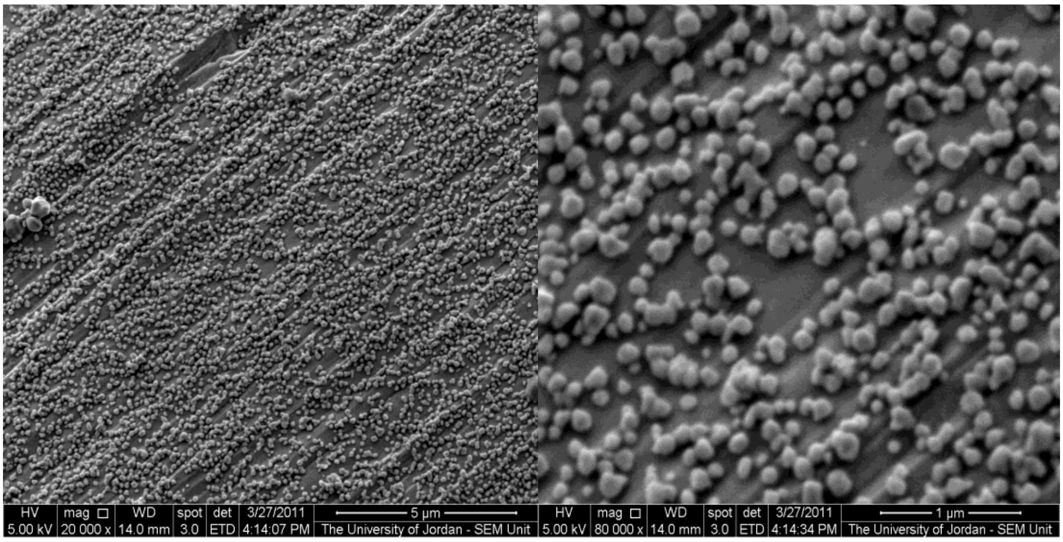


Figure 60: SEM images deposition of silver nanostructures on tantalum. Parameters of the experiment E_L = -0.6, E_H = 0.00 V centered at = -0.3V, amplitude = 0.6V, frequency = 100 Hz, silver concentration 10^{-3} M, time = 60 seconds and scan rate of 100 mV/ s.

3.2.1.3. The concentration effect of deposition of nanostructures of silver

Figure 61 shows the results extracted from the cyclic voltammograms of deposited silver nanostructures produced by application of square wave potential regime with different concentration (10^{-3} and 10^{-4}) M. The total surface area at the concentration of 10^{-4} M is larger than the concentration 10^{-3} M. This is attributed to the fact that the size of the particles produced at higher concentration is larger as evidenced from the SEM micrographs. This might be explained on basis of the enhanced rate particle growth at higher concentration. The smaller particles contribution to the surface area is greater than the larger and aggregated particles.

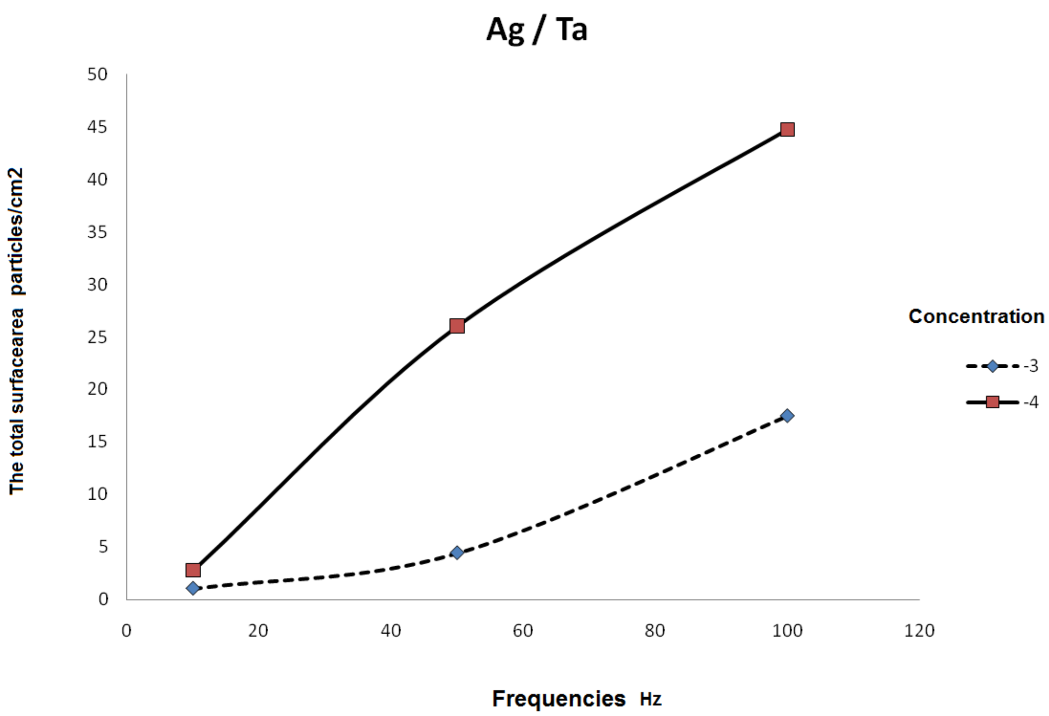


Figure 61: plot of surface area vs. frequency of deposition silver nanostructures on tantalum. Parameters of the experiment E_l = -0.5 V, E_h = - 0.1V centered at = -0.3V, amplitude = 0.4V, time = 60 seconds and scan rate of 100 mV/ s.

Figure 62 shows the SEM micrographs of silver nanostructures at 10^{-3} M silver concentration with various shapes. Further investigation of the deposited nanoparticles indicates that the obtained particles are larger particles, growth of particles and the total surface is smaller covered with silver nanostructures.

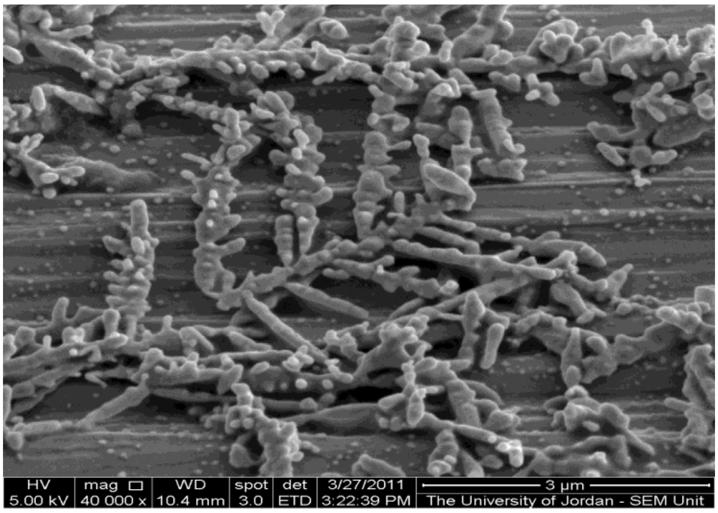


Figure 62: SEM image deposition silver nanostructures on tantalum. Parameters of the experiment E_L= -0.5, E_H = + 0.1 V centered at = -0.3V, amplitude = 0.4V, frequency = 100 Hz, silver concentration 10^{-3} M, time = 60 seconds and scan rate of 100 mV/ s.

Figure 63 shows the SEM micrographs of silver nanostructures at 10^{-4} M silver concentration with egalitarian shape formed; homogenous; similar size of nanoparticles formed and distribution on the surface. Further investigation of the deposited nanoparticles indicates that the obtained particles are larger than concentration 10^{-3} M silver solution used in deposition with an average distribution of 2.20×10^{9} particles/cm^{2}.

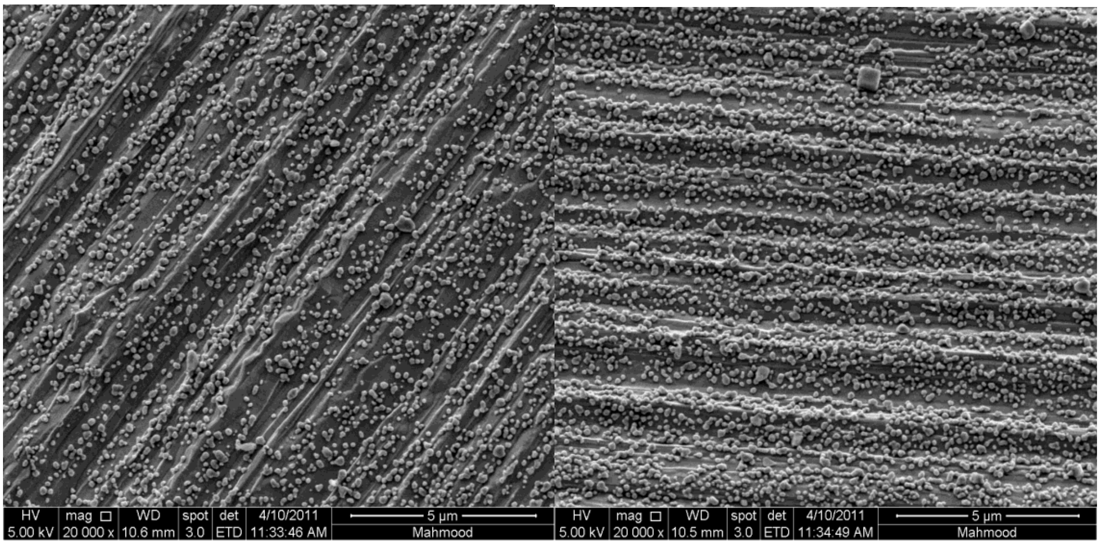


Figure 63: SEM images deposition silver nanostructures on tantalum. Parameters of the experiment E_L = -0.5V, E_H = + 0.1 V centered at = -0.3V, amplitude = 0.4V, frequency = 100 Hz, silver concentration = 10^{-4} M, time = 60 seconds and scan rate of 100 mV/ s.

The concentration 10^{-4} M of silver solution used in deposited is better than the concentration 10^{-3} M. at concentration 10^{-4} M the total surface area is larger than the concentration 10^{-3} M uses in deposited of silver nanostructures.

3.2.1.4. Frequency effect on the deposited nanostructures

Figures 64 and 65 show the SEM images of deposited silver nanostructures produced by application of square wave potential regime with frequency 10 Hz and 100 Hz. Frequency significantly affects the size of the nanoparticles, uniformity and their distribution on the surface.

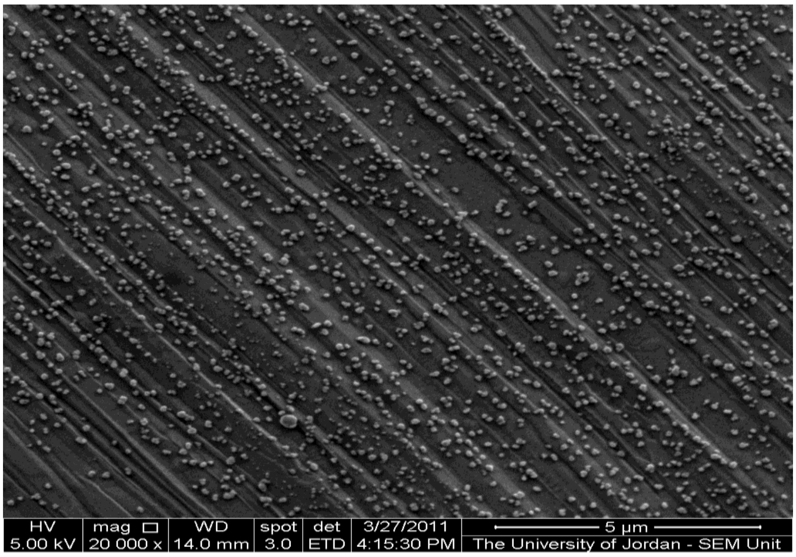


Figure 64: SEM images deposition of silver nanostructures on tantalum. Parameters of the experiment E_L = -0.7, E_H = - 0.1 V centered at = -0.4V, amplitude = 0.6V, frequency = 10 Hz, silver concentration 10^{-3} M, time = 60 seconds and scan rate of 100 mV/ s.

Figure 64 shows the SEM micrographs of silver nanostructures at frequency 10 Hz with same shape formed a layer; homogenous; similar size of nanoparticles formed and distribution on the surface. Further investigation of the deposited nanoparticles indicates that the obtained particles have an average distribution of 2.40 $\times 10^9$ particles/cm^2.

Figure 65 shows the silver nanostructures deposited at 100 Hz frequency square wave where an egalitarian shape is formed; homogenous, with similar size of nanoparticles and uniform distribution on the surface. Further investigation of the deposited nanoparticles indicates that the obtained particles are distributed systemically, with good uniformity, similar shape, size of nanoparticles and the number of nanoparticles is larger than the frequency 10 Hz with an average distribution of 3.50×10^9 particles/cm^2.

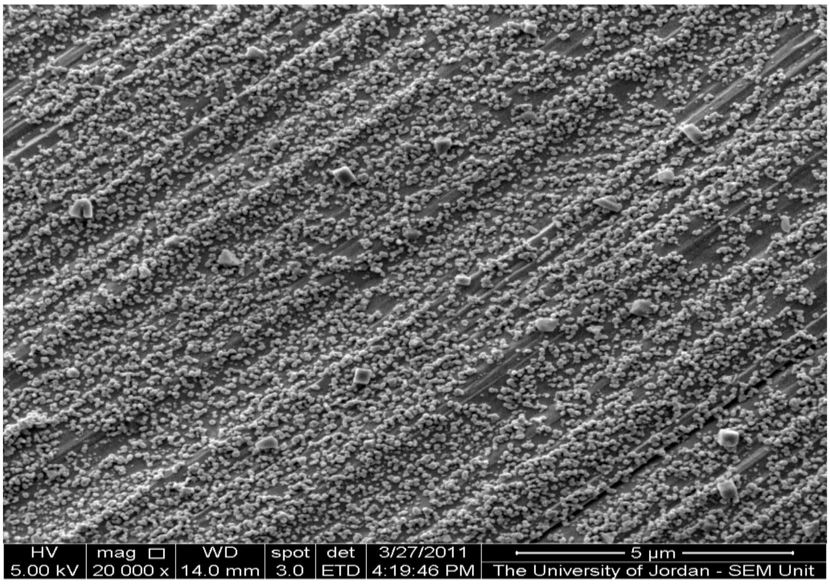


Figure 65: SEM image deposition silver nanostructures on tantalum. Parameters of the experiment: E_L = -0.7V, E_H = - 0.1 V centered at = -0.4V, amplitude = 0.6V, frequency = 100 Hz, silver concentration = 10^{-3} M, time = 60 seconds and scan rate of 100 mV/ s.

Figure 66 shows the relation between the total surface area calculated from SEM images and frequencies. The total surface area increases with the frequencies increase 10, 50 and 100 Hz respectively. At frequency 100 Hz total surface area is the largest.

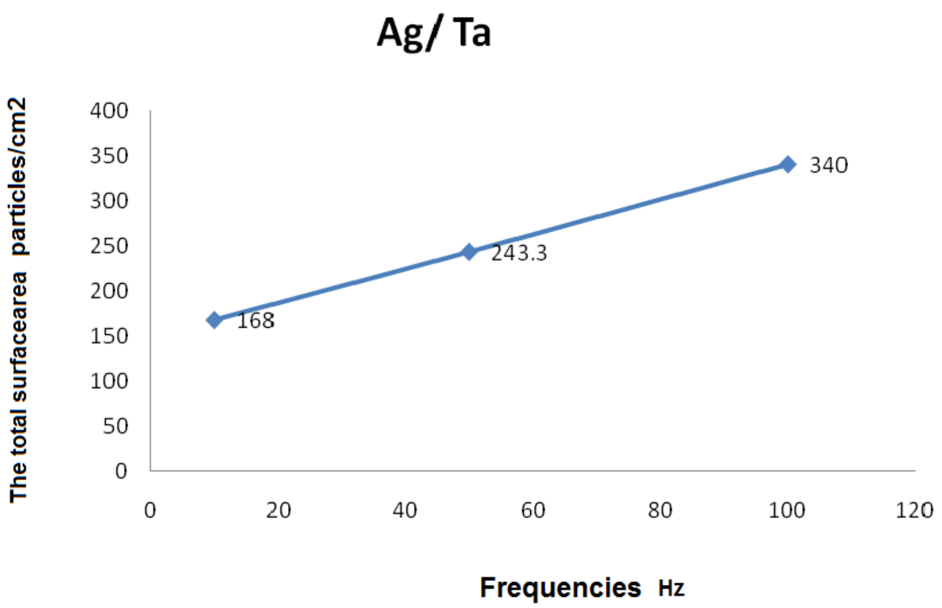
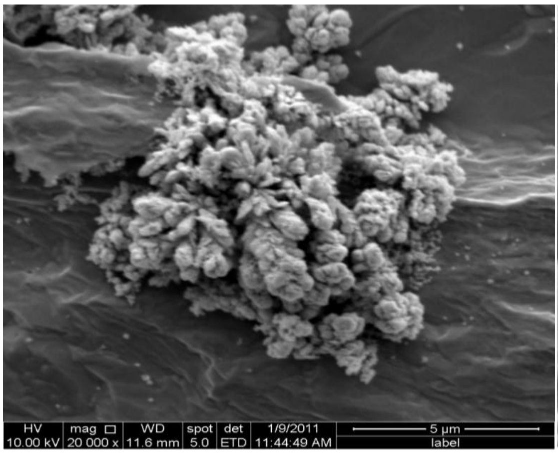


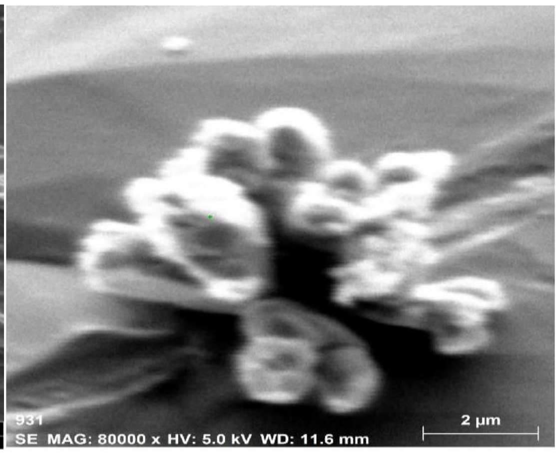
Figure 66: a plot the number of particles × 10^7 (particles/cm^2) vs. deposited gold nanoparticles on tantalum substrate. Frequency Hz. parameters of the experiments potential = -0.4V, amplitude = 0.6 V, time= 60s and different frequency 10, 50 and 100Hz.

3.2.2. Microstructures of silver

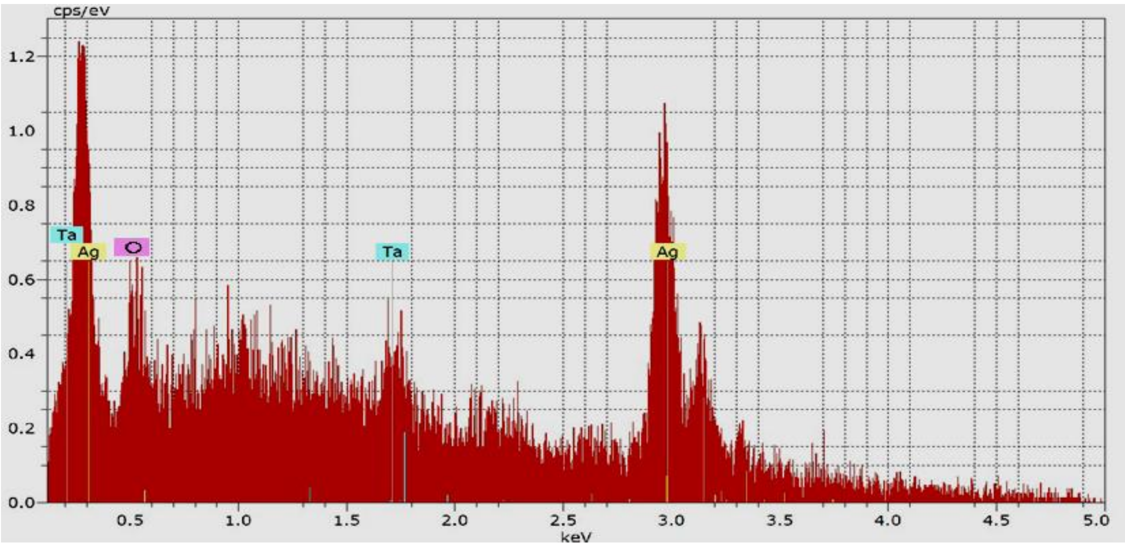
Figure 67 shows the SEM and EDX micrographs of flower-like silver nanostructures which are prepared at higher concentration of 10^{-3} M and 250s deposition time. Figure 65-c shows the EDX spectrum analysis of flower-like silver which proves that the result is silver oxide.



67-a



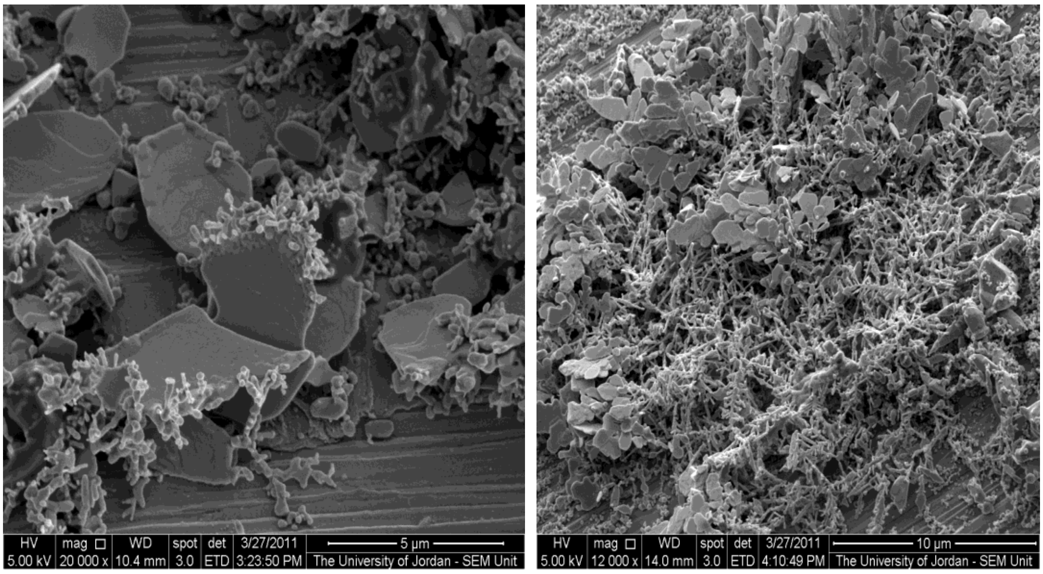
67-b



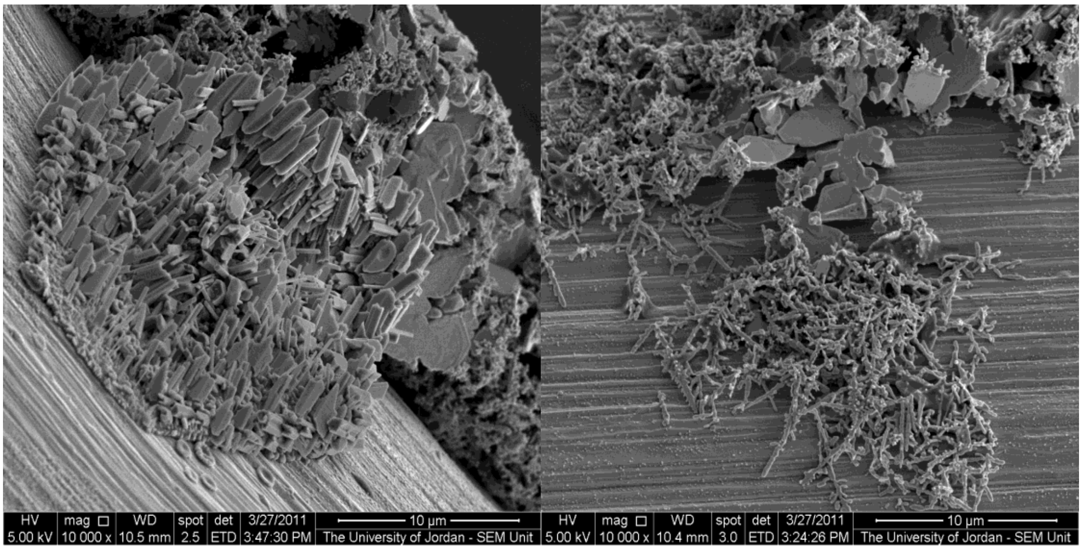
67-c

Figure 67: SEM images (a and b) deposition silver nanostructures on tantalum. Parameters of the experiment E_L = -0.8 , E_H = - 0.2 V centered at = -0.5V, amplitude = 0.6V, frequency = 100 Hz, silver concentration = 10^{-3} M, time = 250 seconds and scan rate of 100 mV/ s. 67-(c)EDX spectra of flower-like silver deposited on tantalum substrate.

Figure 68 shows the SEM micrographs of the plates of silver oxide have been prepared from silver solution 10^{-3} M and 60s deposition time.



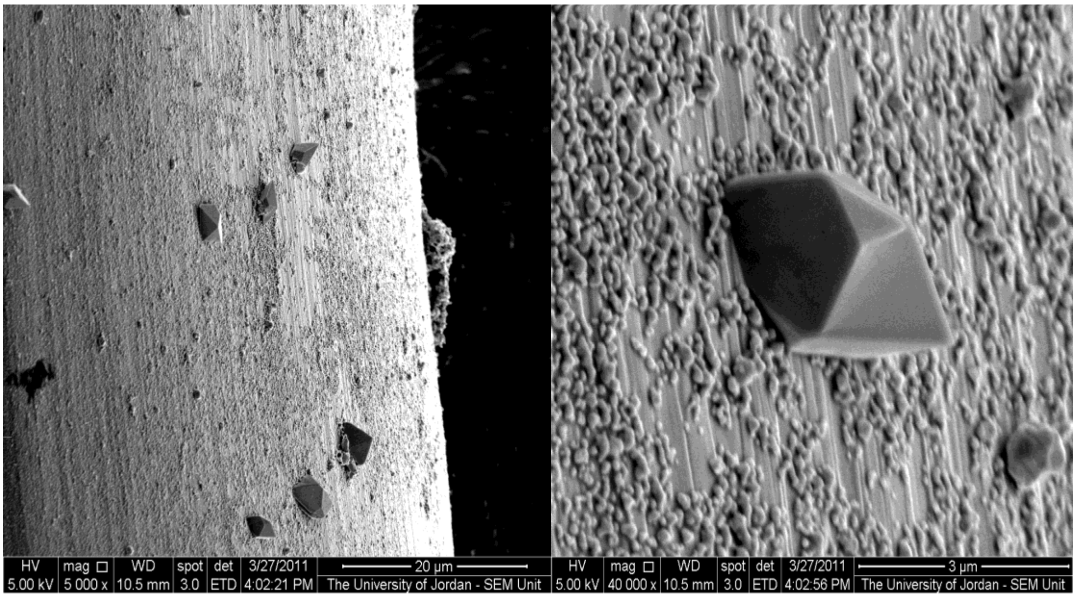
a b



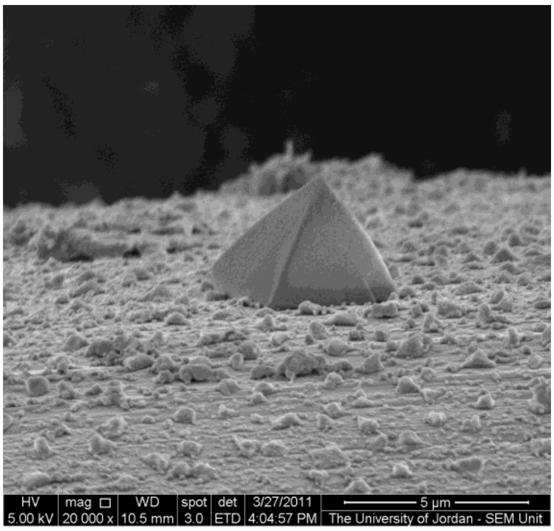
c d

Figure 68: SEM images (a ----- d) deposition silver nanostructures on tantalum. Parameters of the experiment E_L = -0.7, E_H = - 0.1 V centered at = -0.4V, amplitude = 0.6V, frequency = 10 Hz, silver concentration = 10^{-3} M, time = 60 seconds and scan rate of 100 mV/ s.

Figure 69 shows that the SEM micrographs of the microcrystal silver oxide which was successfully prepared at conditions chosen. Microcrystals those were formed on the surface were not of regular shape and were undistributed.



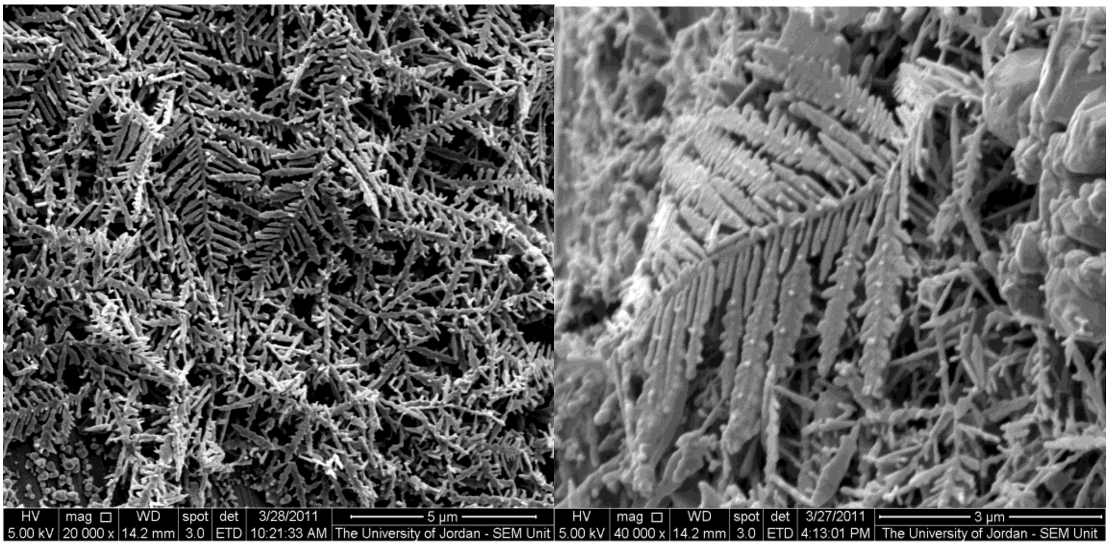
a b



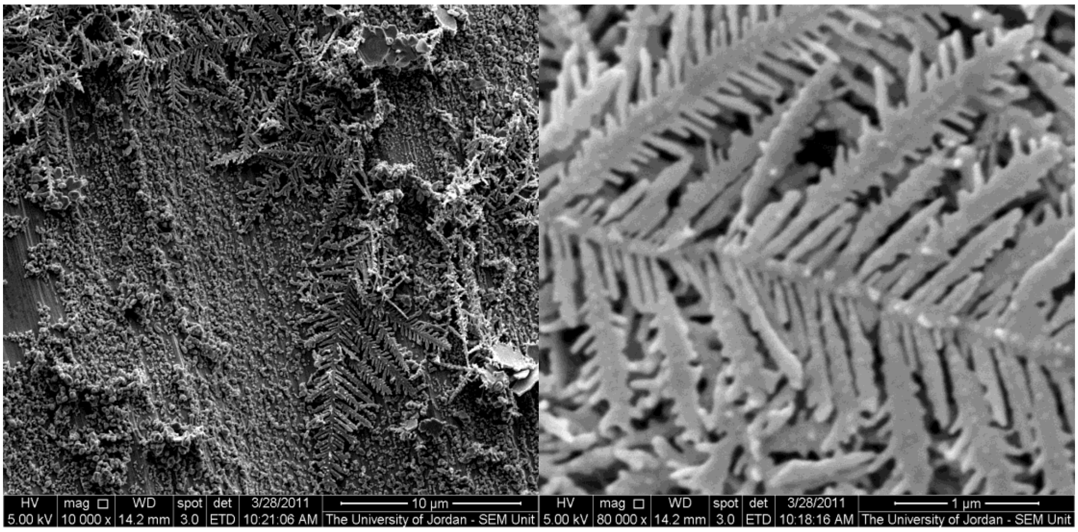
c

Figure 69: SEM images (a b and c) deposition of silver nanostructures on tantalum. Parameters of the experiment E_L = -0.7, E_H = - 0.1 V centered at = -0.4V, amplitude = 0.6V, frequency = 50 Hz, silver concentration = 10^{-3} M, time = 60 seconds and scan rate of 100 mV/ s.

Figure 70 shows the SEM micrographs of nanodendrites silver nanostructures. It has been formed at high concentration10^{-3} M and 10^{-2} M with different parameters. Excellent dendritic structure of silver, and a new pole material, has the ability to very high specific area along with latest sites and many sharp edges that could promising in applications in electrochemical systems. Nano/microdendritic of metallic silver was observed upon application of square wave potential regime under different conditions.



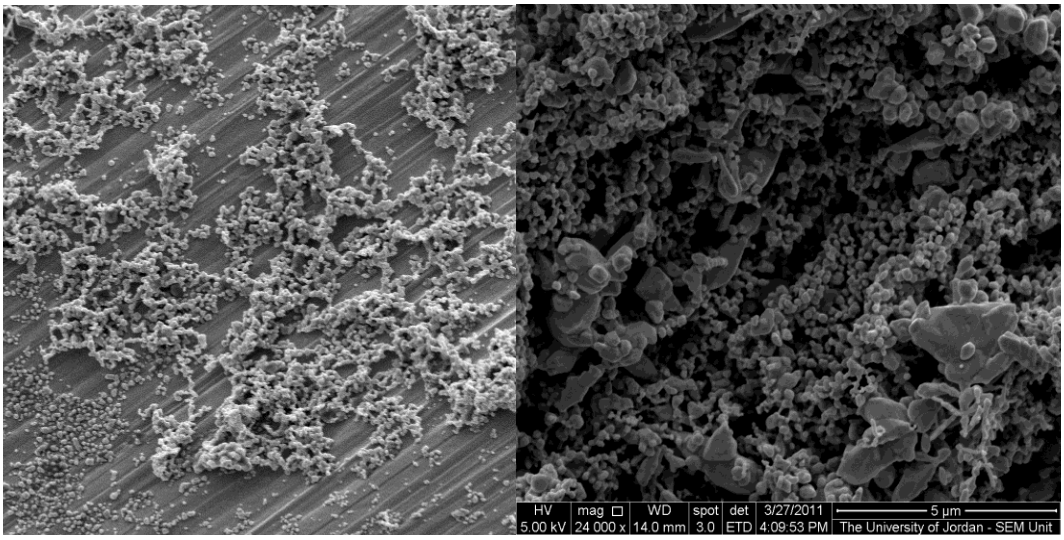
a b



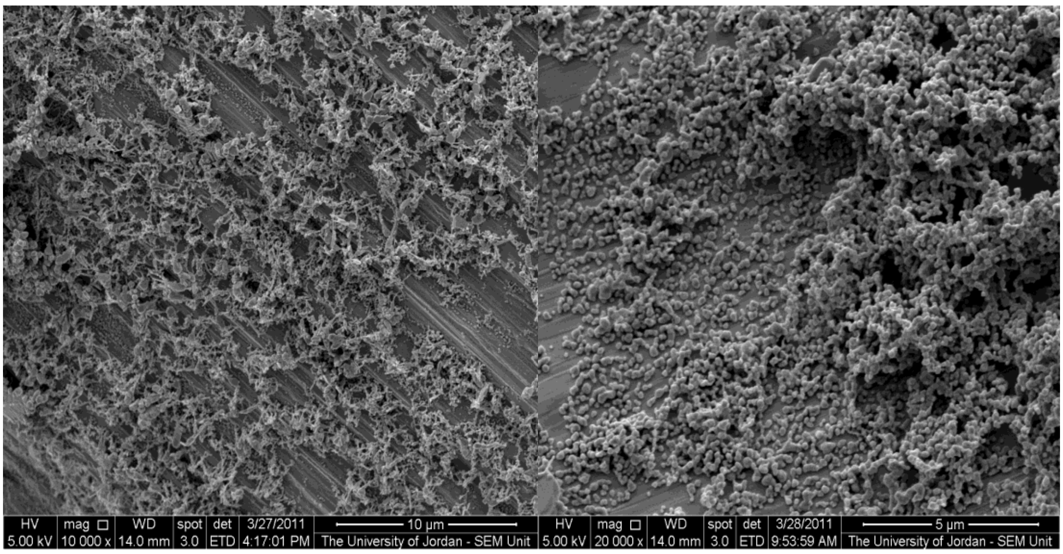
c d

Figure 70: SEM images (a——d) deposition silver nanostructures on tantalum. Formed at different conditions.

Figure 71 shows the SEM micrographs of silver nanoagglomeration that have been observed at higher concentration.



a b



c d

Figure 71: SEM images (a--- d) deposition silver nanostructures on tantalum. Parameters of the experiment: E_L = -1.0, E_H = - 0.4 V centered at = -0.7V, amplitude = 0.6V, frequency = 50 Hz, silver concentration = 10^{-3} M, time = 60 seconds and scan rate of 100 mV/ s.

Table (5): campaigning of all experiments of the silver deposited.

Metal	CV figure	SEM figure	EDX figure	E_H V	E_L V	Center V	Amplitude V	Frequency Hz	Concentration M	Time seconds	Scan rate mV/s	Size nm	Area Particles cm^{-2}
silver	54	55	-----	0.00	-0.4	-0.2	0.4	100	10^{-3}	60	100	------	--------
silver	-------	56	-------	-0.1	-0.7	-0.4	0.6	50	10^{-3}	60	100	------	2.43×10^{9}
silver	-------	57	-------	0.00	-0.8	-0.4	0.8	50	10^{-3}	60	100	------	4.30×10^{9}
silver	-------	58	--------	-0.1	-0.9	-0.4	1.0	50	10^{-3}	60	100	------	7.00×10^{9}
silver	-------	59	------	0.00	-0.6	-0.3	0.6	100	10^{-3}	120	100	------	--------
silver	-------	60	--------	0.00	-0.6	-0.3	0.6	100	10^{-3}	60	100	------	3.50×10^{9}
silver	-------	62	-------	-0.4	-0.1	-0.3	0.4	100	10^{-3}	60	100	------	--------
silver	-------	63	------	-0.4	-0.1	-0.3	0.4	100	10^{-4}	60	100	-----	2.20×10^{9}
silver	-------	64		-0.1	-0.7	-0.4	0.6	10	10^{-3}	60	100	-----	2.40×10^{9}
silver	-------	65		-0.1	-0.7	-0.4	0.6	100	10^{-3}	60	100	-----	3.50×10^{9}
silver	-------	67	67-c	-0.2	-0.8	-0.5	0.6	100	10^{-3}	250	100	------	---------
silver	-------	68	------	-0.1	-0.7	-0.4	0.6	10	10^{-3}	60	100	------	---------
silver	-------	69	------	-0.1	-0.7	-0.4	0.6	50	10^{-3}	60	100	-------	---------
silver	-------	71	------	-0.1	-0.7	-0.4	0.6	50	10^{-3}	60	100	-------	---------

3.3. Copper nanostructures

3.3.1. The effect of concentration of copper solution on the deposited nanoparticles

Figure 72 shows the copper nanostructures at 10^{-4} M with egalitarian shape formed homogenous; with similar size of nanoparticles with a uniform distribution on the surface.

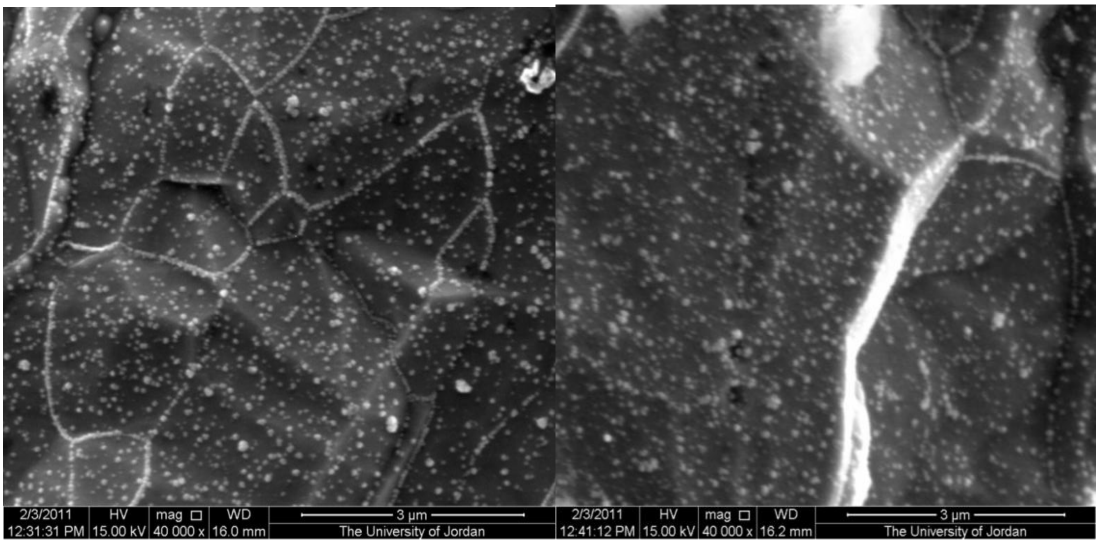
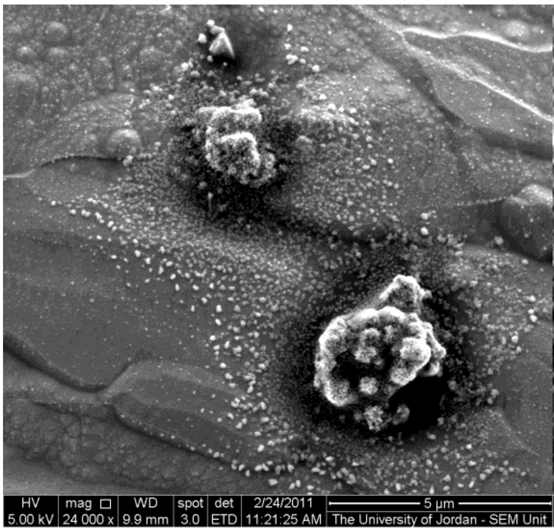
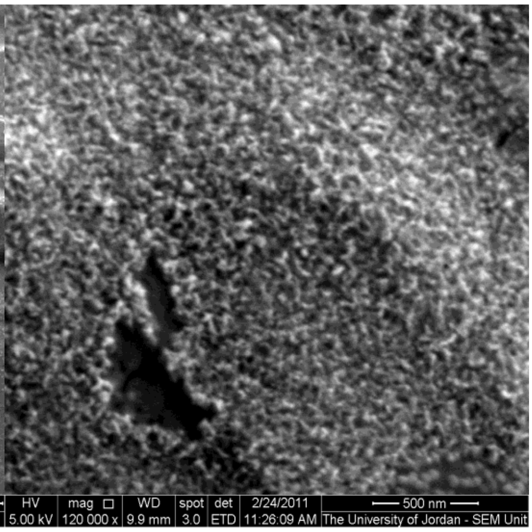


Figure 72: SEM images deposition copper nanostructures on tantalum. Parameters of the experiment E_L= -0.6, E_H = 0.00 V centered at = -0.3V, amplitude = 0.6V, frequency = 100 Hz, copper concentration = 10^{-4} M, time = 120 seconds and scan rate of 100 mV/ s.

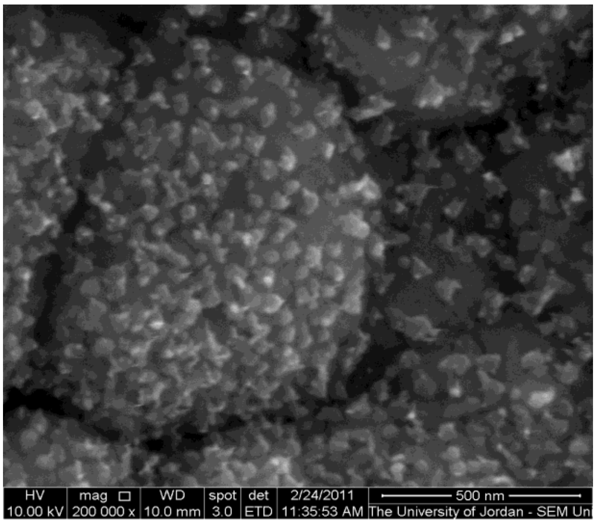
Further investigation of the deposited nanoparticles indicates that the obtained particles are distributed systemically, with good uniformity, similar shape and size of nanoparticles with an average distribution of 3.42×10^9 particles/cm^2. The copper concentration has a significant impact on the resulting nanoparticles.

Figures 73 shows the SEM micrographs of copper nanostructures deposited on tantalum substrate of higher concentration of 10^{-2} M. The formed copper nanoparticles are larger than those copper nanoparticles formed at lower concentration of 10^{-4} M. The shape of nanoparticles formed from 10^{-2} M is cube-like.





a b



c

Figure 73: SEM image (a, b and c) of nanorodes formation on copper wire. Parameters of the experiment E_L = -0.8 V, E_H = - 0.2V centered at = -0.5V, amplitude = 0.6V, frequency = 100 Hz, copper concentration = 10^{-2} M, acidic media, time = 120 seconds and scan rate of 100 mV/ s.

3.3.2. The effect of deposition time

Figures 74 and 75 show the effect of deposition time on the nanoparticles. Figure 74 shows the SEM micrograph for the deposited nanoparticles produced at 60 s deposition time. The nanoparticles are separately scattered on the tantalum surface with a high degree of uniformity.

Figures 74 shows the SEM micrographs of deposited copper nanostructures produced by application of square wave potential regime at 60 s time. A rough estimate of nanoparticles amounts to a value of 3.90×10^9 particle/cm^2.

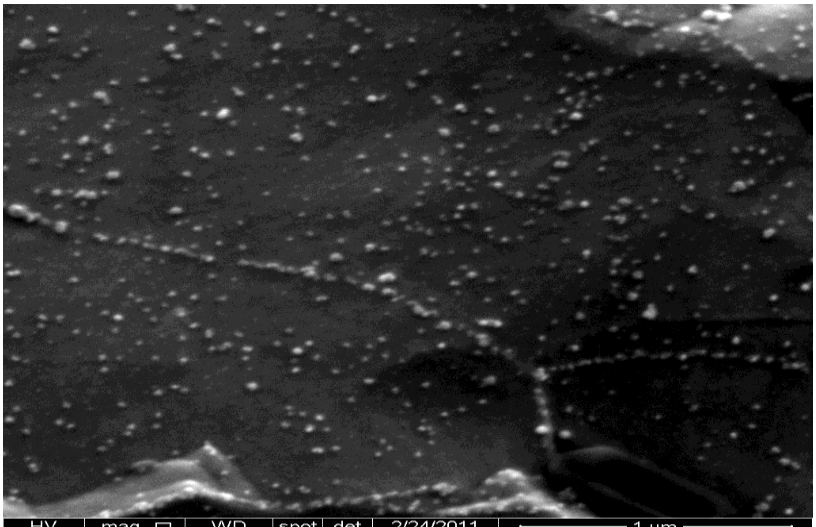
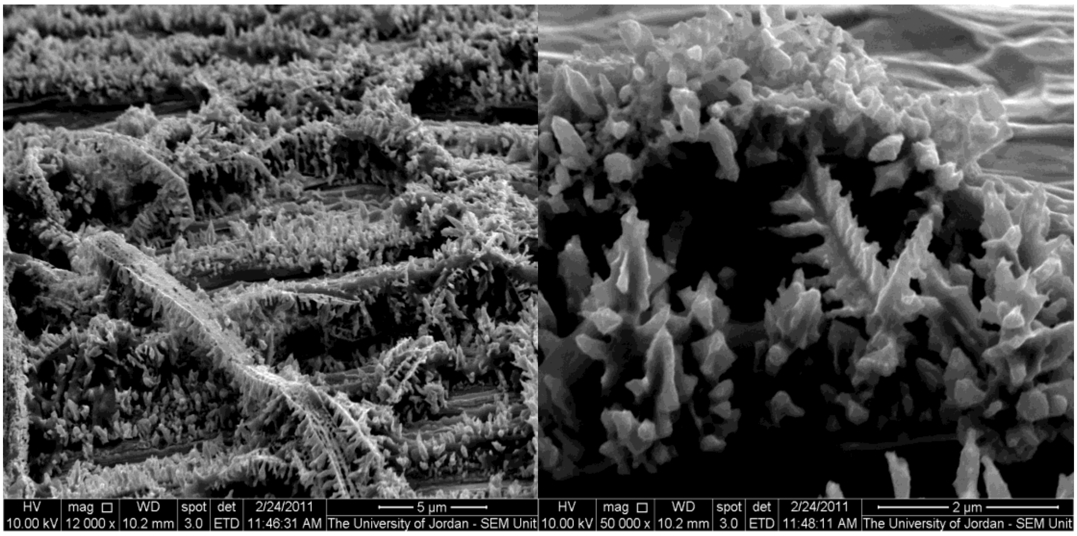
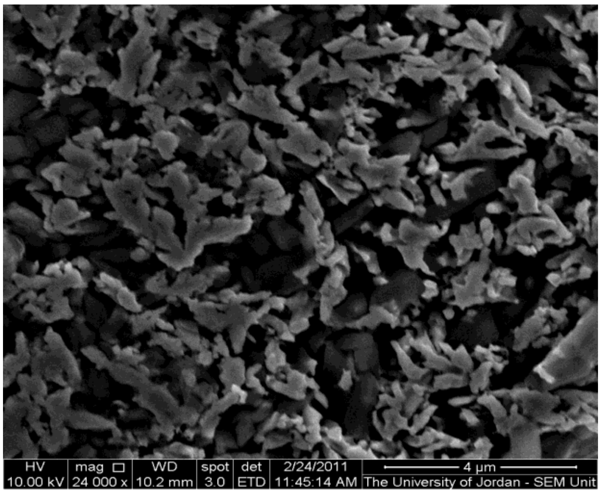


Figure 74: SEM images deposition copper nanostructures on tantalum. Parameters of the experiment E_L = -0.6 V, E_H = 0.00 V centered at = -0.3V, amplitude = 0.6V, frequency = 100 Hz, copper concentration = 10^{-3} M, acidic media, time = 60 seconds and scan rate of 100 mV/ s.

Figure 75 shows the SEM micrograph for the deposited ear-like copper structures obtained at a deposition time of 120s. Further investigation of the deposits indicates that the obtained particles are larger with different shape formation than the experiment carried out at the same conditions at 60s deposition time. Figure 75-c shows the SEM images of flacks-like copper nanostructures.



a b



c

Figure 75: SEM images (a, b and c) deposition copper nanostructures on tantalum. Parameters of the experiment E_L = -0.6 V, E_H = 0.00 V centered at = -0.3V, amplitude = 0.6V, frequency = 100 Hz, copper concentration = 10^{-3} M, acidic media, time = 120 seconds and scan rate of 100 mV/ s.

3.3.3. The effect of frequency of the square wave on the deposited nanoparticles

Figure 76 shows the SEM micrograph for the deposited nanoparticles obtained at 100 Hz frequency of the square wave. Investigation of the deposited nanoparticles indicates that the obtained particles are larger than the frequency 1 kHz with the same conditions used in deposited silver on tantalum.

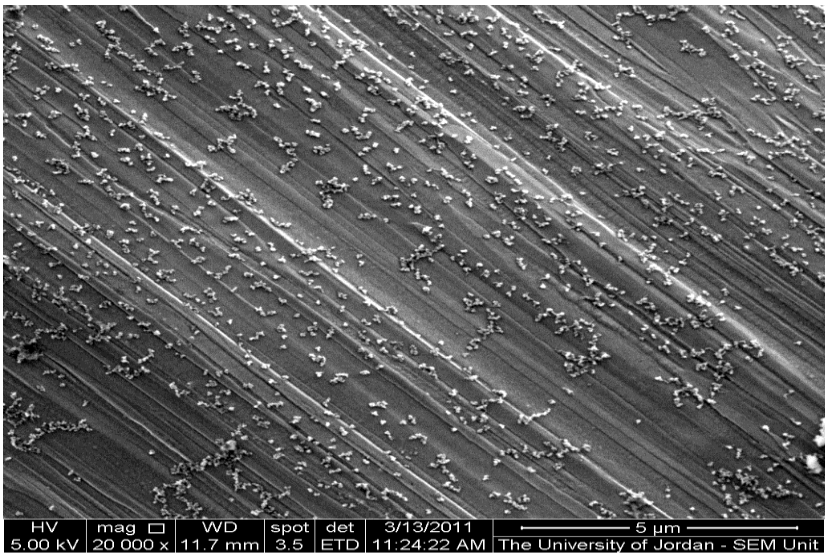


Figure76: SEM image deposition copper nanostructures on tantalum. Parameters of the experiment E_L = -0.5 V, E_H = -0.1V centered at = -0.2V, amplitude = 0.6V, frequency = 100 Hz, copper concentration = 10^{-3} M, acidic media, time = 60 seconds and scan rate of 100 mV/ s.

Figure 77 shows the SEM micrograph for the deposited nanoparticles obtained at frequency 1 kHz used in deposition. the total surface area at frequency 100 Hz; figure 76; are larger than the total surface area at frequency 1 kHz are carried out under the same conditions of both two experiments; the figures shows 76 and 77.

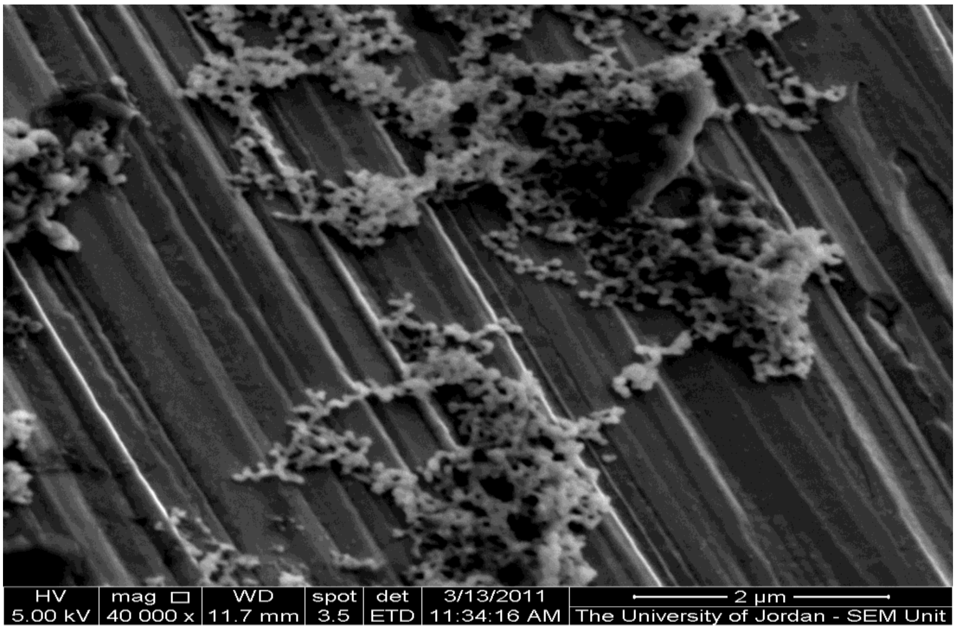


Figure 77: SEM image deposition copper nanostructures on tantalum. Parameters of the experiment E_L = -0.5 V, E_H = -0.1 V centered at = -0.2V, amplitude = 0.6V, frequency = 1 kHz, copper concentration = 10^{-3} M, acidic media, time = 60 seconds and scan rate of 100 mV/ s.

3.3.4. The effect of medium of deposition on the produced and nanostructures:

Figure 78 shows the SEM images of copper oxide nanostructures obtained in acidic media with a uniformity shape formed.

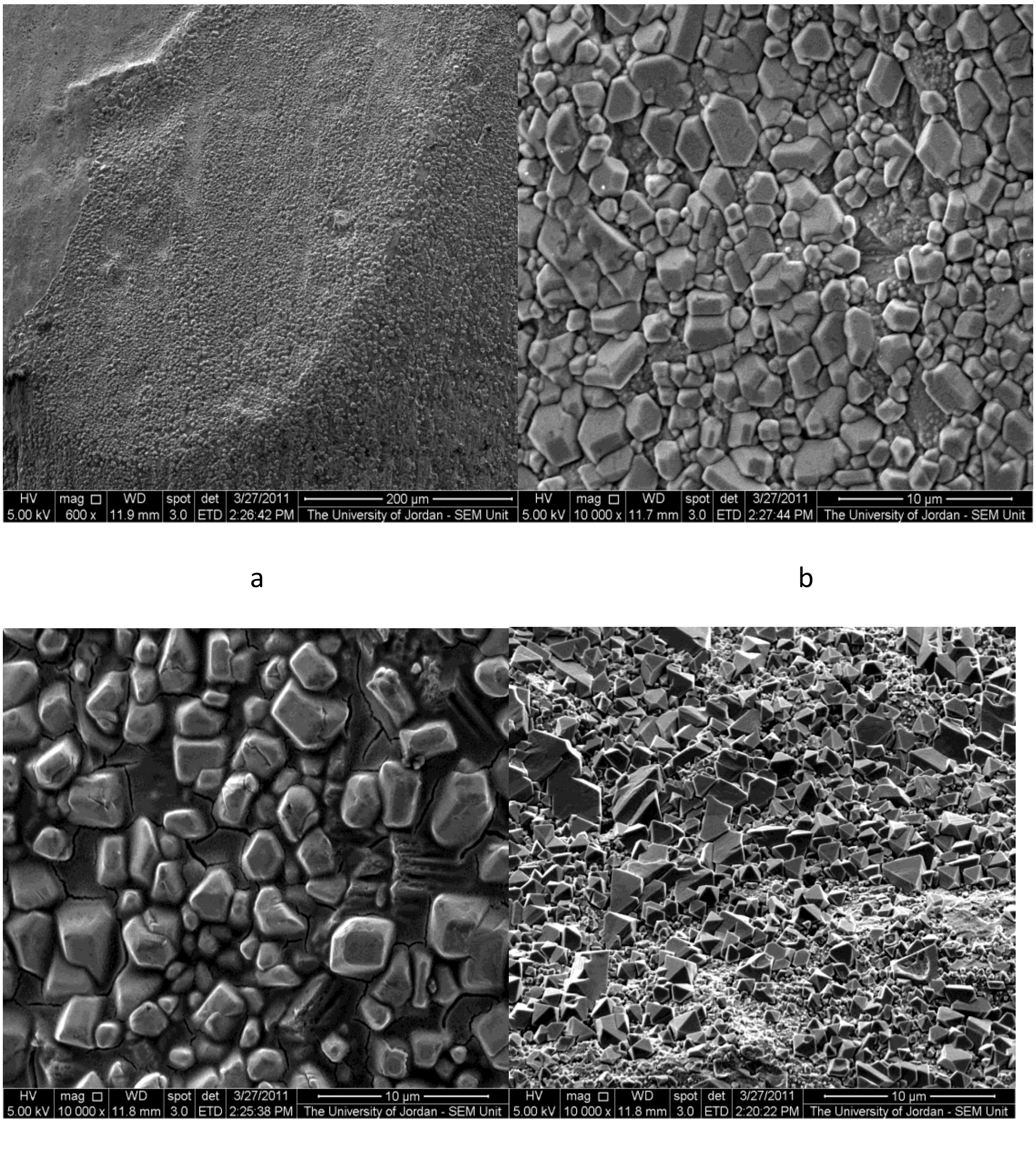


Figure 78: SEM images (a--d) deposition copper nanostructures on copper. Parameters of the experiment E_L = -1.0 V, E_H = -0.5V centered at = -0.75V, amplitude = 0.5V, frequency = 100 Hz, silver concentration = 10^{-3} M, acidic media, time = 60 seconds and scan rate of 100 mV/ s.

Figure 79 shows the SEM images of copper nanostructures obtained in basic media with nanofibers. It is not the only form of the deposits, spongy deposits are formed. In basic media is formed spongy-like copper and nanofibers on the surface. Changing the pH used in deposited also formation of different shape and size of the produced at carried out the same conditions.

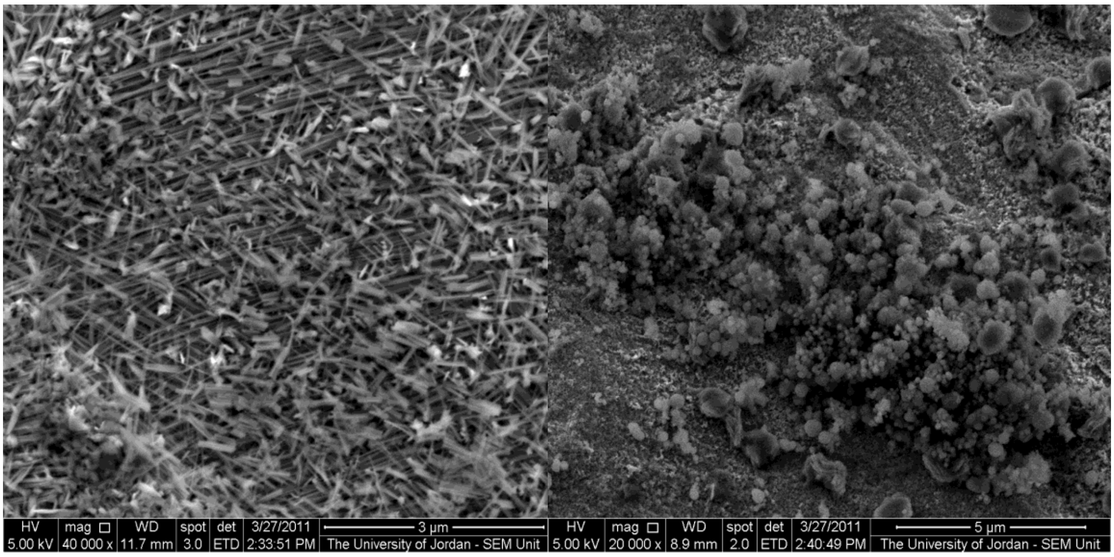
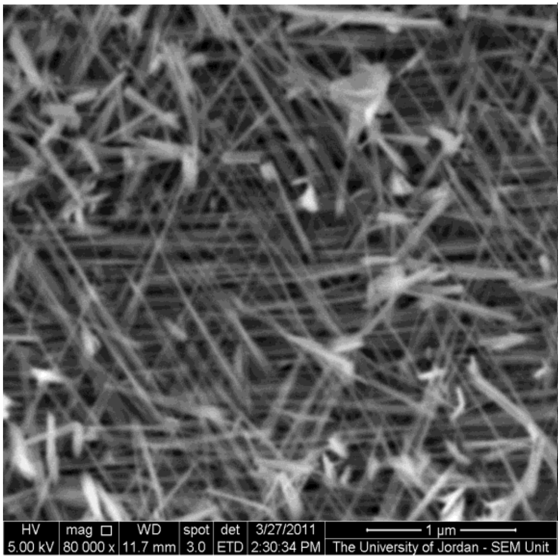
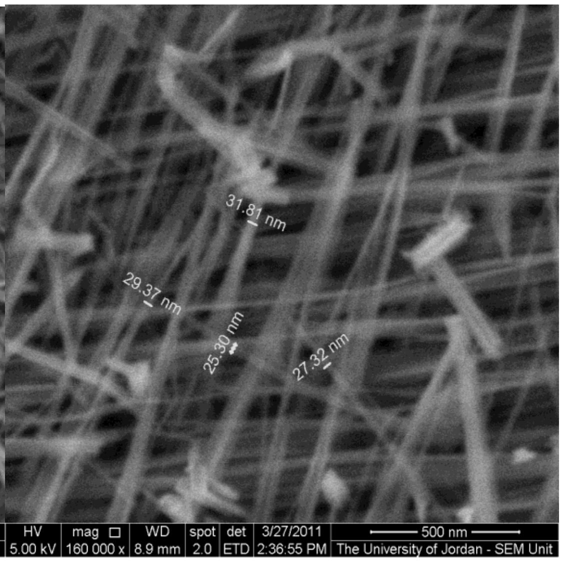


Figure 79: SEM images deposition copper nanostructures on copper. Parameters of the experiment E_L= -1.0 V, E_H = -0.5V centered at = -0.75V, amplitude = 0.5V, frequency = 100 Hz, silver concentration = 10^{-3} M, basic media, time = 60 seconds and scan rate of 100 mV/ s.

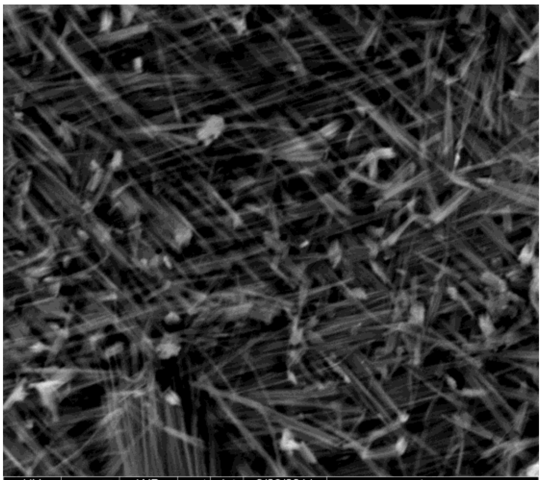
3.3.4. Nanostructures of copper:

Figures 80 and 81 show the SEM micrographs of nanofibers were fabricated by electrodeposition process. The synthesis of nanofibers copper nanostructures occur in basic media. Figure 80 shows, these copper nanofibers were distributed homogeneously on the surface of copper electrode. Copper nanofibers formed as a network. The average size of nanofibers of the copper 28.5 nm.





a b



c

Figure 80: SEM images (a, b and c) deposition of copper nanostructures on tantalum. Parameters of the experiment :E_L = -1.0 V, E_H = -0. 5V centered at = -0.75V, amplitude = 0.5V, frequency = 100 Hz, copper concentration = 10^{-4} M, basic media, time = 60 seconds and scan rate of 100 mV/ s.

Figure 81 shows the SEM micrographs of copper nanofibers formed on tantalum electrode by using copper perchlorate dissolved in 0.5 M sulfuric acid. Copper nanofibers connecting nanoparticles on the surface of the metal and the quantity is small compared to the nanofibers formed in basic media.

.

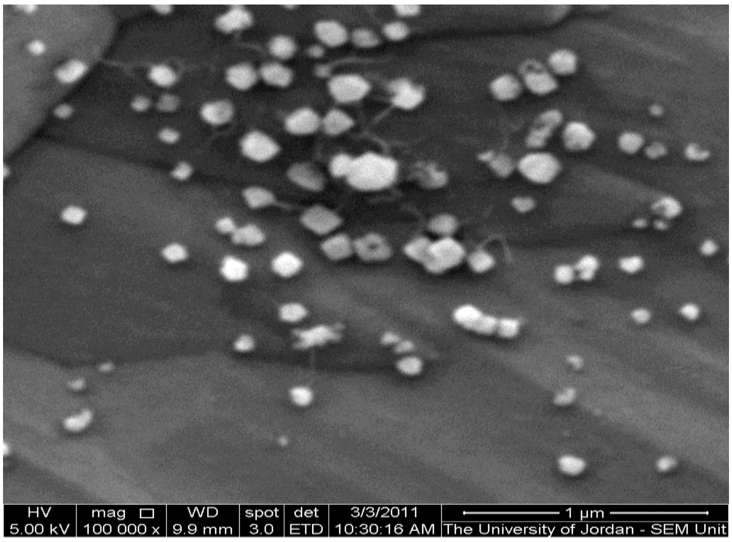
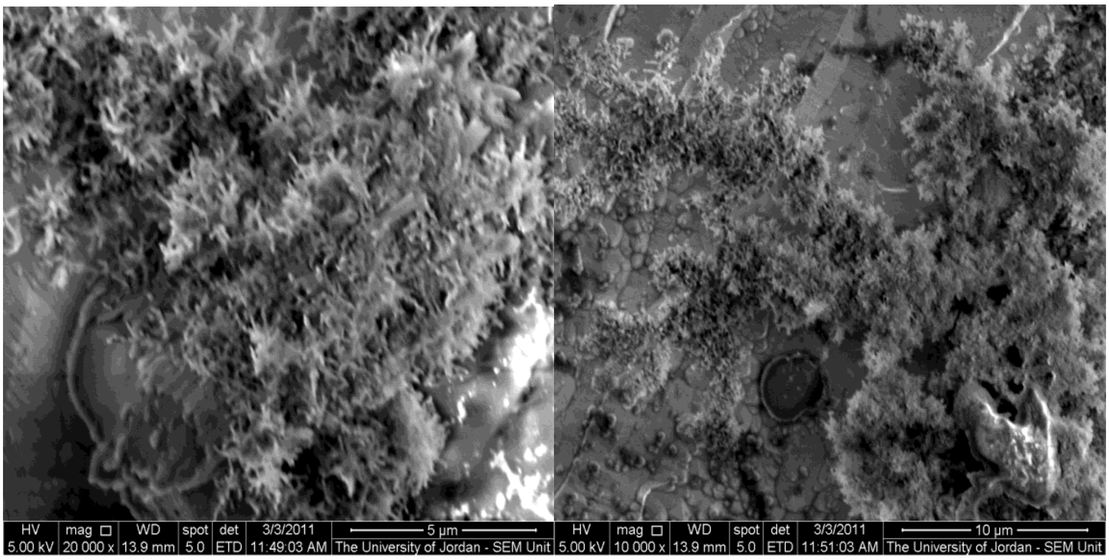
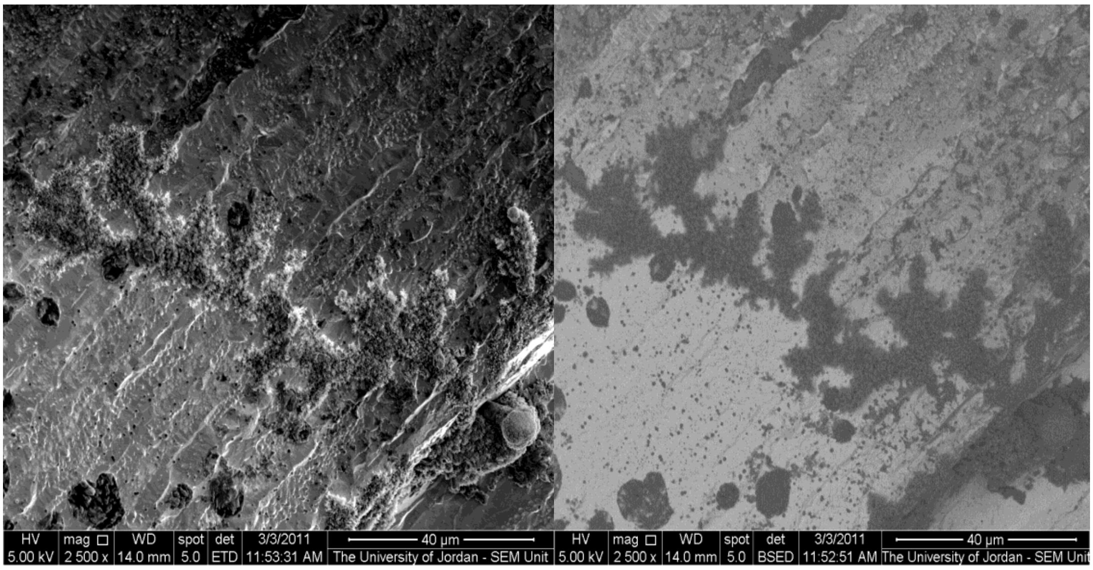


Figure 81: SEM image of nanofibers of copper deposition copper nanostructures on tantalum. Parameters of the experiment E_L = -1.3 V, E_H = -0. 7V centered at = -1.0V, amplitude = 0.6V, frequency = 100 Hz, copper concentration = 10^{-3} M, acidic media, time = 60 seconds and scan rate of 100 mV/ s.

Figure 82 shows the SEM micrographs of spongy copper nanostructures which are formed by deposition from 1×10^{-2} M Cu^{+2} basic solution.



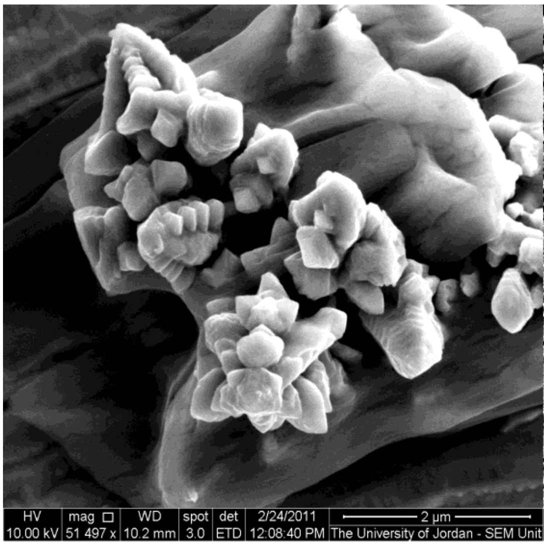
a b

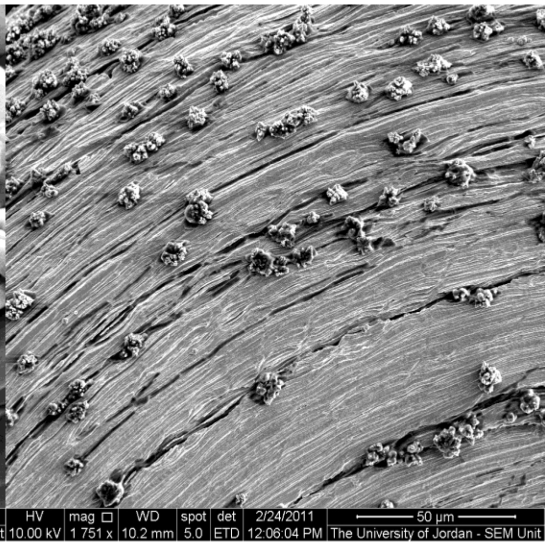


c d

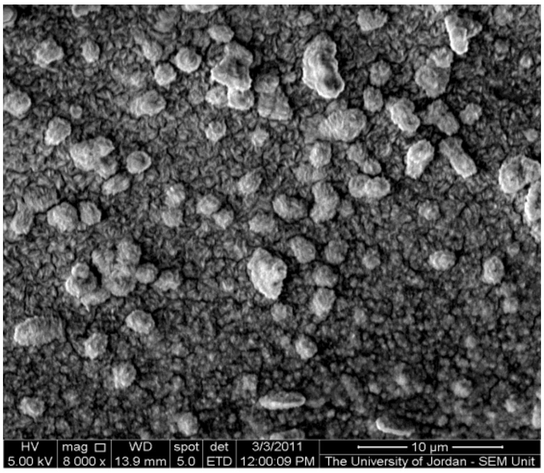
Figure 82: SEM image (a, b, and c) of deposition of copper nanostructure on tantalum substrate. (d) image back scattering for the sample (c). Parameters of the experiment E_L = -1.4 V, E_H = -0. 8V centered at = -1.1V, amplitude = 0.6V, frequency = 100 Hz, copper concentration = 10^{-2} M, basic media, time = 120 seconds and scan rate of 100 mV/ s.

Figure 83 shows the SEM micrographs of flower-like copper nanostructures are formed by deposition from 0.5 M sulfuric acid solution.





a b



c

Figure 83: SEM image (a, b and c) deposition copper nanostructures on tantalum. Parameters of the experiment :E_L = -1.4 V, E_H = -0. 8V centered at = -1.1V, amplitude = 0.6V, frequency = 100 Hz, copper concentration = 10^{-2} M, acidic media, time = 60 seconds and scan rate of 100 mV/ s.

Figures 84 and 85 show the SEM micrographs of deposited copper nanorods produced by application of square wave potential regime at different time of 120 and 300 seconds.

Figure 84 shows the SEM images of copper nanorods at 120s deposition time; the less time required for the deposition the greater the number of nanorods formed on the surface.

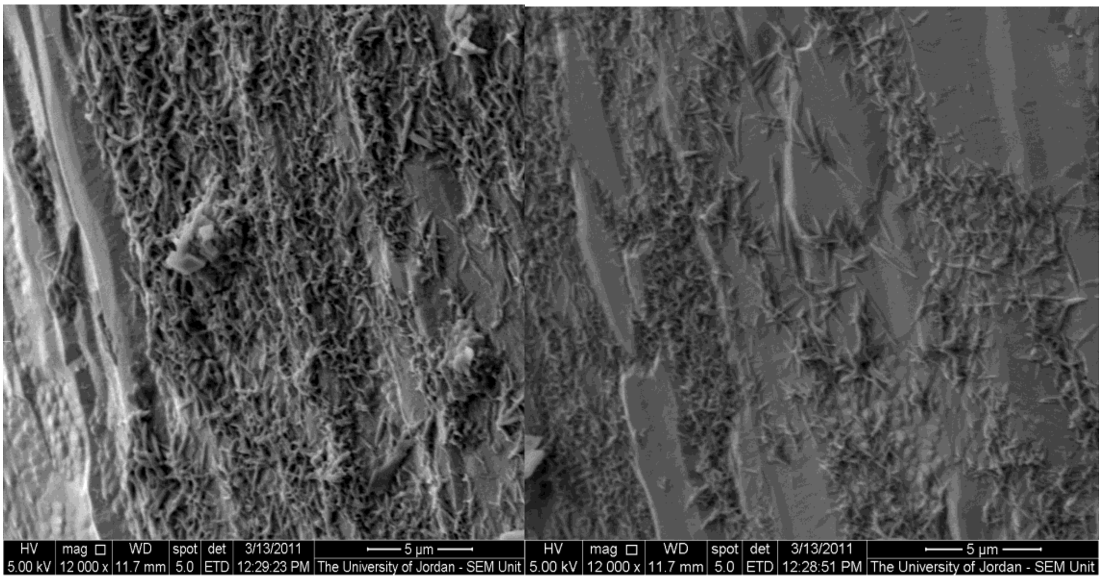


Figure 84: SEM image deposition of copper nanorods on tantalum. Parameters of the experiment E_L = -1.05 V, E_H = -0. 65V centered at = -0.85V, amplitude = 0.4V, frequency = 100 Hz, copper concentration = 10^{-3} M, basic media deposition, time = 120 seconds and scan rate of 100 mV/ s.

Figure 85 shows the SEM micrographs of copper nanorods formed at 300s deposition time. Compared with the figure 84; the amount of nanorodes are smaller and different size of copper nanorodes.

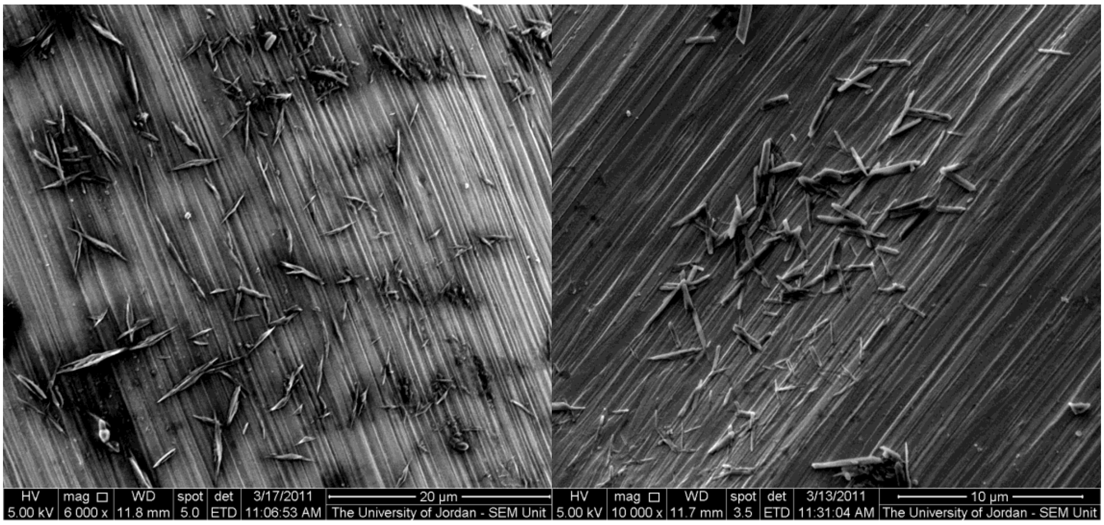
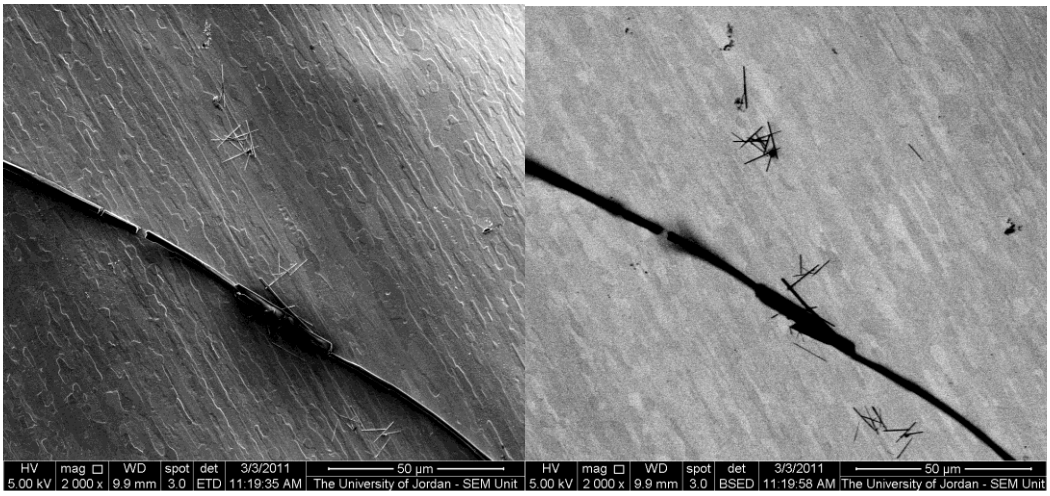
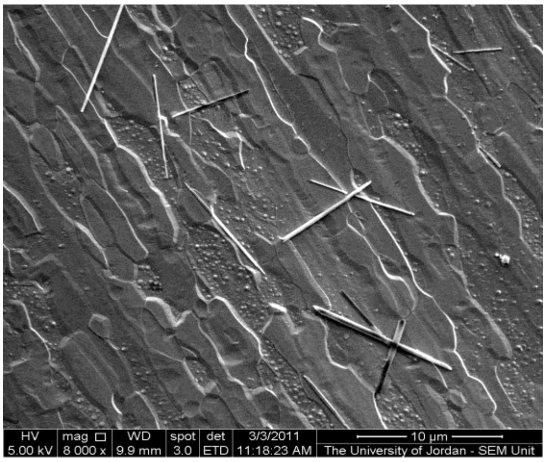


Figure 85: SEM image deposition copper nanorods on tantalum. Parameters of the experiment E_L= -1.15 V, E_H = -0. 55V centered at = -0.85V, amplitude = 0.6V, frequency = 100 Hz, copper concentration = 10^{-3} M, basic media deposition, time = 300 seconds and scan rate of 100 mV/ s.

Figure 86 shows the SEM micrographs of copper nanorods which are formed at 60s deposition time from 0.5 M sulfuric acid and 1× 10^{-3} M Cu^{+2}. Figure 86-b shows the back scattering of micrographs.



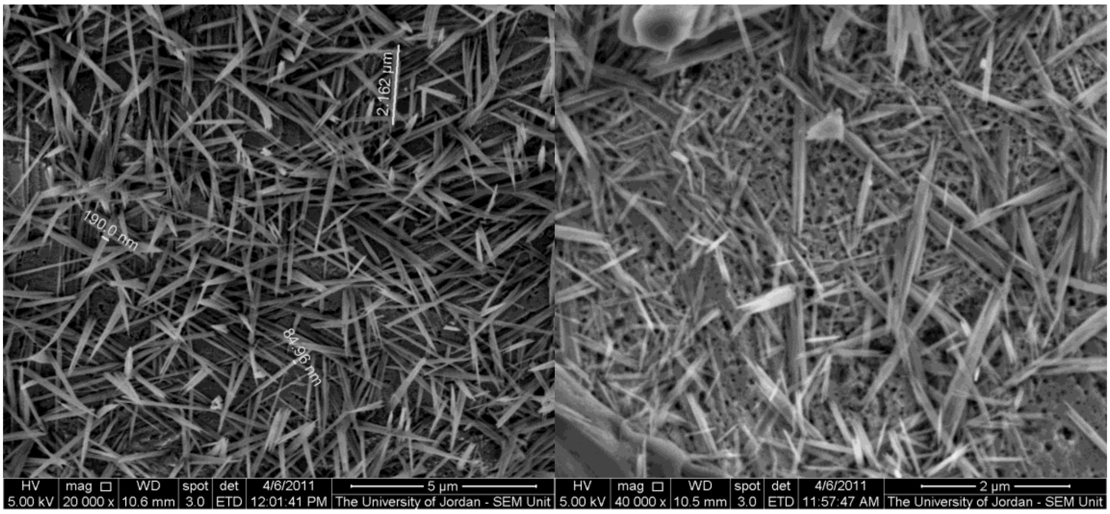
a b



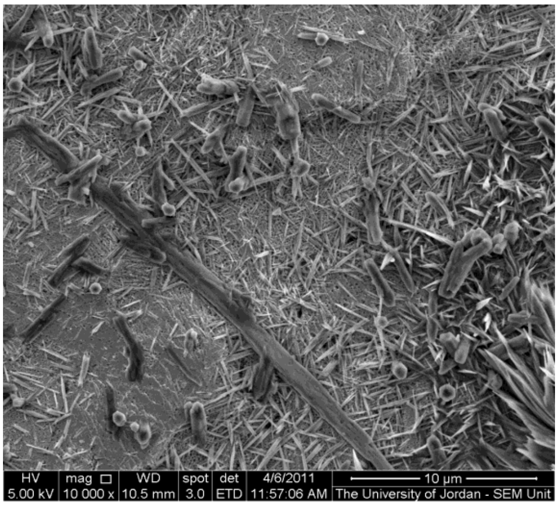
c

Figure 86: SEM images (a and c) deposition copper nanorods on copper substrate. Parameters of the experiment: E_L= -1.15 V, E_H = -0. 55V centered at = -0.85V, amplitude = 0.6V, frequency = 100 Hz, copper concentration = 10^{-3} M, acidic media, time = 60 seconds and scan rate of 100 mV/ s.(b) back scattering.

Figures 87-89 show the SEM micrographs of deposited copper nanorods produced by application of square wave potential regime at different time of 15, 30 and 60 seconds with amplitude square wave 0.5 V centered at -1.25 V. Figure 87 shows the SEM image of copper nanorods which were formed at 15s deposition time on copper substrate, the copper nanorods undisturbed and of different size. The average size of copper nanorodes formed 137 nm and the length of nanorod 2 μm.



a　　　　b



c

Figure 87: SEM images (a, b and c) deposition copper nanostructures on copper substrate. Parameters of the experiment E_L = -1.5 V, E_H = -1.V centered at = -1. 25V, amplitude = 0.5V, frequency = 100 Hz, copper concentration = 10^{-4} M, basic media, time = 15 seconds and scan rate of 100 mV/ s.

Figure 88 shows the SEM image of copper nanorods which were formed at 30s deposition time on copper substrate. The copper nanorods undisturbed, different size and presence of nanoparticles between nanorods. The average size of copper nanorodes formed are larger than the copper nanorods formed at 15s deposition time on copper substrate.

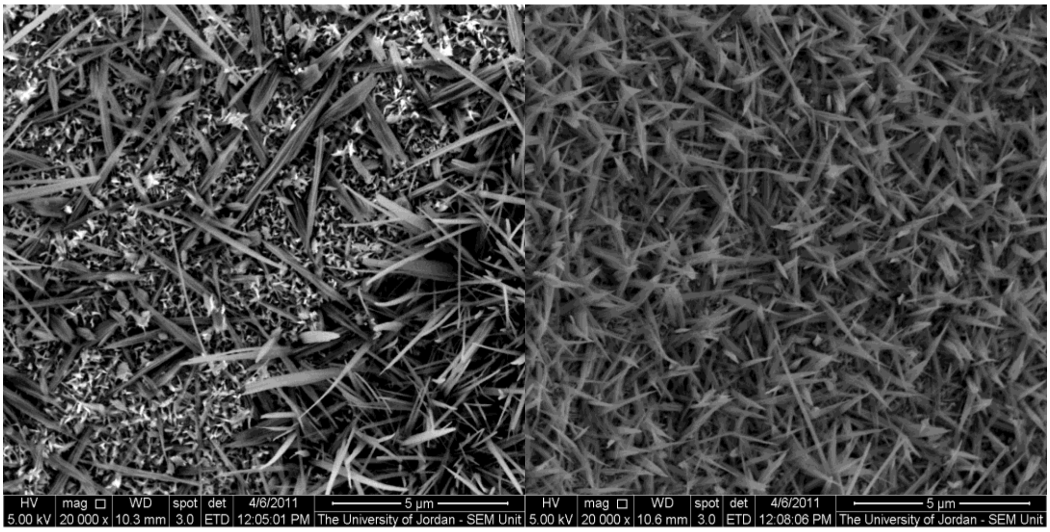


Figure 88: SEM images deposition copper nanorods on copper substrate. Parameters of the experiment E_L = -1.5 V, E_H = -1.V centered at = -1.25V, amplitude = 0.5V, frequency = 100 Hz, copper concentration = 10^{-4} M, basic media, time = 30 seconds and scan rate of 100 mV/ s.

Figure 89 shows the SEM image of copper nanorods which were formed at 60s deposition time on copper substrate. The copper nanorods disturbed, similar size and uniformly. Figure 89-d shows the presence of needles copper between nanorods. The average sizes of copper nanorodes formed are larger than the copper nanorods formed at 15s and 30s deposition time on copper substrate.

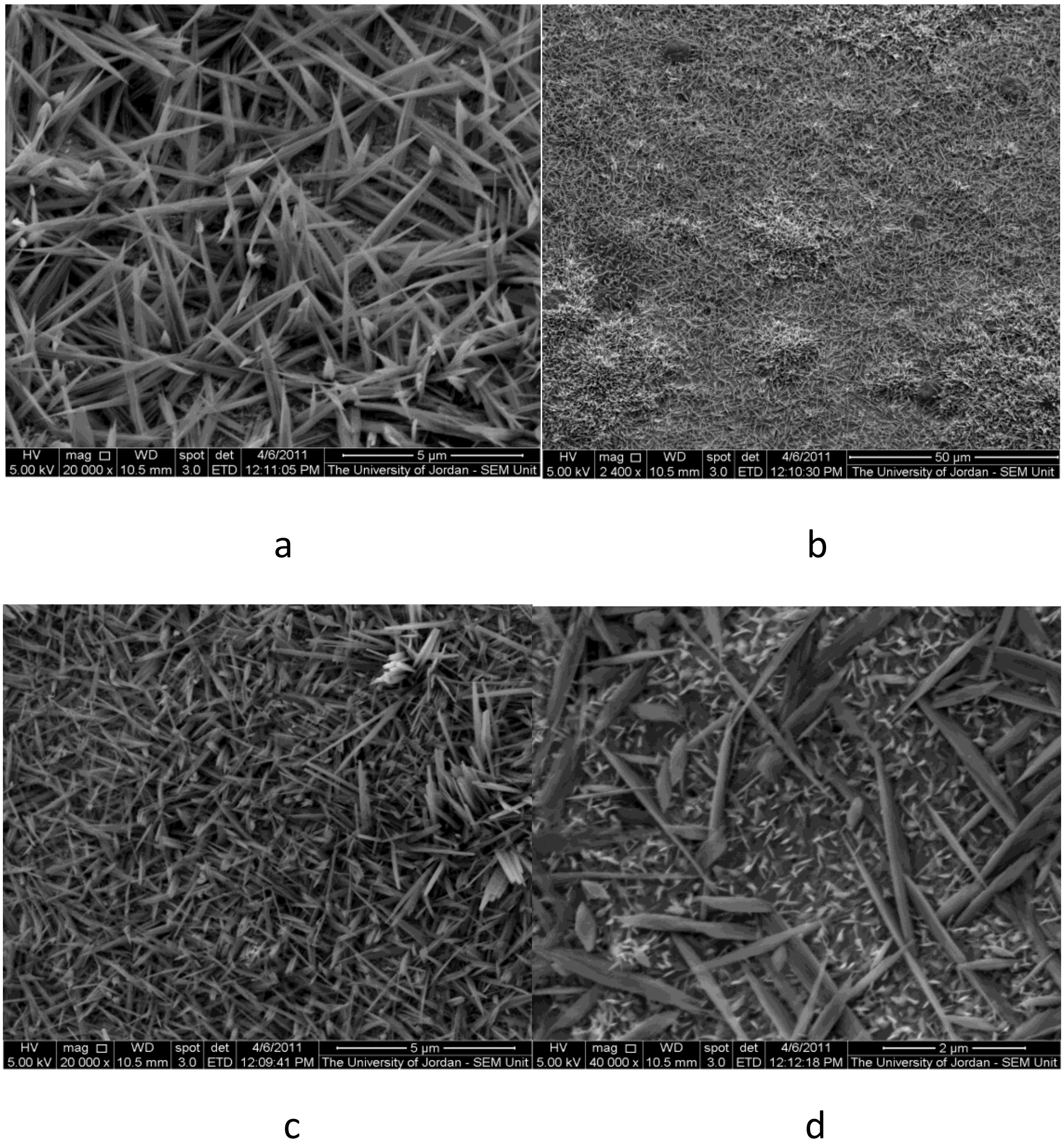
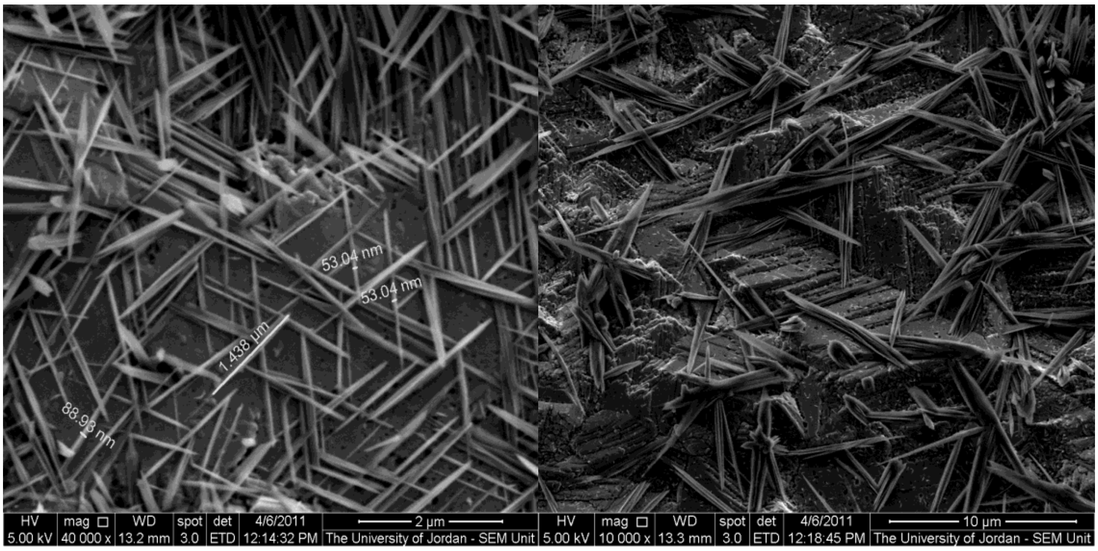
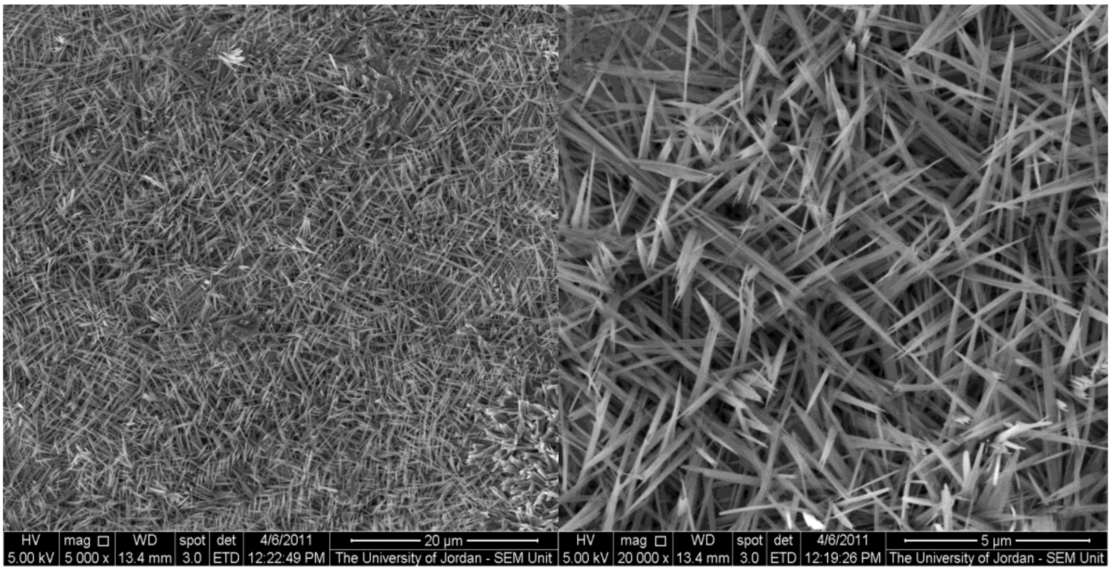


Figure 89: SEM images (a, b c and d) deposition of copper nanorods on copper substrate. Parameters of the experiment E_L = -1.5 V, E_H = -1.V centered at = -1.25V, amplitude = 0.5V, frequency = 100 Hz, copper concentration = 10^{-4} M, basic media, time = 60 seconds and scan rate of 100 mV/ s.

Figure 90 shows the SEM micrographs of copper nanorodes on copper substrate at 60s deposition time with amplitude square wave 0.5 V centered at -1.75V. Increase the potential of square wave potential regime increase the size of nanorodes of the copper with the same conditions used in the experimental for the formation CuO nanorodes, comparing the experiment; figure 87-89 show; for the potential used E = -1.25 V and the experiment; figure 89 shows; the potential -2.25 V the amount of copper nanorodes at potential -2.25 V centered at amplitude square wave 0.5 V are larger than when using the potential -1.25V centered at 0.5 V amplitude square wave. Figure 90 shows the average size of CuO nanorodes synthesis 65 nm.



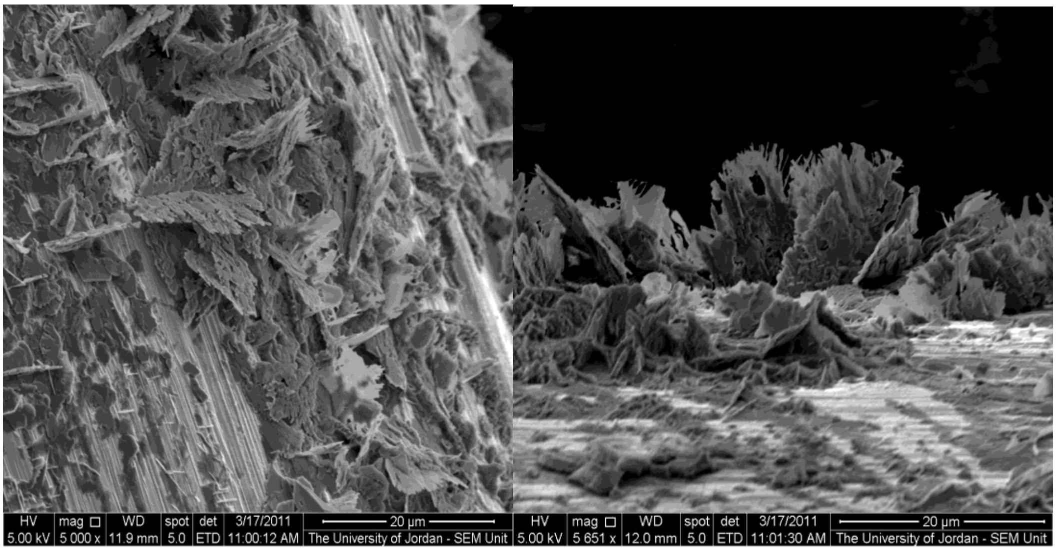
a b



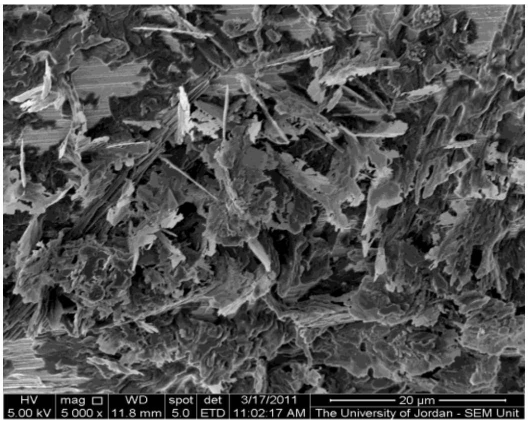
c d

Figure 90: SEM image (a –d) deposition copper nanorods on copper substrate. Parameters of the experiment E_L = -2.25 V, E_H = -1.75V centered at = -2.0V, amplitude = 0.5V, frequency = 100 Hz, copper concentration = 10^{-4} M, basic media, time = 60 seconds and scan rate of 100 mV/ s.

Figure 91 shows the SEM image of plates of copper oxide which are formed by dissolving copper salts in basic media at 1 M KOH, the plates of copper oxide formed on tantalum substrate in the form of epitaxial growth and distributed irregular on the surface.



a b



c

Figure 91: SEM images (a, b and c) deposition copper nanostructures on tantalum. Parameters of the experiment: E_L = -1.15 V, E_H = -0.55V centered at = -0.85 V, amplitude = 0.6V, frequency = 100 Hz, copper concentration = 10^{-3} M, basic media, time = 300 seconds and scan rate of 100 mV/ s.

Figure 92 shows the SEM micrographs which are formed of copper needles on copper substrate, the average size of needles 24 nm and the average length of needles 200 nm. It formation between nanorods; the better distribution, uniformity, size and shape.

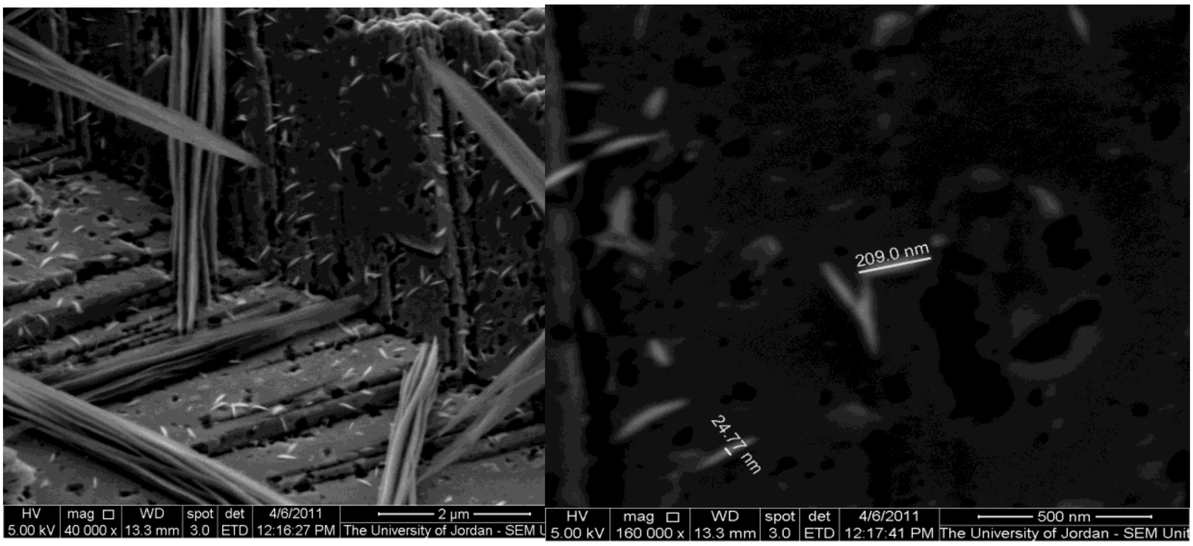
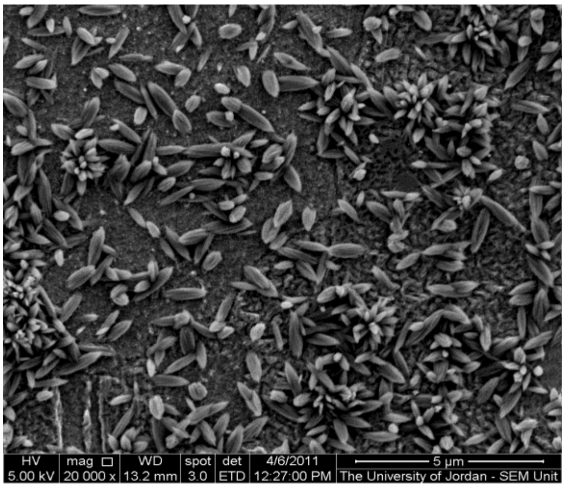
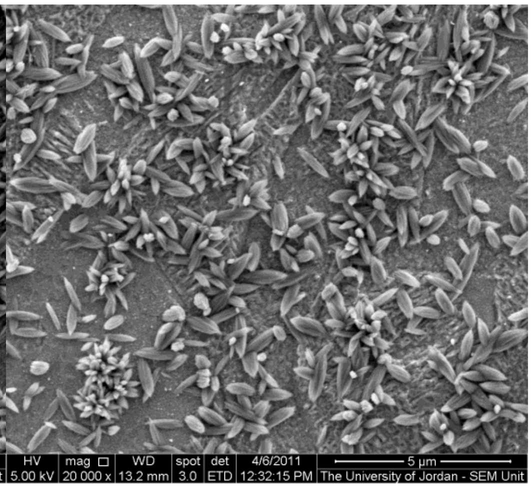


Figure 92: SEM images deposition of copper nanostructures on tantalum. Parameters of the experiment: E_L = -1.5 V, E_H = -1.V centered at = -1.25V, amplitude = 0.5V, frequency = 100 Hz, copper concentration = 10^{-4} M, basic media, time = 60 seconds and scan rate of 100 mV/ s.

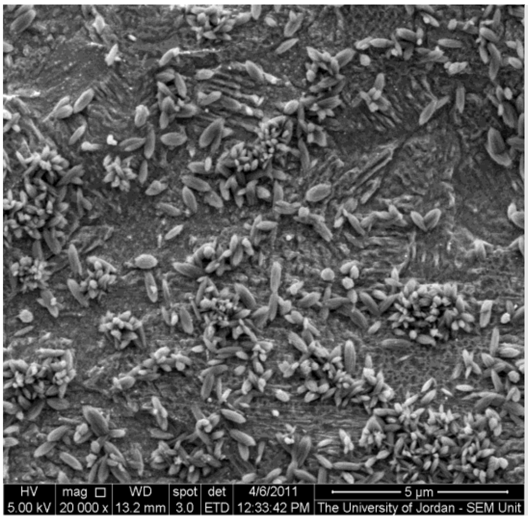
Figures 93 and 94 show the SEM and EDX micrographs of deposited copper nanostructures produced by application of square wave potential regime. Figure 93 shows grains of copper deposited from 1 M KOH and 1×10^{-4} M Cu^{+2} solutions. The grain formation consists of a group of nanorodes combined with each other in the form of grain particles. The average numbers of grain particles on the surface 2×10^{8} particles/ cm^{2}.



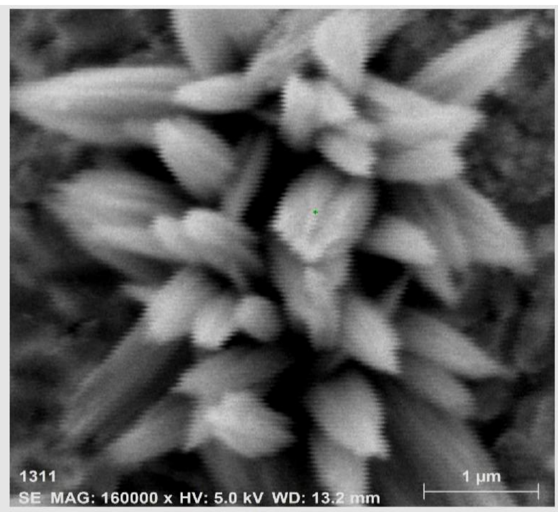
a



b



c



d

Figure 93: SEM images (a, b, c and d) deposition of copper nanostructures on tantalum. Parameters of the experiment E_L = 0.00 V, E_H = + 0.5V centered at = +0.25V, amplitude = 0.5V, frequency = 100 Hz, copper concentration = 10^{-4} M, basic media, time = 30 seconds and scan rate of 100 mV/ s.

Figure 94 shows the EDX spectra the analysis of grains evidence and proof are formed the grains particles copper oxide.

Spectrum: Acquisition 1261

El	AN	Series	unn. C [wt.%]	norm. C [wt.%]	Atom. C [at.%]	Error [%]
O	8	K-series	25.44	25.44	57.54	8.5
Cu	29	L-series	74.56	74.56	42.46	24.2
		Total:	100.00	100.00	100.00	

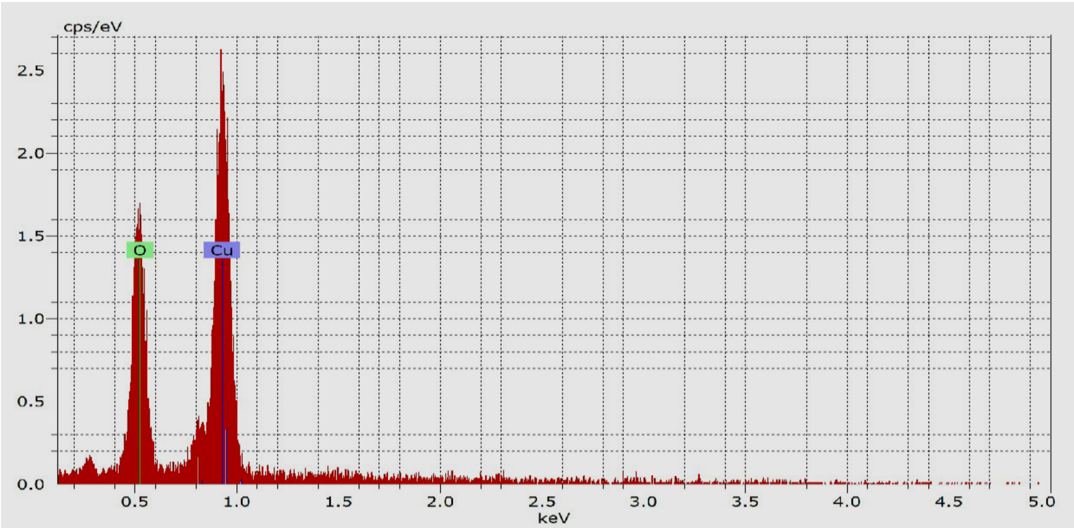


Figure 94: EDX the analysis of the produced. Parameters of the experiment :E_L = 0.00 V, E_H = + 0.5V centered at = +0.25V, amplitude = 0.5V, frequency = 100 Hz, copper concentration = 10^{-4} M, basic media, time = 30 seconds and scan rate of 100 mV/ s.

Figures 95 and 96 show the SEM micrographs of plam leave-like of copper oxide formed by application of square wave potential regime at different deposition time of 15 and 30 seconds with amplitude square wave of 0.5 V centered at -1.25 V.

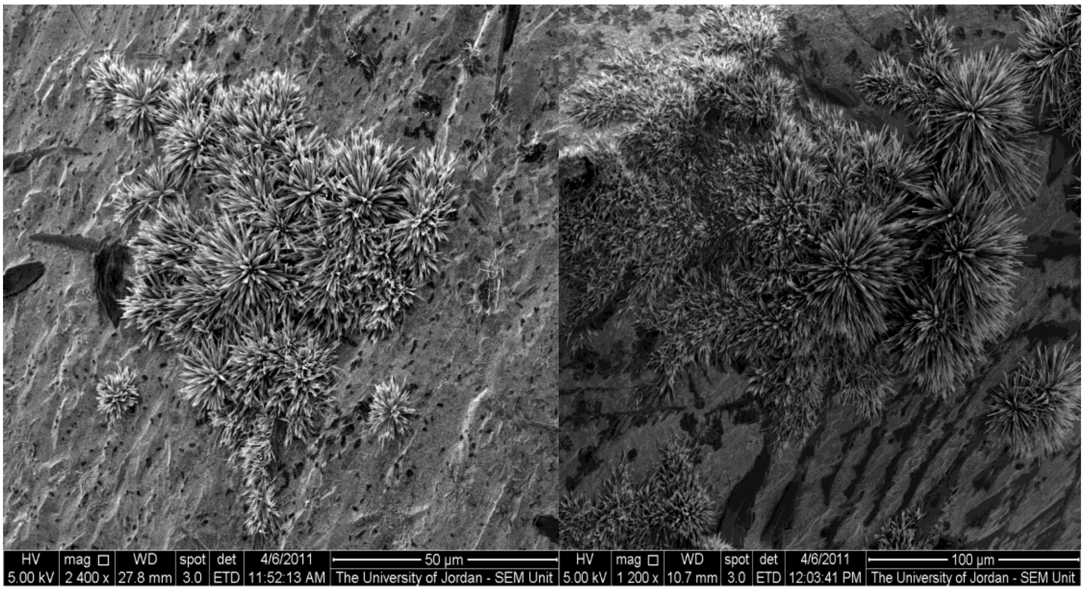


Figure 95: SEM image of plam leave-like formation on copper wire. Parameters of the experiment :E_L = -1.5 V, E_H = - 1.0V centered at = -1.25V, amplitude = 0.5V, frequency = 100 Hz, copper concentration = 10^{-4} M, basic media, time = 30 seconds and scan rate of 100 mV/ s.

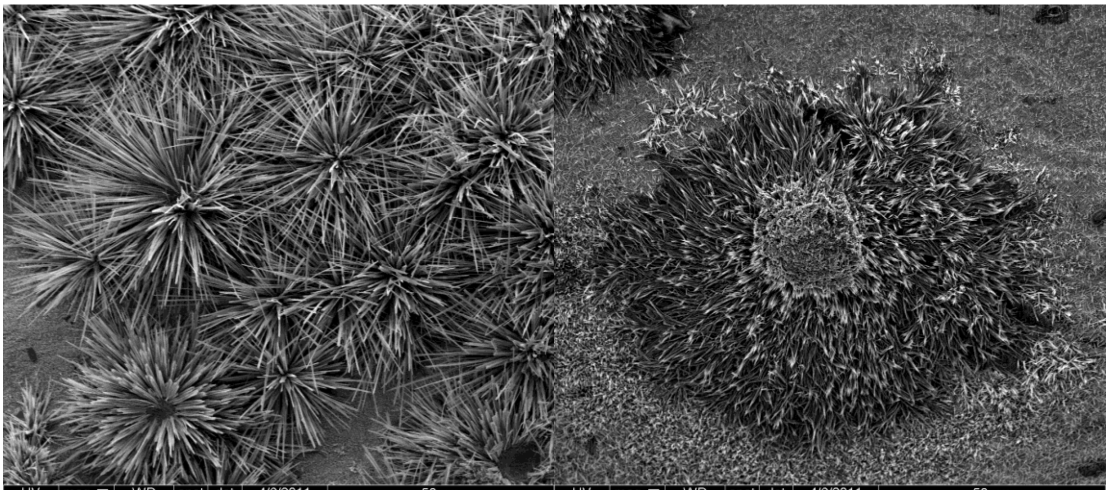
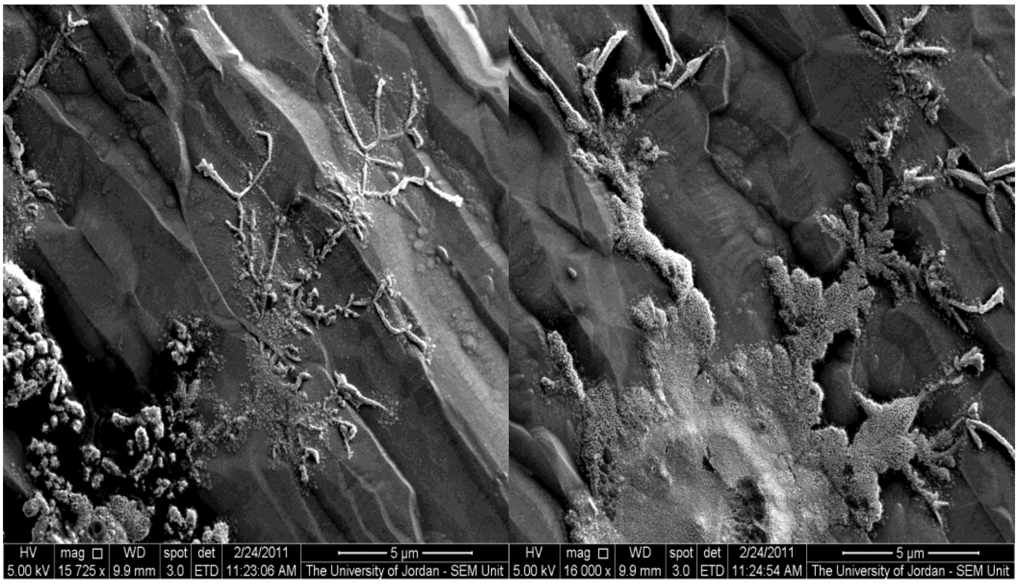


Figure 96: SEM image of plam leave-like formation on copper wire. Parameters of the experiment E_L = -1.5 V, E_H = - 1.0V centered at = -1.25V, amplitude = 0.5V, frequency = 100 Hz, copper concentration = 10^{-4} M, basic media, time = 15 seconds and scan rate of 100 mV/ s.

Figure 97 shows the SEM micrographs of tree-like copper nanostructures which are deposited on tantalum substrate. Figure 98 shows the EDX spectrum analysis of the result and evidence the formation of copper oxide nanostructures.

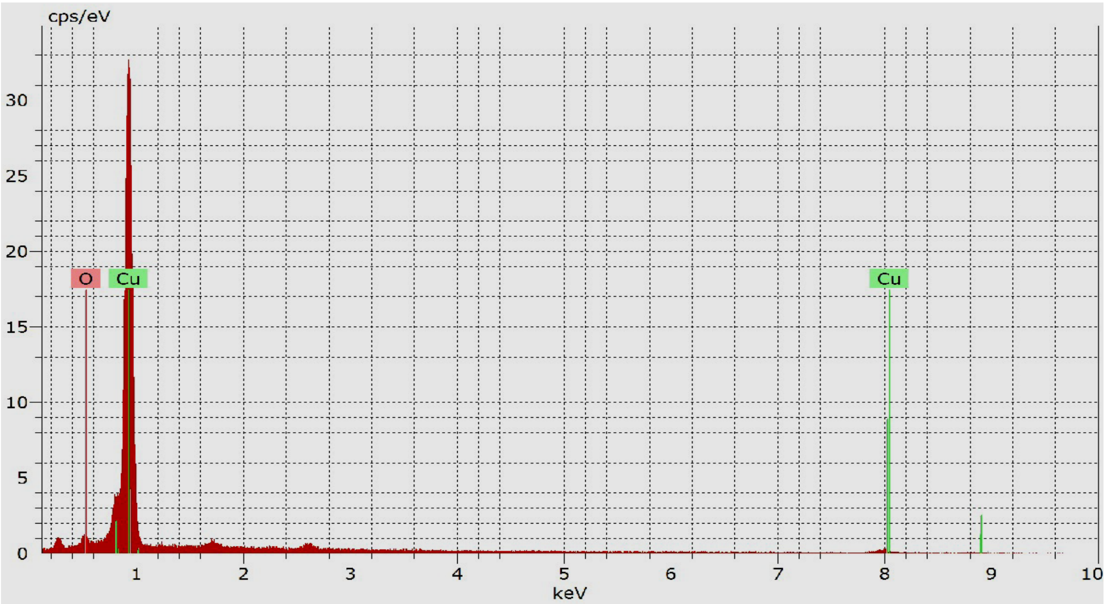


a

Figure 97-a: SEM image of tree-like formation on copper wire. Parameters of the experiment: E_L= -0.8 V, E_H = - 0.2V centered at = -0.5V, amplitude = 0.6V, frequency = 100 Hz, copper concentration = 10^{-2} M, acidic media, time = 120 seconds and scan rate of 100 mV/ s.

Spectrum: Acquisition 1035

El	AN	Series	unn. C [wt.%]	norm. C [wt.%]	Atom. C [at.%]	Error [%]
O	8	K-series	1.53	1.53	5.82	0.6
Cu	29	L-series	98.47	98.47	94.18	30.2
		Total:	100.00	100.00	100.00	



b

Figure 97-b: EDX spectra analysis of the results. Parameters of the experiment E_L = -0.8 V, E_H = -0.2V centered at = -0.5V, amplitude = 0.6V, frequency = 100 Hz, copper concentration = 10^{-2} M, acidic media, time = 120 seconds and scan rate of 100 mV/ s.

Figure 98 shows the SEM micrographs of nanofibers of copper formed by application of square wave potential regime at 15s deposition time with amplitude square wave of 0.5 V centered at -1.25 V.

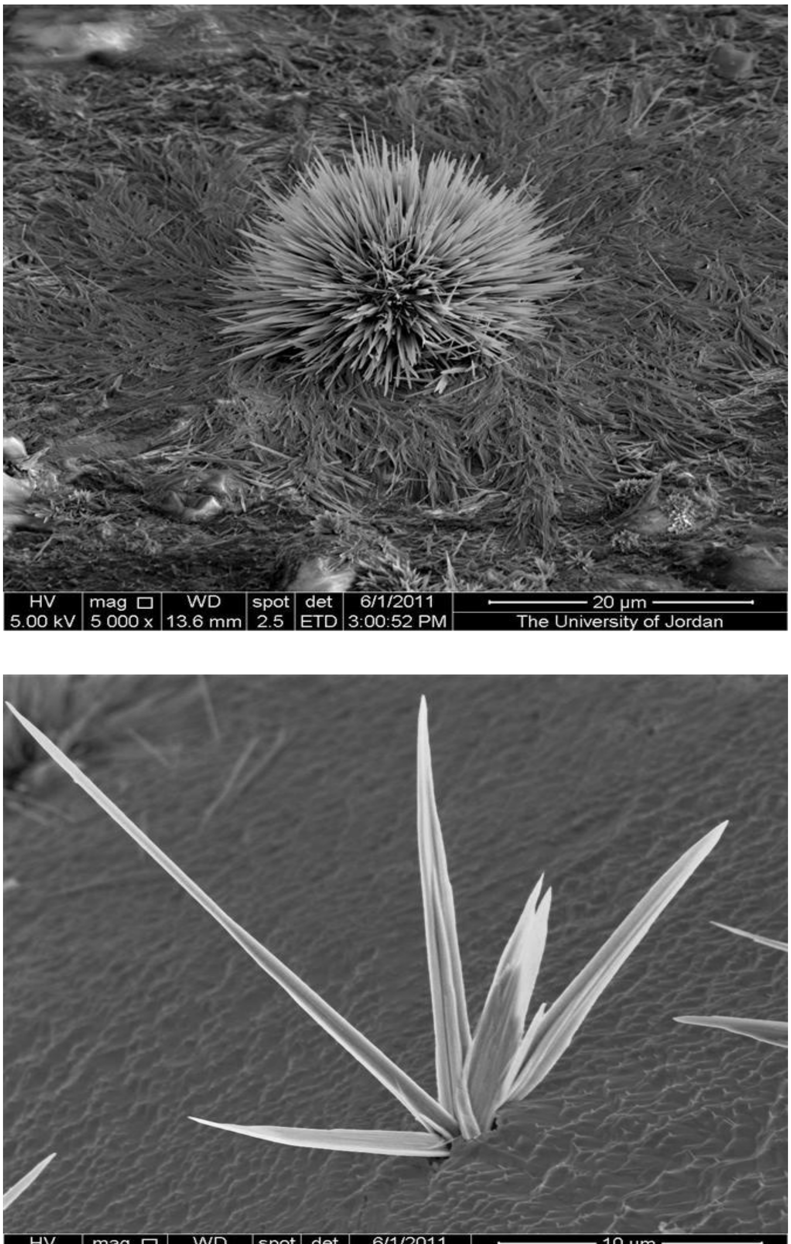


Figure 98: SEM image of plam leave-like formation on copper wire. Parameters of the experiment E_L = -1.5 V, E_H = - 1.0V centered at = -1.25V, amplitude = 0.5V, frequency = 100 Hz, copper concentration = 10^{-4} M, basic media, time = 15 seconds and scan rate of 100 mV/ s.

Table (6-a): comparing of all experiments of copper deposited.

Metal	Media	SEM figure	EDX figure	E_H V	E_L V	Center V	Amplitude V	Frequency Hz	Concentration M	Time seconds	Scan rate mV/s	Size nm	Area Particles cm^{-2}
copper	acidic	72	-----	0.00	-0.6	-0.3	0.6	100	10^{-4}	120	100	------	3.42×10^{9}
copper	acidic	73	-------	0.00	-0.6	-0.3	0.6	100	10^{-2}	120	100	------	---------
copper	acidic	74	-------	0.00	-0.6	-0.3	0.6	100	10^{-3}	60	100	------	3.90×10^{9}
copper	acidic	75	--------	0.00	-0.6	-0.3	0.6	100	10^{-3}	120	100	------	---------
copper	acidic	76	------	-0.1	-0.5	-0.2	0.6	100	10^{-3}	60	100	------	--------
copper	acidic	77	--------	-0.1	-0.5	-0.2	0.6	1000	10^{-3}	60	100	------	3.50×10^{9}
copper	acidic	78	-------	-1.0	-0.5	-0.75	0.5	100	10^{-3}	60	100	------	--------
copper	basic	79	------	-1.0	-0.5	-0.75	0.5	100	10^{-3}	60	100	-----	---------
copper	basic	80	------	-1.0	-0.5	-0.75	0.5	100	10^{-4}	60	100	28.5	--------
copper	acidic	81	-------	-1.3	-0.7	-1.0	0.6	100	10^{-3}	60	100	…….	--------
copper	basic	82	-----	-1.4	-0.8	-1.1	0.6	100	10^{-2}	120	100	------	---------
copper	acidic	83	------	-1.4	-0.8	-1.1	0.6	100	10^{-2}	60	100	------	----------
copper	basic	84	------	-1.05	-0.65	-0.85	0.4	100	10^{-3}	120	100	-------	---------

Table (6-b): comparing of all experiments of copper deposited.

Metal	Media	SEM figure	EDX figure	E_H V	E_L V	Center V	Amplitude V	Frequency Hz	Concentration M	Time seconds	Scan rate mV/s	Size nm	Area Particles cm^{-2}
copper	basic	85	------	-1.15	-0.55	-0.85	0.6	100	10^{-3}	300	100	-------	---------
copper	acidic	86	-------	-1.15	-0.55	-0.85	0.6	100	10^{-3}	60	100	------	---------
copper	basic	87	-------	-1.0	-1.5	-1.25	0.5	100	10^{-4}	15	100	------	--------
copper	basic	88	--------	-1.0	-1.5	-1.25	0.5	100	10^{-4}	30	100	------	---------
copper	basic	89	------	-1.0	-1.5	-1.25	0.5	100	10^{-4}	60	100	------	---------
copper	basic	90	--------	-2.25	-1.75	-0.2	0.5	100	10^{-4}	60	100	------	-------
copper	basic	91	-------	-1.15	-0.55	-0.85	0.6	100	10^{-3}	300	100	------	--------
copper	basic	92	------	-1.0	-1.5	-1.25	0.5	100	10^{-4}	60	100	-----	---------
copper	basic	93	94	0.00	+0.5	+0.25	0.5	100	10^{-4}	30	100	-------	2×10^{8}
copper	basic	95	-------	-1.0	-1.5	-1.25	0.5	100	10^{-4}	30	100	…….	--------
copper	basic	96	-----	-1.0	-1.5	-1.25	0.5	100	10^{-4}	15	100	------	---------
copper	basic	97-a	97-b	-0.8	-0.2	-0.5	0.6	100	10^{-2}	120	100	------	----------
copper	basic	98-(a b)	------	-1.0	-1.5	-1.25	0.5	100	10^{-4}	15	100	-------	---------

130

3.3.5. The concentration and potential affected of the deposits in acidic media:

Concentrations and potential used in the deposition of copper from copper (II) perchlorate hexahydrate significantly affect the output of the deposition. The greater the concentration 10^{-3} M from copper(II)perchlorate hexahydrate whenever the result is composed of copper oxides and copper only, but at lower concentration(10^{-3} and 10^{-4})M from copper (II) perchlorate with a high potential used in deposited of nano-structures in 0.5M sulfuric acid. The analysis of the output format proves that the output does not contains copper, but also other elements contributed to the composition copper sulfate or copper sulfide and tantalum oxide in various forms. Thus we can control the composition of copper oxide-specific factors and the most important and central focus being the process of electrodeposition.

Figure 99 shows the SEM micrograph of copper sulfide deposited on tantalum wire at 10^{-3} M copper solution with central at -0.75 V.

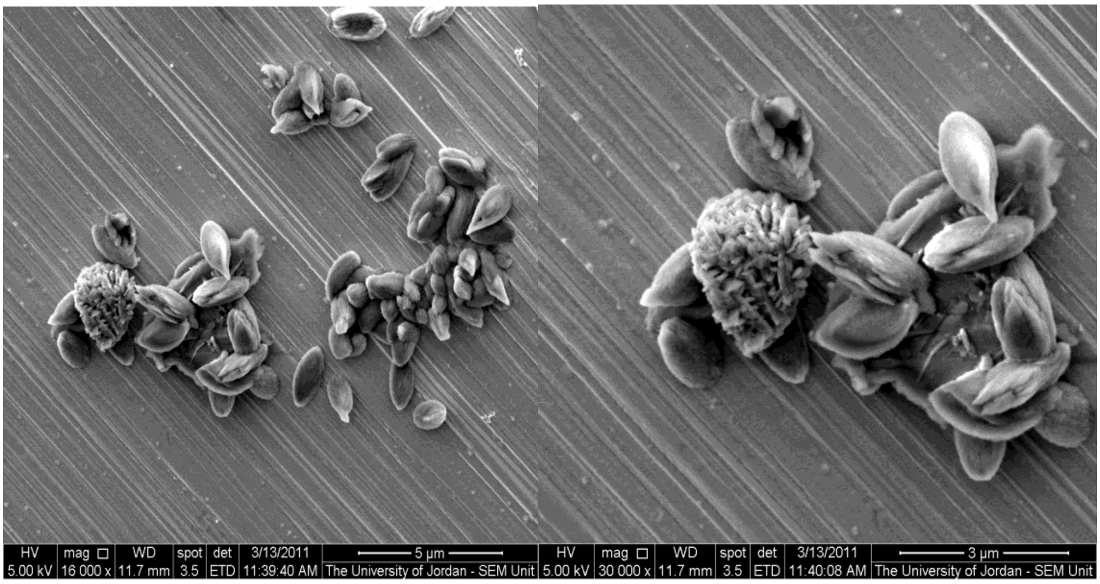


Figure 99: SEM images deposition of copper sulfate nanostructures on tantalum. Parameters of the experiment :E_L = -1.05 V, E_H = -0.45V centered at = -0.75V, amplitude = 0.6V, frequency = 1K Hz, copper concentration = 10^{-3} M, basic media deposition, time = 120 seconds and scan rate of 100 mV/ s.

Figures 100--102 show the SEM and EDX micrographs of deposited copper sulfate nanostructures produced in acidic media at10^{-3} M concentration with high potential.

Figure 100 shows the SEM images copper sulfate of deposited on tantalum wire. The concentration used of deposited nanostructures 10^{-3} M with central at -0.7 V.

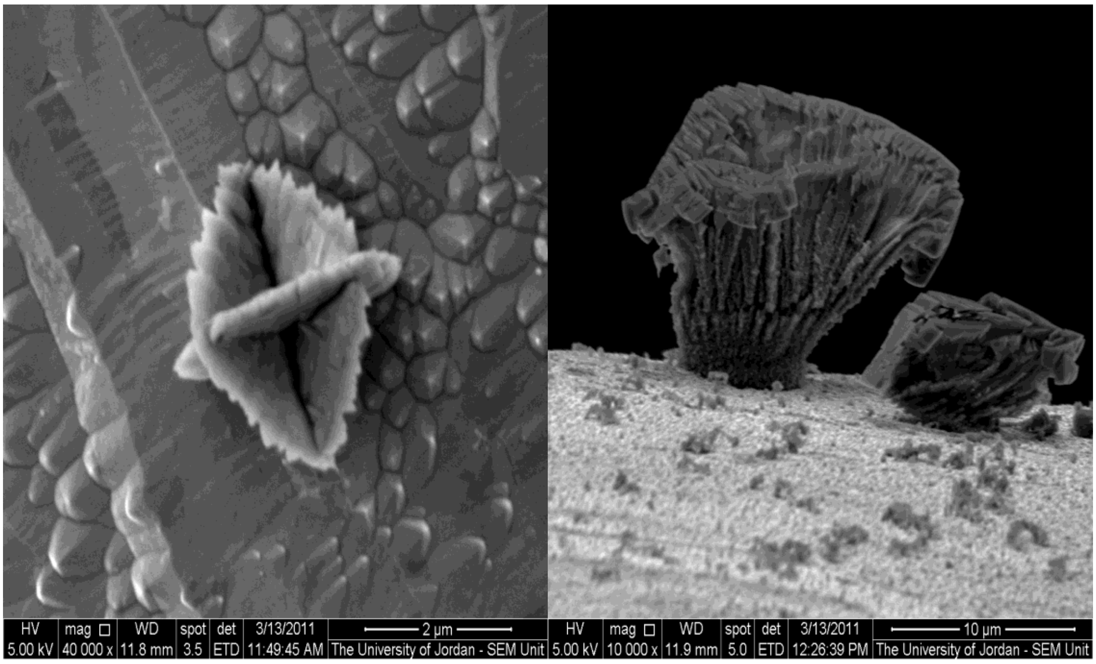
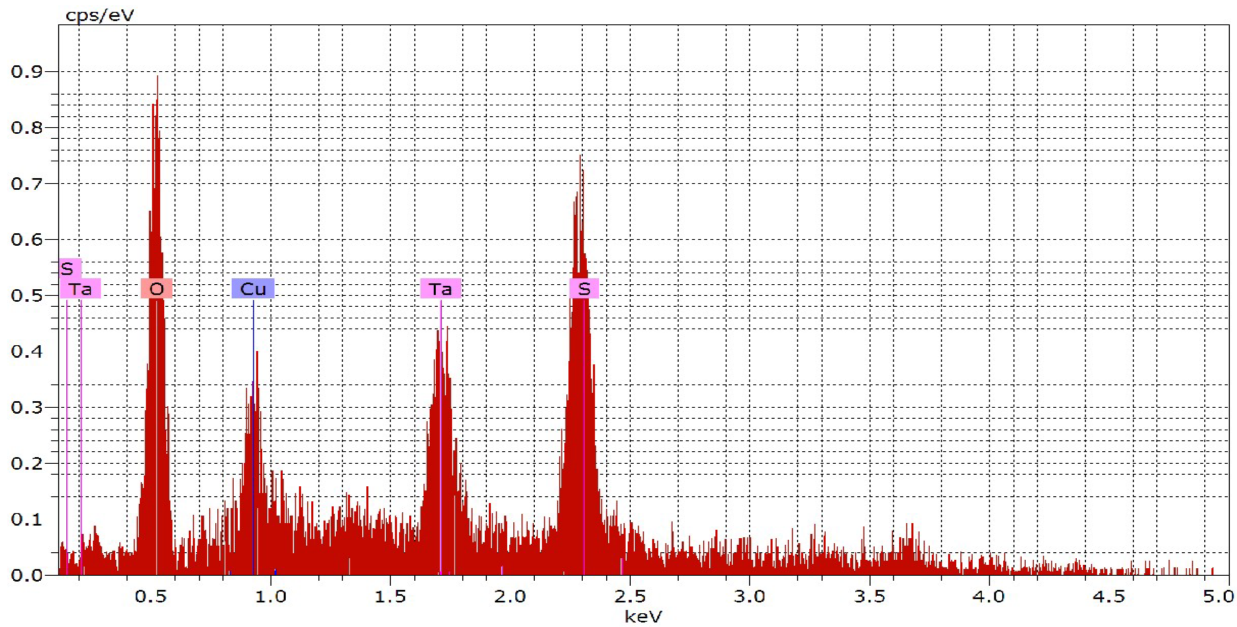


Figure 100: SEM images deposition of copper nanostructures on tantalum. Parameters of the experiment: E_L = -0.9 V, E_H = -0.5V centered at = -0.7V, amplitude = 0.4V, frequency = 1K Hz, copper concentration = 10^{-3} M, basic media, time = 120 seconds and scan rate of 100 mV/ s.

Figure 101 shows the EDX spectra analysis of the results, the analysis of spectra evidence the formation on the surface is copper sulfate.

Spectrum: Acquisition 1103

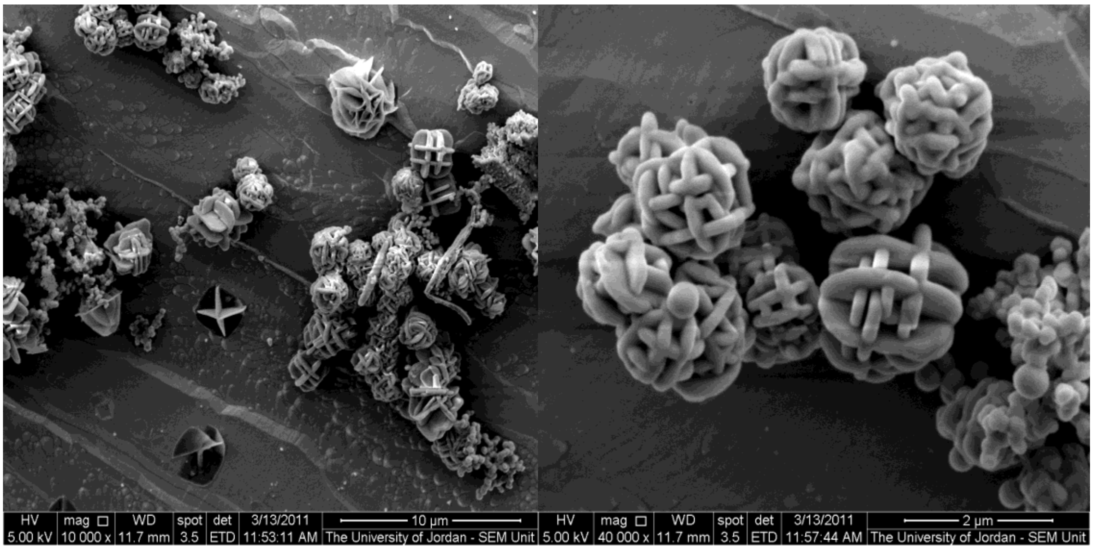
El	AN	Series	unn. C [wt.%]	norm. C [wt.%]	Atom. C [at.%]	Error [%]
O	8	K-series	25.25	32.61	61.27	5.2
S	16	K-series	20.70	26.73	25.05	1.2
Cu	29	L-series	17.47	22.56	10.67	4.6
Ta	73	M-series	14.02	18.11	3.01	0.9
		Total:	77.44	100.00	100.00	



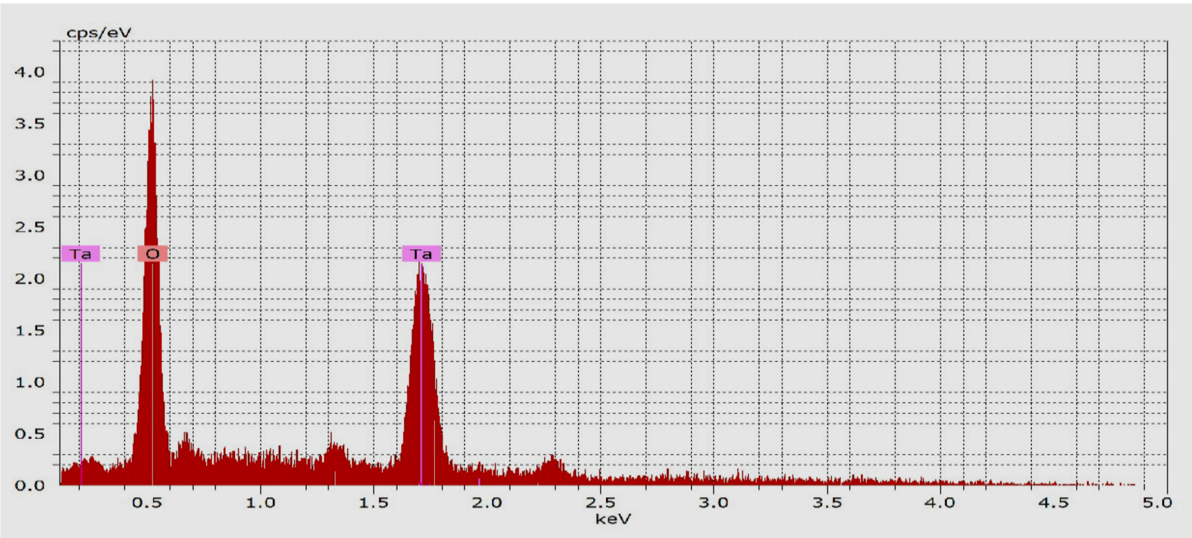
d

Figure 101(d): EDX of the results deposition copper nanostructures on tantalum. Parameters of the experiment E_L = -0.9 V, E_H = -0. 5V centered at = -0.7V, amplitude = 0.4V, frequency = 1K Hz, silver concentration = 10^{-3} M, basic media deposition, time = 120 seconds and scan rate of 100 mV/ s.

Figure 102 shows the SEM images tantalum oxide of deposited on tantalum wire. The concentration used of deposited nanostructures 10^{-3} M with central at -0.7 V. conclusion in a single sample which are formed three results copper oxide, copper sulfate and tantalum oxide on the same surface.



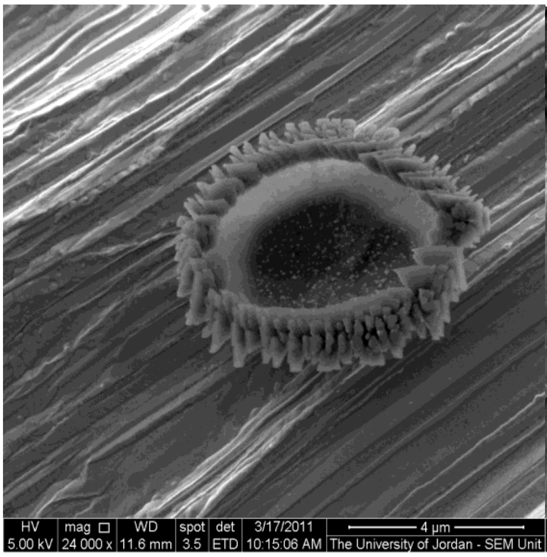
a b

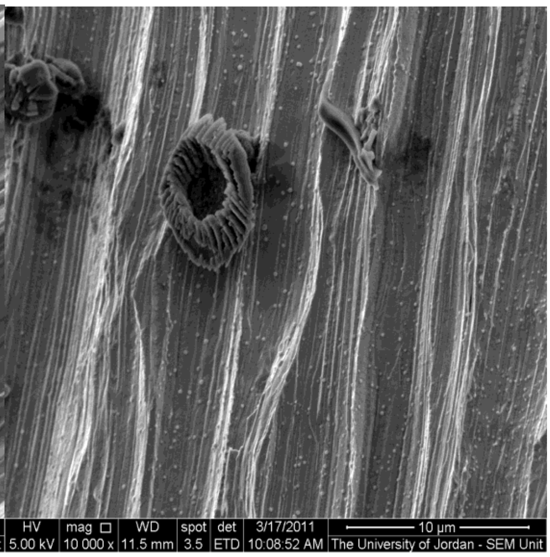


d

Figure 102: SEM image (a and b) tantalum oxide formation on tantalum substrate. (c)EDX spectra of tantalum oxide formation on tantalum substrate. Parameters of the experiment E_L = -0.9 V, E_H= -0.5V centered at = -0.7V, amplitude = 0.4V, frequency = 1K Hz, silver concentration = 10^{-3} M, basic media, time = 120 seconds and scan rate of 100 mV/ s.

Figures 103—105 show the SEM and EDX micrographs of coccolith-like copper sulfate deposited nanostructures produced by application of square wave potential regime.





a b

Figure 103: SEM images (a and b) deposition copper nanostructures on tantalum. Parameters of the experiment E_L = -1.15 V, E_H = -0. 55V centered at = -0.85V, amplitude = 0.6V, frequency = 50 Hz, copper concentration = 10^{-3} M, acidic media, time = 120 seconds and scan rate of 100 mV/ s.

Spectrum: Acquisition 1145

El	AN	Series	unn. C [wt.%]	norm. C [wt.%]	Atom. C [at.%]	Error [%]
O	8	K-series	51.43	50.66	79.46	7.3
S	16	K-series	14.48	14.26	11.16	0.9
Cu	29	L-series	17.87	17.60	6.95	3.5
Ta	73	M-series	17.74	17.47	2.42	1.0
		Total:	101.52	100.00	100.00	

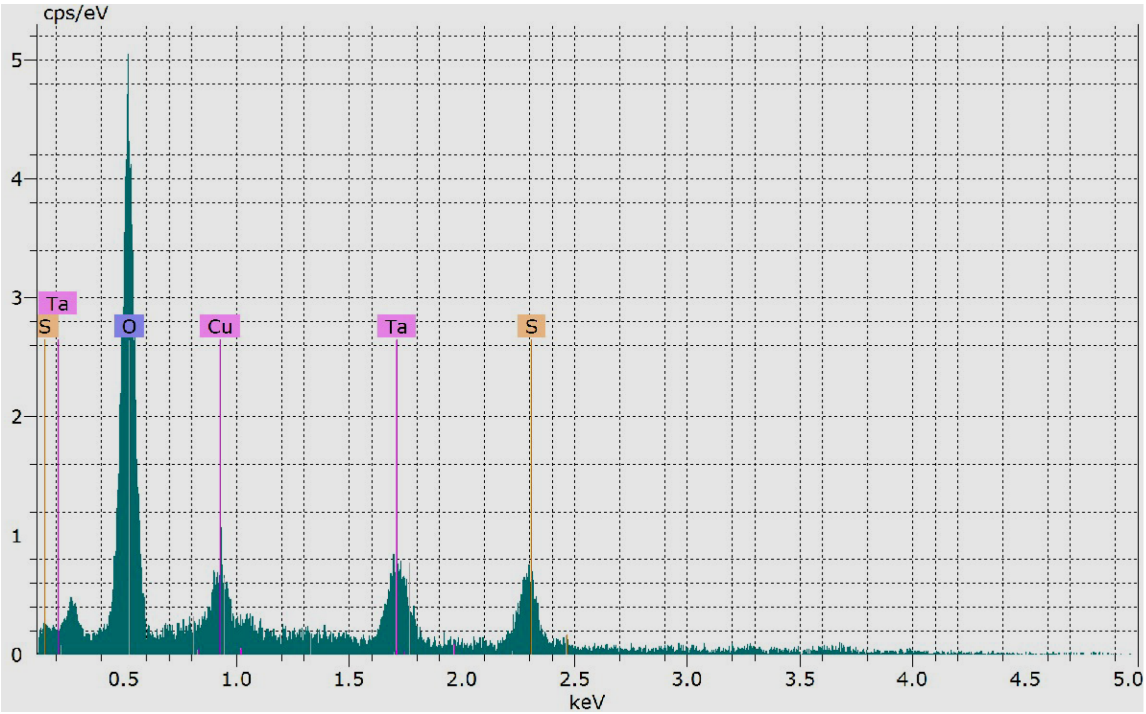
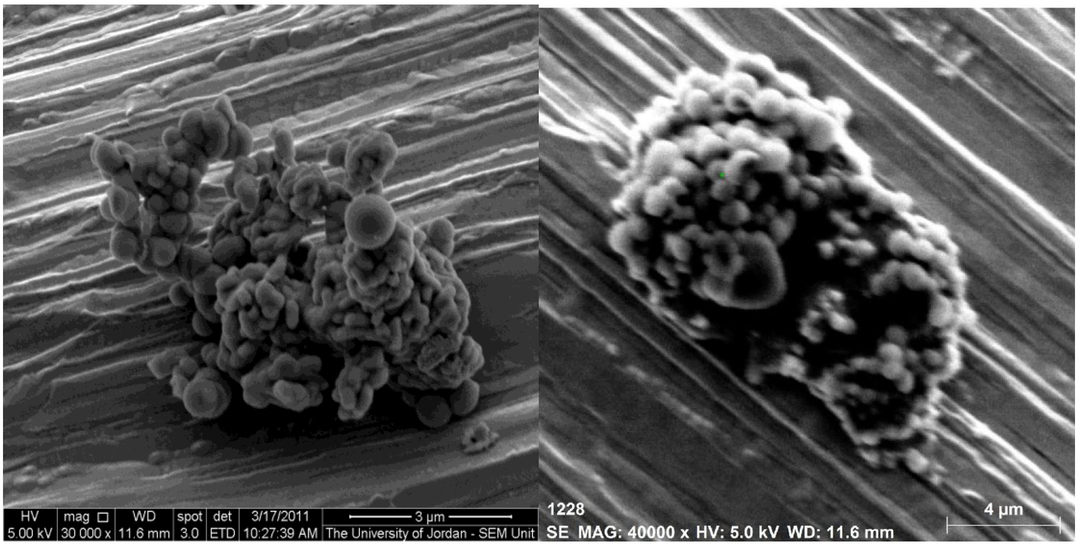


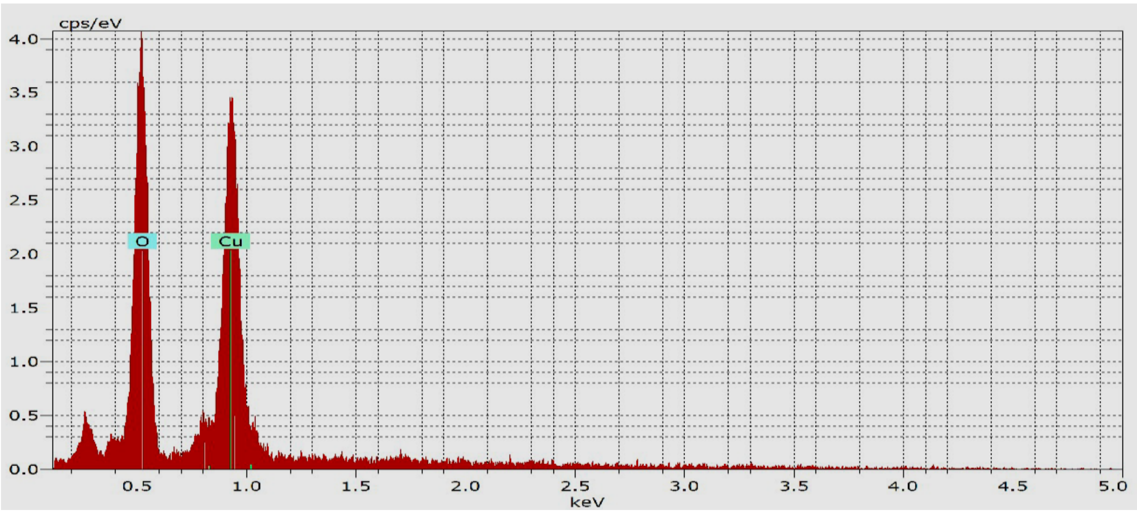
Figure 104: EDX of the results deposition copper nanostructures on tantalum deposition copper nanostructures on tantalum. Parameters of the experiment E_L = -1.15 V, E_H = -0. 55V centered at = -0.85V, amplitude = 0.6V, frequency = 50 Hz, copper concentration = 10^{-3} M, acidic media, time = 120 seconds and scan rate of 100 mV/ s.



a b

Spectrum: Acquisition 1148

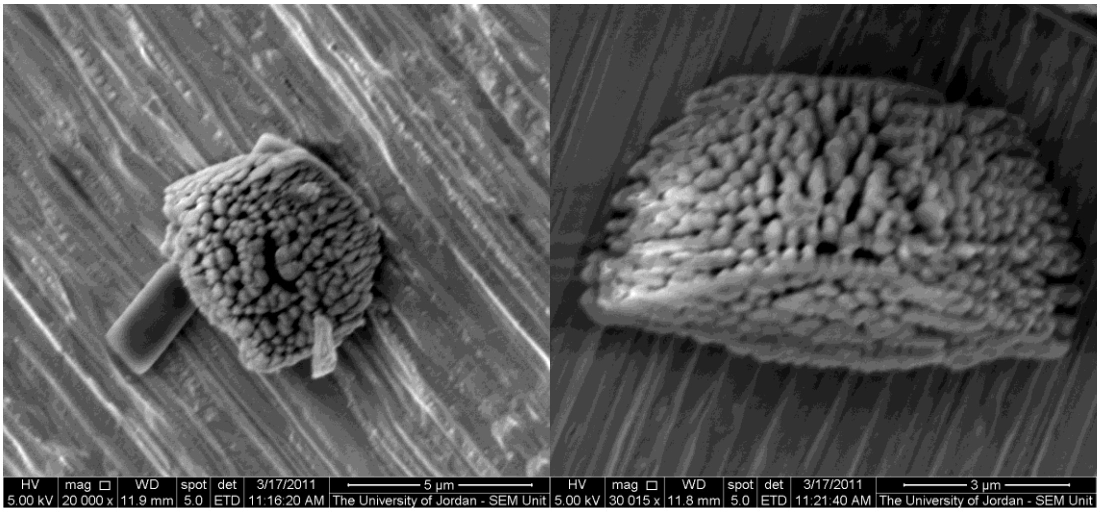
El	AN	Series	unn. C [wt.%]	norm. C [wt.%]	Atom. C [at.%]	Error [%]
O	8	K-series	34.72	34.72	67.87	11.2
Cu	29	L-series	65.27	65.28	32.13	20.9
		Total:	100.00	100.00	100.00	



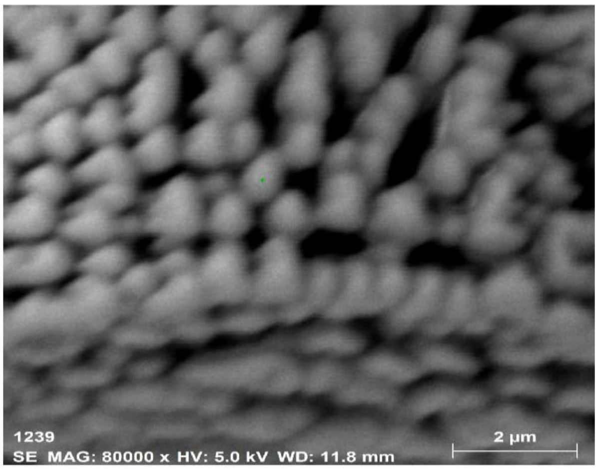
c

Figure 105: SEM images (a and b) and (c) EDX of the results; tantalum oxide formation. Parameters of the experiment E_l = -1.15 V, E_h = -0. 55V centered at = -0.85V, amplitude = 0.6V, frequency = 50 Hz, copper concentration = 10^{-3} M, acidic media, time = 120 seconds and scan rate of 100 mV/ s.

Figures 106 shows the SEM and EDX micrographs of deposited copper sulfate nanostructures produced by application of square wave potential regime.



a b

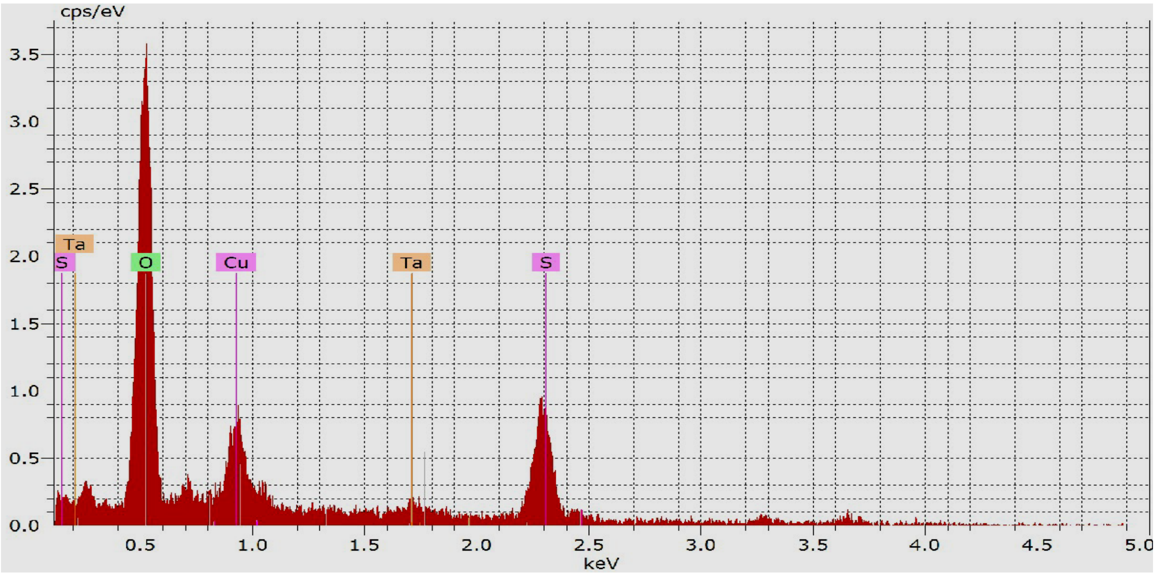


c

Figure 106(a-c) SEM images deposition of copper nanostructures on tantalum. Parameters of the experiment E_l = -1.25 V, E_h = -0. 65V centered at = -0.95V, amplitude = 0.6V, frequency = 100 Hz, copper concentration = 10^{-3} M, acidic media, time = 300 seconds and scan rate of 100 mV/ s.

Spectrum: Acquisition 1158

El	AN	Series	unn. C [wt.%]	norm. C [wt.%]	Atom. C [at.%]	Error [%]
O	8	K-series	50.62	48.44	73.80	7.4
S	16	K-series	21.29	20.37	15.48	1.2
Cu	29	L-series	27.37	26.19	10.05	5.0
Ta	73	M-series	5.23	5.01	0.67	0.4
		Total:	104.51	100.00	100.00	

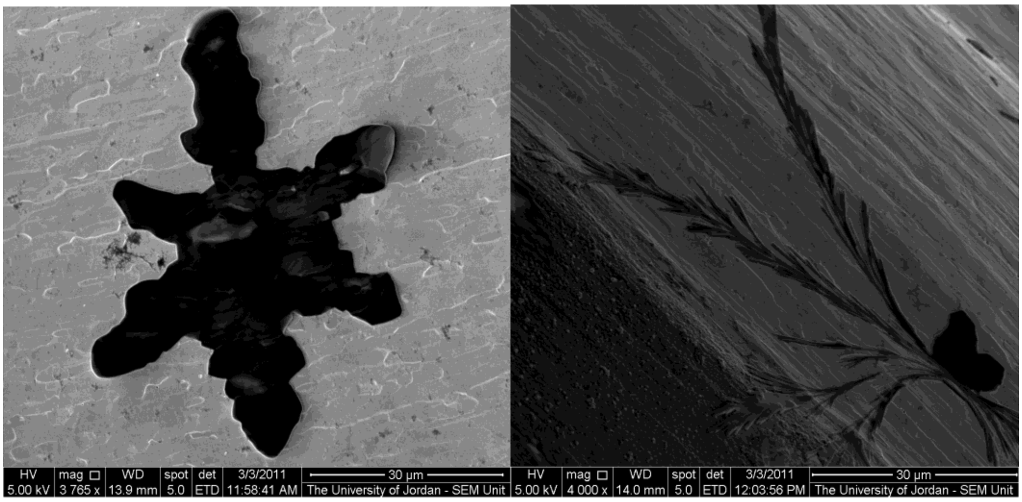


d

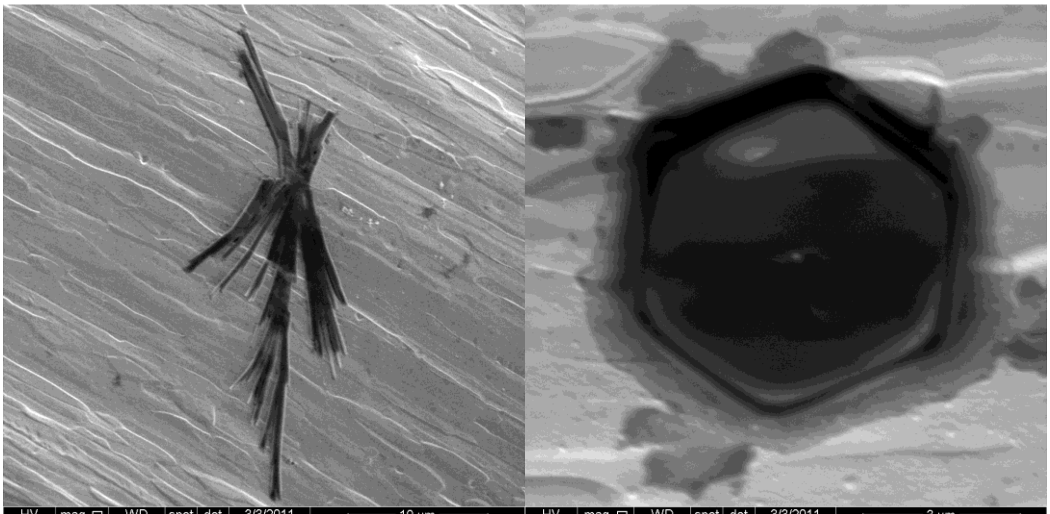
Figure 106-d: EDX of the produces deposition of copper nanostructures on tantalum. Parameters of the experiment E_l = -1.25 V, E_h = -0. 65V centered at = -0.95V, amplitude = 0.6V, frequency = 100 Hz, copper concentration = 10^{-3} M, acidic media, time = 300 seconds and scan rate of 100 mV/ s.

Microcrystals copper oxide:

Figure 107 shows the SEM micrographs of deposited copper oxide nanostructures produced by application of square wave potential regime.



a b



c d

Figure 107: SEM images (a ----- d) deposition copper oxide nanostructures on tantalum. Parameters of the experiment E_L = -1.15 V, E_H = -0. 55V centered at = -0.85V, amplitude = 0.6V, frequency = 100 Hz, copper concentration = 10^{-2} M, acidic media, time = 120 seconds and scan rate of 100 mV/ s.

4- conclusions:

The present study involved development of a technique for formation of electrodes on surface bearing nanostructures. The developed methods rely on application of a square potential regime to an electrode dipped in a solution containing ions of the deposited metal. This method proved successful to deposition of gold, silver and copper nanostructures.

The size of the particles, their shape and uniformity of distribution on the surface of the substrate showed dependence on the experimental conditions. The experimental conditions involve the parameters of the square wave potential regime in addition to the concentration of the ions of the deposited metals, pH of the solution and deposition time.

The frequency of the square wave played a prominent role on the properties of the nanostructures produced. An intermediate frequency of 100 Hz was found as the optimal frequency for deposition as indicate by i-E voltammetry traces and by SEM micrographs. This can be explained on the basis that each cycle represents a potential step experiments, a forward step and reverse step. The optimal frequency that compromises the electrochemical events per one cycle versus the number of events per unit time. On the other hand, it is the frequency that sets a balance between particles growth and nucleation of nanoparticles on the surface.

The amplitude of the square wave also proved to play an important role in the shape, size and composition of the nanoparticles is not unexpected. If the amplitude of the square wave spans through the oxidation region then the nanoparticles will be partially or totally oxidized.

The effect of the concentration of the runs in the solution can be generally explained on basis of the effect of concentration on deposition kinetics. Higher concentrations, generally, will increase the relative super saturation and this enhances the particle growth mechanisms leading to formation of meso- and micro- structures. The effect of time of deposition was found generally to increase the particle size.

Reference

Alper, M., Baykul, M.C., Peter, L., Toth, J., and Bakonyi, I. (2004). Preparation and Characterization of electrodeposited Ni-Cu/Cu Multilayers. **J. of App. Electroc**. 34, 841-848.

Ambrose, J., Barradas, R. G., Shoesmith, D. W. , (1973). Investigations of copper in aqueous alkaline solutions by cyclic voltammetry. **J. Electroanal. Chem.**, vol. 47, PP. 47-64.

Bard, A.; Faulkner, L., (2001). **Electrochemical Methods: Fundamentals and Applications**, (2nd ed.). New York: Wiley & Sons, Inc.

Christensen, P.A., and Hamnett, A. (1994), **Techniques and Mechanisms in Electrochemistry**. London: Blakie Academinc & Professional.

Devers, T. Kante, I. Allam L. and Fleury, V. (2003), Preparation of dendritic tin Nanoaggregates by electrodeposition. **Journal of Non-Crystalline Solids**, 321, 73-80.

Diliberto×, S., Richoux, V., Boulanger, C. and Lecuire, J.M., (2006), pulsed electrodeposition of bismuth telluride films: influence of pulse parameters over nucleation and morphology. **Electrochimica Acta,** 52 (2007) 3053-3060.

Droog, J. M., Alderliesten, C. A., Alderliesten, P. T., Bootsma, G. A., (1980) Initial stages of anodic oxidation of polycrystalline copper electrodes in alkaline solution. **J. Electroanal. Chem.**, vol. 111, PP. 61-70.

Fotouhi, L. and Rezaei, M., (2009), electrochemical synthesis of copper sulfide nanoparticles. **Microchim Acta,** (2009) 167: 247-251.

Gosser, Jr. David. (1993), **Cyclic Voltammetry, Simulation and Analysis of Reaction Mechanisms.** VCH Publishers, INC .

Gleiter, H. (1989).Nanocrystalline materials. **Prog. Mater. Sci**. 33vol. P.223-315.

Holze, R., (2009). **Experimental Electrochemistry**. Germany: Wiley-VCH.

Hourani, M., (1993). Desulfurization of thiophene by electrochemical perturbation. **Electroanalytical chemistry**.368 (1994) 139-142.

Hourani, M., and Ibrahim, K., (1992). **Electrocatalysis and Electroanalysis By Adsorbed-Atom Electrodes**; Palladium on Tantalum and Iodine on Platinum systems.

Hourani, M. and waleed, B., (1998). Exhaustive oxidation of nitrite, nitrate, and hydrazine was achieved b application of square wave potential regime to a platinum electrode. **J. of App. Electroc**.30: 859±864, 2000. 859.

Hourani, M., and Wedian, F. (2000). The effect of adatoms on the corrosion rate of copper. **Corrosion Science**, 42Vol, 2131-2144.

Hourani, M. and Wieckowski, A. (1990), Structural effects in heterogeneous electrocatalysis: Electrohydrogenation of ethylene on preferentially oriented platinum electrodes. **Langmuir**, 6(2): 379-385.

Kounaves, P. Samuel., (1997), Chapter 37: Voltammetric Techniques. In: Settle, A. Frank, **Handbook of instrumental techniques for analytical chemistry**, (2nd ed.). 709-725, Upper Saddle River, NJ: Prentice Hall PTR.

Latimer, W. M., **oxidation potentials**. (2 ed.). Prentice-Hall, Engle Wood Cliffs, New Jersey, 1952, PP. 183.

Nicholson, Richard S. (1965), Theory and Application of Cyclic Voltammetry for Measurement of Electrode Reaction kinetics. **Anal. Chem.,** 37 (11), 1351-1355.

Read, W.T., and Shockley, W., (1950). Dislocation Models of Crystal Grain Boundaries . **Phys. Rev**. 78 (1950), p.275.

Rezaei, B. and Damiri, S., (2010). Electrodeposited silver nanodendrites electrode with strongly enhanced electrocatalytic activity. **J. Talanta**. 83 Vol. (2010) 197–204.

Sawyer, D., Sobkowiak, A., Roberts, J., (1995). **Electrochemistry for Chemists,** (2nd ed.). New York: John Wiley & Sons, Inc.

Sawyer, Donald T., Heineman, William R., and Beebe, Janice M. (1984), **Chemistry Experiments for Instrumental Methods**. John Wiley & Sons.

Schindler×, W., Hugelmann, P., Hugelmann, M., and Lorenz b, W.J. (2005), Nanoelectrochemistry and nanophysics at electrochemical interfaces. **Surface Science**, 597 (2005) 156–172.

Skoog, Douglas A., Holler, James F., and Nieman, Timothy A. (1998), **Principle of Instrumental Analysis**, (5th ed.). Brooks/Cole: Thonson Learning.

Taylor, G.I., (1934). The Mechanism of Plastic Deformation of Crystals. **Proc. Roy. Soc.** London Ser. A 145 vol. 388.

Valentine, Z. and Manuele, D. (2009), iron-chromium alloy nanoparticles produced by pulsed sonoelectrochemistry: Synthesis and characterization. **Acta Materialia**, 58 (2010) 311-319.

Wang, Joseph. (2000), **Analytical Electrochemistry**, (2nd ed.). A John Wiley & sons, Inc., Publication.

Wang, J., (2006). **Analytical Electrochemistry**, (3rd ed.). New York: Wiley-VCH.

Wieckowski×, A. and Hourani, M., (1989). Structural effects in Heterogeneous Electrocataysis: Electrohydogenation of Ethylene on Preferentially Oriented Platinum Electrodes. **Langmuir**. 1990, 6, 379.

Yunhuai Zhang×, Yannan Yang, Peng Xiao, Xiaoning Zhang a, Lu Lua, Lu Li (2009), Preparation of Ni nanoparticle–TiO2 nanotube composite by pulse electrodeposition. **Materials Letters**, 63 (2009) 2429–2431.

تحضير و تعريف دقائق نانونية من الذهب و الفضة و النحاس بالترسيب الكهروكيميائي بإستخدام برنامج جهد موجة مربعة

إعداد

وائل محمد محمود

المشرف

الأستاذ الدكتور "محمد خير" عودة الحوراني

ملخص

في هذه الدراسة تم تحضير البنية النانواية من معادن الذهب و الفضة و النحاس بتطبيق برنامج جهد موجة مربعة على سطح معدن التانتلوم. اولا تحضير محلول الذهب من تركيز 1.9×10^{-3} مولار في كلوروواورريك اسيد و تخفيف المحلول الى تراكيز مختلفة 10^{-2} ، 10^{-3} و 10^{-4} مولار في محلول حامض الكبريتيك بتركيز0.5 مولار. الأشكال الرئيسية التي نتجت كانت جزيئات النانو، النمو الأفقي، الزهور، الإبر، حدود الصفائح، شوكة و البلورات.

أما محلول الفضة المستخدم في عملية الترسيب ثم تحضيره من هيدرات بيركلورات الفضة بتراكيز مختلفة 10^{-2}، 10^{-3} و 10^{-4} مولار في وسط حمضي. و الأشكال الرئيسية الناتجة هي جزيئات النانو، اسفنج، الصفائح، سعفة النخيل، الزهرة، التكتلات النانواية.

ثم تحضير بناءات نانو النحاس المعدنية من سداسي هيدرات بيركلورات النحاس الثنائي في وسطين مختلفين حمضي و قاعدي بتراكيز مختلفة 10^{-2}، 10^{-3} و 10^{-4} مولار. ووجد أن الأشكال الرئيسية الناتجة في الوسط القاعدي هي جزيئات الناو و ألياف النانو و الاسفنج و الصفائح و حدود الصفائح و الحبوب والبلورات. أما في الوسط الحمضي فتم تحضير النحاس باشكال مختلفة و هي الجزيئات النانواية،النانو قضيب و الاسفنج و ألياف النانو والكوكوليت و الزهور و البلورات.

و تم الكشف ان لكل من التركيز و السعة و التردد و الزمن و الجهد تأثير على الحجم و التوزيع و الشكل للمادة المراد ترسيبها. و قد تم التعرف على خصائص الذهب والفضة و النحاس باستخدام الفولتاموغرامات و الماسح الضوئي الالكتروني و الالكترون التشتتي باستخدام الأشعة السينة.